



QEX

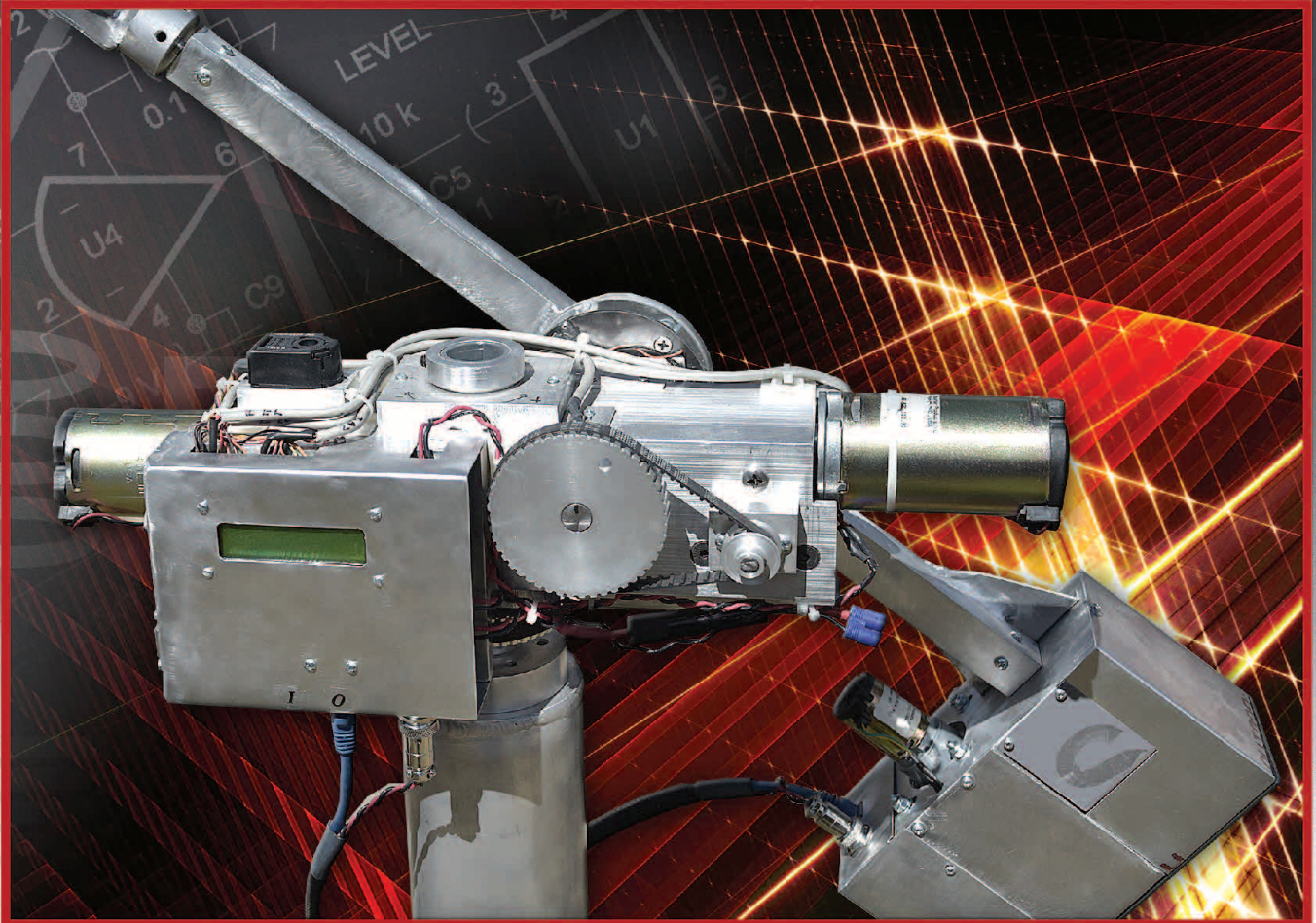
March/April 2017

www.arrl.org

\$7

A Forum for Communications Experimenters

Issue No. 301



KE7FEF steps through several generations of satellite tracking antenna positioners.

New

APRS® / D-STAR®

TH-D74A 144/220/430 MHz Tribander

Introducing the TH-D74A for the ultimate in APRS and D-STAR performance. KENWOOD has already garnered an enviable reputation with the TH-D72A handheld APRS amateur radio transceiver. And now it has raised the bar even further with the new TH-D74A, adding support for D-STAR, the digital voice & data protocol developed by the JARL, and enabling simultaneous APRS and D-STAR operation – an industry first.



- ▼ APRS compliance using packet communication to exchange real-time GPS position information and messages
- ▼ Compliant with digital/voice mode D-STAR digital amateur radio networks
- ▼ Built-in high performance GPS unit with Auto Clock Setting
- ▼ Wide-band and multi-mode reception
- ▼ 1.74" (240 x 180 pixel) Transflective color TFT display
- ▼ IF Filtering for improved SSB/CW/AM reception
- ▼ High performance DSP-based audio processing & voice recording
- ▼ Compliant with Bluetooth, microSD & Micro-USB standards
- ▼ External Decode function (PC Decode 12kHz IF Output, BW:15 kHz)
- ▼ Free software for Memory and Frequency Control Program
- ▼ Data Import / Export (Digital Repeater List, Call sign, Memory Channel)
- ▼ Four TX Power selections (5/2/0.5/0.05 W)
- ▼ Dust and Water resistant IP54/55 standards

APRS (The Automatic Packet Reporting System) is a registered American trademark of WB4APR (Mr. Bob Bruninga). D-Star is a digital radio protocol developed by JARL (Japan Amateur Radio League).

KENWOOD

Customer Support/Distribution Customer Support:
(310) 639-4200 Fax: (310) 537-8235


www.kenwood.com/usa



ADS#29016

QEX (ISSN: 0886-8093) is published bimonthly in January, March, May, July, September, and November by the American Radio Relay League, 225 Main Street, Newington, CT 06111-1494. Periodicals postage paid at Hartford, CT and at additional mailing offices.

POSTMASTER: Send address changes to: QEX, 225 Main St, Newington, CT 06111-1494 Issue No 301

Publisher
American Radio Relay League

Kazimierz "Kai" Siwiak, KE4PT
Editor

Lori Weinberg, KB1EIB
Assistant Editor

Zack Lau, W1VT
Ray Mack, W5IFS
Contributing Editors

Production Department

Steve Ford, WB8IMY
Publications Manager

Michelle Bloom, WB1ENT
Production Supervisor

Sue Fagan, KB1OKW
Graphic Design Supervisor

David Pingree, N1NAS
Senior Technical Illustrator

Brian Washing
Technical Illustrator

Advertising Information Contact:

Janet L. Rocco, W1JLR
Business Services
860-594-0203 – Direct
800-243-7768 – ARRL
860-594-4285 – Fax

Circulation Department

Cathy Stepina, QEX Circulation

Offices

225 Main St, Newington, CT 06111-1494 USA
Telephone: 860-594-0200
Fax: 860-594-0259 (24 hour direct line)
e-mail: qex@arrl.org

Subscription rate for 6 issues:

In the US: \$29;

US by First Class Mail: \$40;

International and Canada by Airmail: \$35

Members are asked to include their membership control number or a label from their QST when applying.

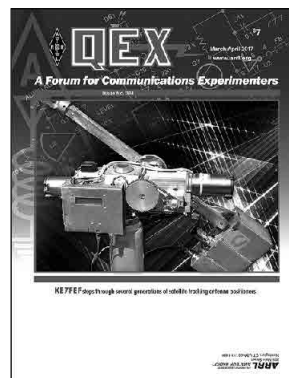
In order to ensure prompt delivery, we ask that you periodically check the address information on your mailing label. If you find any inaccuracies, please contact the Circulation Department immediately. Thank you for your assistance.



Copyright © 2017 by the American Radio Relay League Inc. For permission to quote or reprint material from QEX or any ARRL publication, send a written request including the issue date (or book title), article, page numbers and a description of where you intend to use the reprinted material. Send the request to the office of the Publications Manager (permission@arrl.org).

About the Cover

Bob Harbour, KE7FEF, takes us through his experiences with rotator mechanical designs for positioning antennas to track satellites. This third generation prototype uses belts, cables and boards on the outside of the enclosure.



In This Issue

Features

- 2 Perspectives**
Kazimierz "Kai" Siwiak, KE4PT
- 3 The Polar Explorer**
Brian Machesney, K1LI and Tony Brock-Fisher, K1KP
- 10 The Antenna Equivalent Radius: A Model for Non-Circular Conductors**
David M. Drumheller, K3WQ
- 15 Lessons Learned From Four Generations of Satellite Tracking Rotator Designs**
Bob Harbour, KE7FEF
- 19 Getting Started with DMR and DSDPlus**
Andrew Milluzzi, KK4LWR
- 24 Using FDMA in HF Multimedia Modes**
Rick Peterson, WA6NUT
- 31 An Improved Audio-Frequency Bandpass Filter for Morse Code Reception**
James L. Tonne, W4ENE
- 36 Apparatus for RF Measurements**
Bruce Pontius, N0ADL and Kazimierz "Kai" Siwiak, KE4PT
- 41 Letters to the Editor**
- 42 Upcoming Conferences**

Index of Advertisers

ARRL.....	43, 44, Cover III, Cover IV
DX Engineering:.....	23
Kenwood Communications:.....	Cover II
Nemal Electronics International, Inc:.....	18
RF Parts:.....	39, 41
Tucson Amateur Packet Radio:.....	9

The American Radio Relay League

The American Radio Relay League, Inc. is a noncommercial association of radio amateurs, organized for the promotion of interest in Amateur Radio communication and experimentation, for the establishment of networks to provide communications in the event of disasters or other emergencies, for the advancement of the radio art and of the public welfare, for the representation of the radio amateur in legislative matters, and for the maintenance of fraternalism and a high standard of conduct.



ARRL is an incorporated association without capital stock chartered under the laws of the state of Connecticut, and is an exempt organization under Section 501(c)(3) of the Internal Revenue Code of 1986. Its affairs are governed by a Board of Directors, whose voting members are elected every three years by the general membership. The officers are elected or appointed by the Directors. The League is noncommercial, and no one who could gain financially from the shaping of its affairs is eligible for membership on its Board.

"Of, by, and for the radio amateur," ARRL numbers within its ranks the vast majority of active amateurs in the nation and has a proud history of achievement as the standard-bearer in amateur affairs.

A *bona fide* interest in Amateur Radio is the only essential qualification of membership; an Amateur Radio license is not a prerequisite, although full voting membership is granted only to licensed amateurs in the US.

Membership inquiries and general correspondence should be addressed to the administrative headquarters:

ARRL
225 Main Street
Newington, CT 06111 USA
Telephone: 860-594-0200
FAX: 860-594-0259 (24-hour direct line)

Officers

President: Rick Roderick, K5UR
PO Box 1463, Little Rock, AR 72203

Chief Executive Officer: Tom Gallagher, NY2RF

The purpose of *QEX* is to:

- 1) provide a medium for the exchange of ideas and information among Amateur Radio experimenters,
- 2) document advanced technical work in the Amateur Radio field, and
- 3) support efforts to advance the state of the Amateur Radio art.

All correspondence concerning *QEX* should be addressed to the American Radio Relay League, 225 Main Street, Newington, CT 06111 USA. Envelopes containing manuscripts and letters for publication in *QEX* should be marked Editor, *QEX*.

Both theoretical and practical technical articles are welcomed. Manuscripts should be submitted in word-processor format, if possible. We can redraw any figures as long as their content is clear. Photos should be glossy, color or black-and-white prints of at least the size they are to appear in *QEX* or high-resolution digital images (300 dots per inch or higher at the printed size). Further information for authors can be found on the Web at www.arrl.org/qex/ or by e-mail to qex@arrl.org.

Any opinions expressed in *QEX* are those of the authors, not necessarily those of the Editor or the League. While we strive to ensure all material is technically correct, authors are expected to defend their own assertions. Products mentioned are included for your information only; no endorsement is implied. Readers are cautioned to verify the availability of products before sending money to vendors.

Kazimierz "Kai" Siwiak, KE4PT

Perspectives

In this Issue

Our intent in *QEX* is to cover a wide range of technologies in each issue. Herein, the technologies span using arbitrary cross-section conductors for antenna elements, FDMA modulation techniques, polar modulation, satellite tracking positioners, a digital voice tutorial, CW filters, and a low cost RF measurement apparatus.

David M. Drumheller, K3WQ, explains how to model antennas made from angle stock, wires cages, tape measures and other unconventional conductors; Rick Peterson, WA6NUT, shows how FDMA technology can be used for new sound card modes; Brian Machesney, K1LI, and Tony Brock-Fisher, K1KP, use polar modulation to implement a linear amplifier; Bob Harbour, KE7FEF, takes us through several iterations of antenna positioners for tracking satellites; Andrew Milluzzi, KK4LWR, introduces digital voice modulations with this simple tutorial; James L. Tonne, W4ENE, explains how to make better sounding add-on audio filters for the CW operator; and Bruce Pontius, NØADL and Kai Siwiak, KE4PT, describe an inexpensive apparatus for very low level RF and digital signal measurements.

Please continue to support *QEX*, and help it remain a strong technical publication. Help determine the content of future *QEX* issues by putting your favorite topic or innovative measurement on paper. Share it on these pages with fellow readers. Just follow the details on the www.arrl.org/qex-author-guide web page, and contact us at qex@arrl.org or via US Mail to *QEX*, ARRL HQ, 225 Main St, Newington, CT 06111. We value your feedback, comments and opinions about these pages.

73,

Kazimierz "Kai" Siwiak, KE4PT

Editor

Dr. Ulrich Rohde, N1UL, Recognized for Pioneering Work on SDR

Dr. Ulrich L. Rohde, N1UL, of Synergy Microwave Corp. was invited to give the *6th Sir J C Bose Memorial Lecture* at IEEE Hyderabad Section on Dec 2, 2016 in Hyderabad, India. This was a joint session of the IEEE MTT, AP and EMC Societies. Dr. Rohde delivered the talk entitled, "Next Generation Networks: Software Defined Radio – Emerging Trends." While working at RCA in 1982, Dr. Rohde's department developed the first SDR with the COSMAC (Complementary Symmetry Monolithic Array Computer) chip working under a DoD contract. The RCA CDP1802, a 40-pin LSI integrated circuit chip, is an 8-bit CMOS microprocessor introduced by RCA in early 1976 and was the company's first single-chip microprocessor. Dr. Rohde was one of the first to present publically on this topic when he gave a talk entitled, "Digital HF Radio: A Sampling of Techniques" at the Third International Conference on HF Communication Systems and Techniques, London, England, February 26-28, 1985.

The lecture is named in honor of Sir Jagadish Chandra Bose, a Bengali scientist and expert in math, physics, biology, and archaeology who lived in British India. He pioneered the investigation of radio and microwave optics, made significant contributions to plant science, and laid the foundations of experimental science doing most of his work in during the late 1800's and early 1900's. Sir J.C. Bose did much of his original scientific work in the area of microwaves. He was the first to use a semiconductor junction to detect radio waves. The IEEE named him one of the fathers of radio science. [Source: Microwave Journal, www.microwavejournal.com.]

The Polar Explorer

You may never look at your “linear amplifier” the same way again.

If you're like me, you have a love/hate relationship with your linear amplifier. While this piece of “big iron” has cranked out the legal limit for almost 20 years, it also presents some significant challenges. It seems to take forever to warm up — especially when sitting down to work an all-time new one! Because of the size and weight, it occupies its own piece of reinforced furniture in the shack. I have to keep it within easy reach because it doesn't tune automatically. New tubes are not available, so the dwindling supply of matched pairs on the “new old stock” (NOS) market is driving up the price, even though they aren't guaranteed to last. Rather than simply spending several thousand dollars to replace this venerable sidekick of my 100 W transceiver, I decided to explore the feasibility of using a technique called *polar modulation* to reduce the size, weight and cost of a legal-limit ham transmitter, hence the moniker, “Polar Explorer.”

The Cost of RF Power

The high cost of high power is rooted in the evolution of ham radio technology and equipment. Figure 1A shows the traditional modulation process of a high-power output stage operating at the carrier frequency with the modulation process at the high power output stage. Figure 1B shows the single sideband modulation process moved away from that high-power output stage back to an intermediate frequency (IF) operating at a very low power level. SSB signals generated at less than one watt at the IF are heterodyned to the carrier frequency and passed through three or more stages of amplification to reach levels useful for reliable communication over long distances with average antennas. Unlike CW and AM, SSB and other quadrature

amplitude modulated signals must undergo a relatively inefficient *linear* amplification to increase signal levels without distortion. To balance cost and performance, slightly nonlinear Class AB amplifiers¹ are often used, requiring low-pass filters between stages to remove harmonic distortion products, and adding cost to the transmitter without adding value to the signal.

Since the VFO and IF circuitry — including the expensive electromechanical sideband filter — can be shared between the transmit and receive, manufacturers increasingly combined the formerly separate receiver and transmitter into a single “transceiver” to keep equipment prices within reach of the ham population. But,

Efficiency and Amplifier Classes

Amplifiers traditionally employed in amateur RF amplifiers - classes A, AB, B and C - operate the active device in its linear region for some part of the RF cycle. This means that there is voltage across the device while there is current flowing through the device, resulting in power dissipation in the device. By contrast, amplifier in the switch-mode classes D, E, F and their variants [superscript 9-11] switch the active device between cutoff - zero current through the device - and saturation - zero voltage across the device. Switching amplifiers minimize power dissipated in the active device by minimizing the overlap of the periods of nonzero current and nonzero voltage, resulting in higher efficiency. The output networks of the switching amplifier classes are designed to optimize this behavior.

this marriage of convenience came at a price. Transmitter improvements have been largely outpaced by receiver improvements, as advances in silicon technology integration spawned digital integrated circuits that supplanted analog circuits in a number of performance-critical roles.

A “pay as you go” power upgrade path was provided in what came to be known as a “linear amplifier” to augment the comparatively low output power of an affordable SSB transceiver. Because more efficient nonlinear amplifiers cannot be used to amplify SSB signals, about 40% more dc power needs to be provided to the “linear” amplifier to produce the same output power as a Class-C amplifier of a CW or AM transmitter.

As the convenience of no-tune solid-state amplifier technology displaced vacuum tube circuits, the single high-Q band-switched tank circuit gave way to a switched bank of five or six low-pass filters to control spurious emissions. Each filter section requires several custom-wound inductors and ceramic capacitors that can sustain high RF currents, once again adding cost without adding value to the signal.

In today's era of concern over energy efficiency, it's easy to lose track of the fact that a significant fraction of the total cost of an RF power amplifier is driven by the need to generate nearly twice as much dc power as the RF power that will be sent up the transmission line, and the need to dissipate the difference. This inefficiency also requires RF transistors to be made with exotic insulating materials that can survive high energy densities, plus high-conductivity heat sinks and fans to remove the heat produced by the dissipated power.

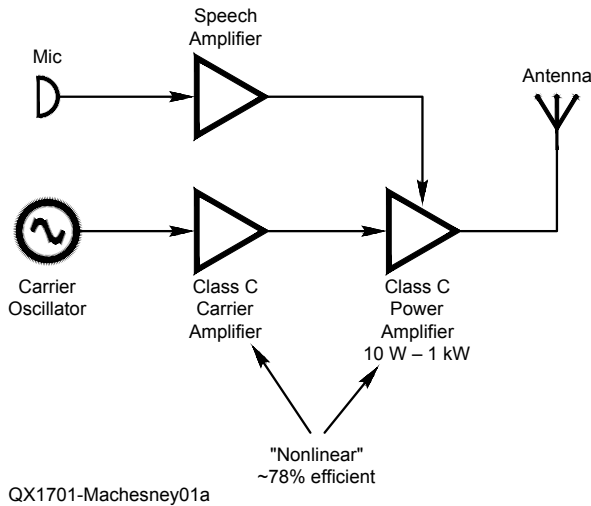


Figure 1A — AM transmission was accomplished by directly modulating a relatively efficient, high-power Class C output stage.

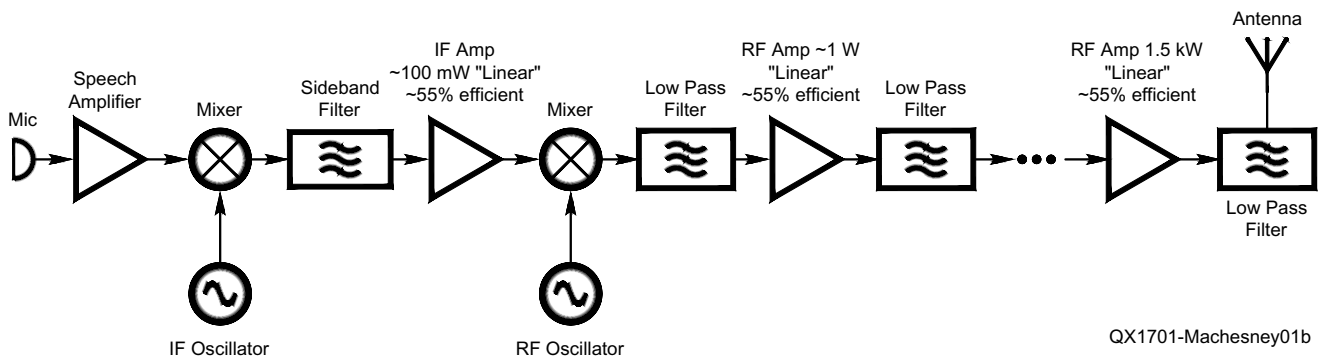


Figure 1B — The filter approach to SSB transmission generates a low-power waveform at an IF and heterodynes the waveform to the transmitting frequency, achieving high power levels through a series of relatively inefficient linear amplifiers.

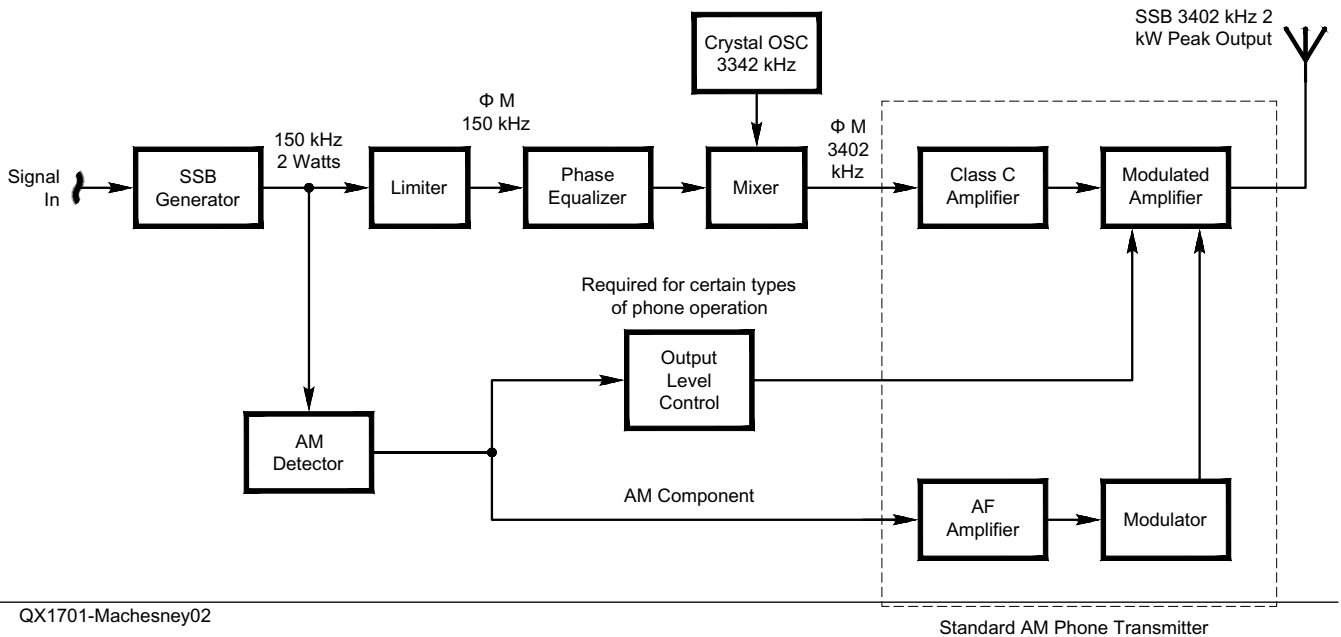


Figure 2 — A block diagram of the Kahn EER system to generate SSB.

A High Efficiency Amplifier Approach

The weaknesses in the arguments favoring SSB were not lost on RF practitioners of the day. In 1952, Leonard Kahn published a technical paper explaining how to make SSB transmissions by envelope elimination and restoration.² As shown in Figure 2, Kahn separated the amplitude and phase components of a low-level SSB signal, then amplified and applied the components to a more-efficient conventional Class-C AM transmitter, reproducing the original SSB signal at higher power. David Cripe, NMØS, used this approach in his award winning 5 W to 50 W 40-meter SSB amplifier costing just \$32.³ His secret was to use short lengths of copper wire as a heat sinks for his amplifier. Because the high efficiency amplifier dissipated very little power, very little heat needed to be removed.

Advances in semiconductor technology introduce opportunities to modernize Kahn's approach. As shown in Figure 3, a digital signal processor (DSP) chip can generate the envelope signal, which is then amplified with a high-efficiency circuit similar to the audio amplifier in modern entertainment equipment. Likewise, a DSP can generate the phase modulation signal at a baseband frequency, followed by a quadrature digital upconverter (QDUC) that numerically heterodynes it to the carrier frequency.

By generating the envelope- and phase-modulation signals numerically, rather than separating them from an existing SSB signal, it is reasonable to anticipate improvements in output signal quality.

In this hybrid approach to Kahn's architecture, the number of inter-stage low pass filters can be dramatically reduced to cut cost. The substantially lower power

dissipation resulting from use of a high efficiency switch-mode power amplifier operated in Class D, E or F allows the use of inexpensive transistors in plastic packages intended for other high-volume markets. The same is true for the modulator and power supply, cutting the size, weight and cost of heat sinks and fans for thermal management. It may soon be possible for transmitter

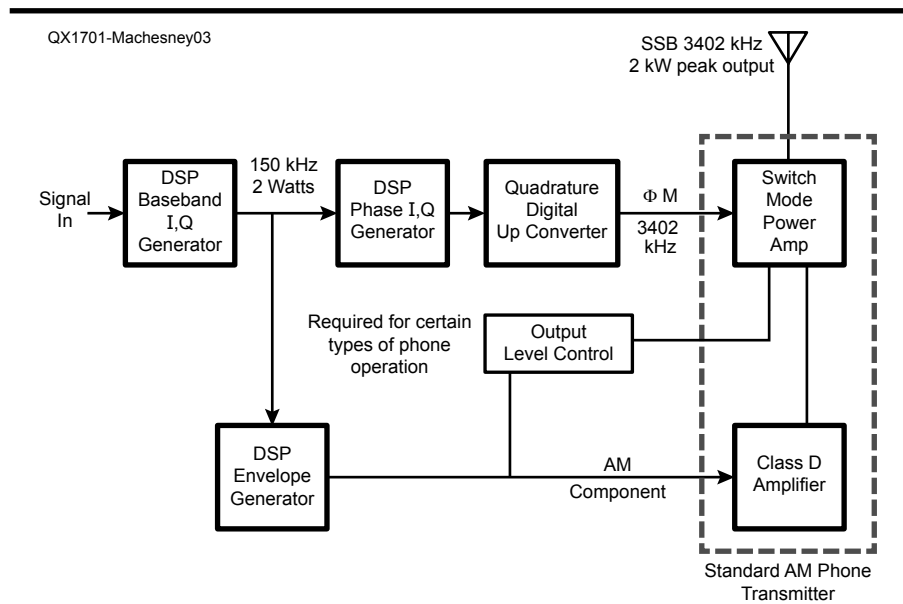


Figure 3 — Direct generation of envelope and phase signals using modern silicon devices.

Quadrature Digital Upconverter

As shown in the functional block diagram of the Analog Devices AD9957 in Figure A, a QDUC converts baseband digital I and Q signals to an analog signal at a carrier output frequency.

Normalizing the I and Q inputs to the envelope amplitude results in an analog output from the QDUC, which has the constant peak amplitude required by the phase-modulation input of Polar Explorer Class E amplifier. The digital outputs of the numerically controlled oscillators (NCO) represent the sine and cosine values of a carrier at the programmed frequency. The QDUC combines the results from a pair of high-speed digital multipliers, which heterodynes interpolated up-samples of the input, then converts the result to analog. By choosing whether the combining of I and Q is additive or subtractive, the output signal is upper sideband (USB) or lower sideband (LSB).

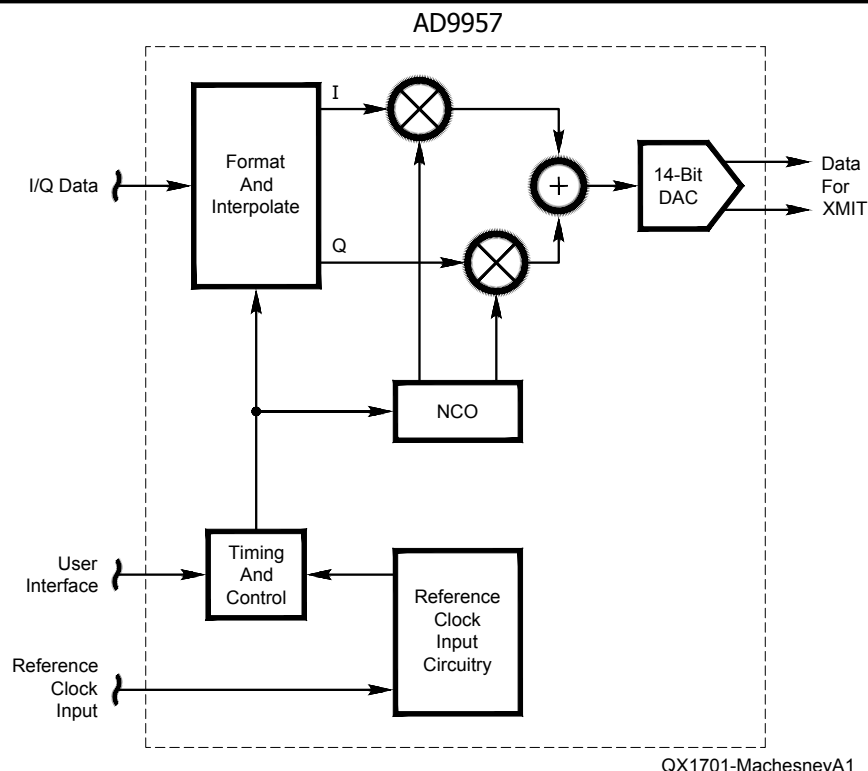


Figure A — Functional block diagram of the Analog Devices AD9957.

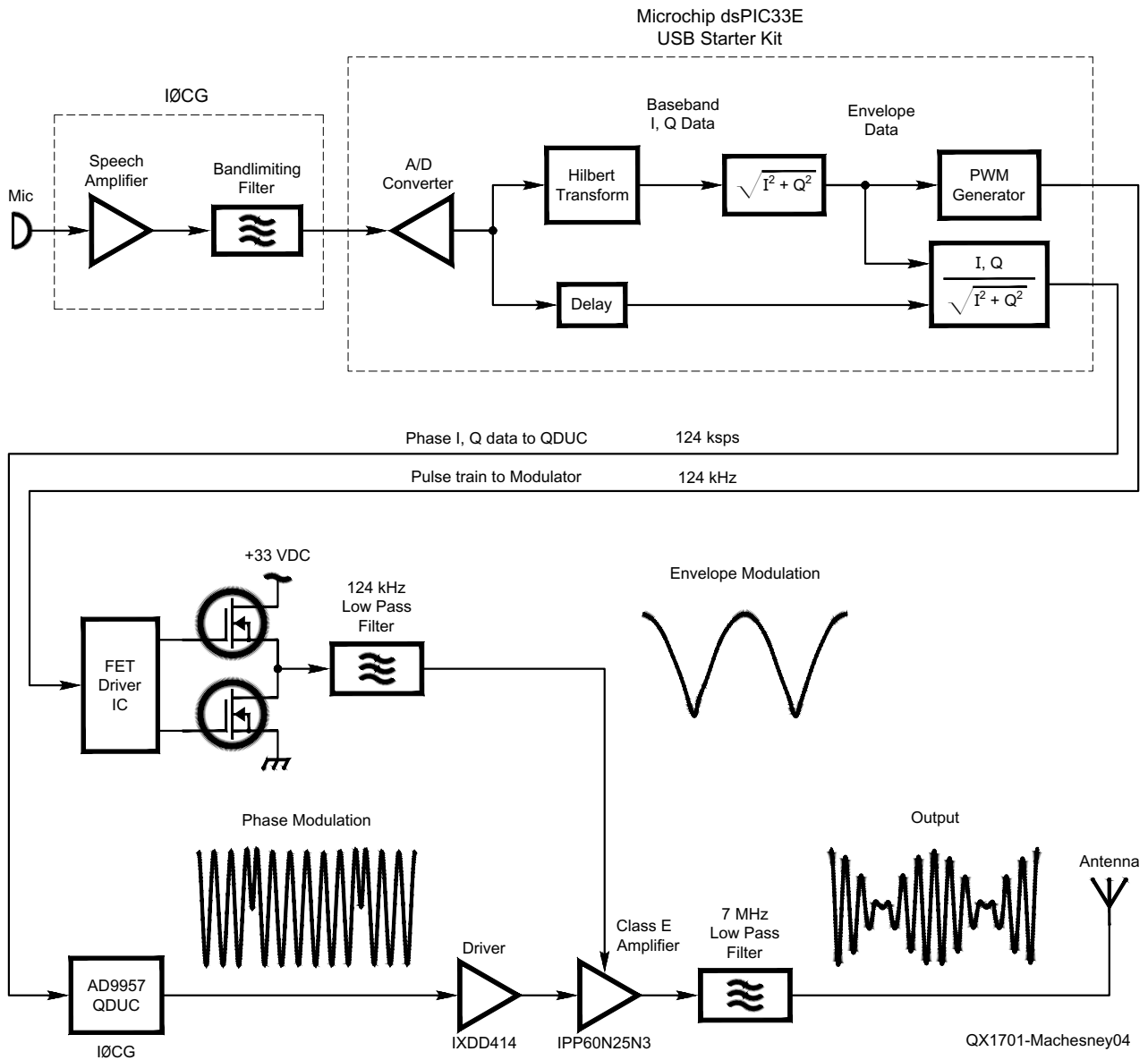


Figure 4 — The polar explorer block diagram.

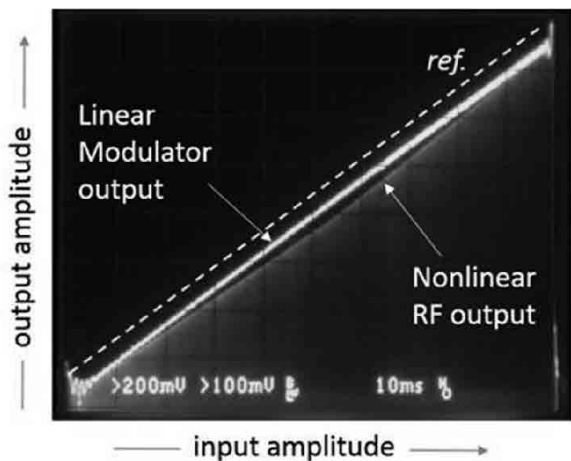


Figure 5A — The uncompensated power amplifier gain sags by about 5% in the middle of its range.

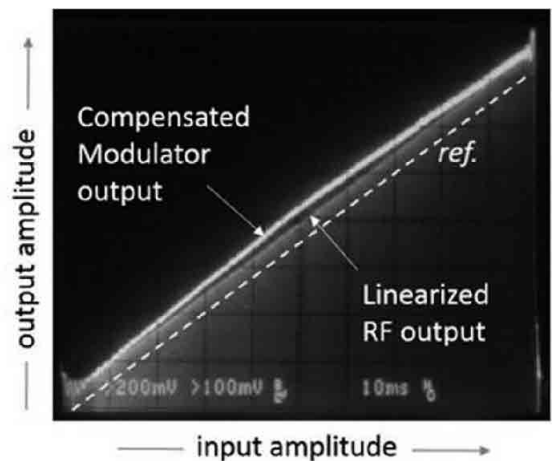


Figure 5B — Linearized power amplifier RF output.

technology improvements to catch up with receivers. Together with the recent influx of highly capable “software defined radios” (SDR), the flexibility of separate units will be restored. See *Sidebar-1: Efficiency and Amplifier Classes*.

Polar Modulation Basics

First dubbed “quadruplex telegraph,” what we now call polar modulation was invented by Thomas Edison in 1874 as a means of allowing the simultaneous transmission of four telegraph signals on a single wire. Single sideband is a special case of quadrature modulation, whereby the quadrature (Q) component of the signal is derived from the in-phase (I) component by the mathematical operation of a Hilbert transform.⁴ Applying the trigonometry of a right triangle, the amplitude of the signal is the square root of the sum of the squares of the I and Q components of the SSB signal, while the phase angle is derived from their ratio. These and other calculations take advantage of the unique architecture of a DSP to develop the baseband envelope and phase modulating signals at very low cost.

As seen in Figure 3, the phase modulation to the switch-mode power amplifier must operate at the RF carrier frequency. The baseband phase modulation is heterodyned to this frequency by a quadrature digital up-converter (QDUC). Whereas the QDUC would produce SSB from the baseband I and Q signals, polar modulation requires a phase modulation signal of constant amplitude. This is accomplished by dividing each I and Q value by the corresponding envelope value before sending to the QDUC.

The Hardware

It was time to bring Kahn’s approach to the 21st century of Amateur Radio. I invited Tony Brock-Fisher, K1KP, to partner with me on the development of Polar Explorer, a platform for experimentation with polar modulation and switching amplifiers. Figure 4 shows its ‘building block’ circuit boards, some of which we designed and others that we obtained elsewhere. Giuliano Carmignani, IØCG, kindly supplied us with bare circuit boards from his software defined transmitter project.⁵ One of his boards amplifies and band-pass filters the incoming audio, which is then sampled at 15.5 kilo-samples per second (ksps) by the 12-bit A/D converter on a Microchip dsPIC33E USB Starter kit.

The dsPIC applies a Hilbert transform to the sampled audio, producing the baseband analytic I and Q signal pair, then computes the envelope and the I and Q pairs for the phase modulation signals. Interpolation filters in the dsPIC up-sample the phase and envelope signals to 124 ksps. The phase modulation I and Q data is sent to another IØCG board, which uses an Analog

Devices AD9957 QDUC chip to numerically heterodyne the phase modulation signal to the RF carrier frequency and convert it to analog with an on-chip D/A converter. See *Sidebar-2 Quadrature Digital Upconverter*. The output of the AD9957 is amplified and applied to the gate input of the Class E switching amplifier.

The dsPIC also converts the envelope signal to a 124 kHz pulse width modulated (PWM) wave train with 8 ns resolution. This digital signal is sent to a Class D switching modulator and low-pass filter that removes the 124 kHz component and passes baseband audio. The 33 V (peak) modulated drain voltage for the Class E switching amplifier produces peak RF output of about 55 W.

The Numbers

As described earlier, the audio information sampled at 15.5 ksps is used by the DSP to calculate the phase modulation I and Q data. Those I and Q pairs are up-sampled by a factor of 8 to produce interpolated phase modulation data for the AD9957 QDUC at 124 ksps. The programmable QDUC hardware up-samples the phase modulation data a further factor of 1008, to 125 MHz. Why all this up-sampling? Because the final rate, in this case 125 MHz, determines the spacing between the spurious replicas (aliases) of the input data that result from the sampling process. This high sample rate pushes the spurs outside the pass bands of the low-pass filters used between the amplifier output and the antenna.

The goals of the project include generating legal-limit output power as cleanly, efficiently and cheaply as possible. Modern receivers combine advanced digital and analog design to achieve very high performance with regards to receiver intermodulation distortion (IMD). Rob Sherwood, NCØB, has documented extensive measurements of this parameter across a large number of commercial transceivers.⁶ He estimates that a receiver operating in a band crowded with strong signals needs to have at least 80 dB of close-in (2 kHz) IMD dynamic range for CW, but only 70 dB for SSB.

Sherwood observes that contemporary transceivers have so much IMD on their *transmitted* signals that the ultimate performance of our equipment is limited by our transmitters, not our receivers.

While receivers have made giant strides in performance over the past three decades, transmitters, in particular the power output stages, have not fundamentally changed or improved since the 1970s.

Prototype Results

The goal of the first Polar Explorer prototype was to produce 100 W with low transmitted IMD on any HF Amateur

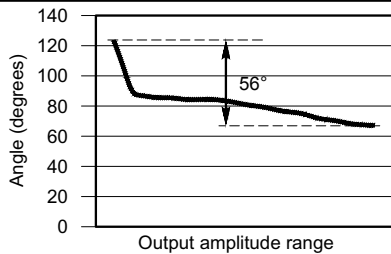
Radio frequency up to 30 MHz. While it served as an excellent platform for experimentation, we quickly discovered some design shortcomings. Contrary to the performance of its SPICE simulation model, the IXDD614 driver chip for the PA MOSFET did not work above 14 MHz. Once we had Polar Explorer working on 40 meter SSB, we made a few contacts and received welcome compliments on how good it sounded! We tried many different approaches to the software calculations and the hardware implementation, and learned a tremendous amount about changes for future revisions.

We measured output power directly with a Telepost LP-100A watt meter. PA input power was calculated by multiplying the modulator output voltage by the current measured through a 0.5 Ω resistor inserted between the modulator and the drain of the Class E PA MOSFET. Dividing the output power by the input power, we routinely observed efficiencies above 90%. The highest efficiency we observed was a staggering 97%! The temperature of the output device and its heat sink barely rose above room ambient temperature. Compare that to what you would expect to feel if you touched a 40 W incandescent light bulb, which dissipates about the same amount of heat you would expect from a Class AB amplifier producing 55 W.

The situation was not so rosy for the quality of the transmitted signal. Using SpectrumLab software⁷ and a sound card generator, the ARRL standard 700 Hz and 1900 Hz tones⁸ were injected at the Polar Explorer audio input. Intermodulation distortion products were measured by tuning an Icom 756Pro2, with 3000 Hz DSP filter and with AGC disabled, to an attenuated sample of the RF output. Receiver audio was routed back to the sound card input and analyzed with SpectrumLab.

Initially, the third-order IMD product was just 24 dB down from peak output, considerably worse than nearly all contemporary ham transceivers. After some research into the literature on the subject, we analyzed the system amplitude and phase distortions in search of improvement.

Figure 5A shows that the uncompensated PA gain sags by about 5% in the middle of its range. In Figure 5B the compensated PA has a linearized output. Figure 6 shows that the uncompensated PA phase varies by 56 degrees across the output range. We incorporated an Analog Devices AD8302 gain and phase detector chip into the circuitry to provide a means of correcting these errors. This chip compares the input and output of the PA to provide error measurements to the DSP. On command, the DSP programs the RF output to span across 60 discrete amplifier levels and records the exact gain and phase



QX1701-Machesney06

Figure 6 — The uncompensated power amplifier input vs. output phase varies by 56 degrees across the output range.

response of the PA. These recorded values are then used to pre-distort the gain and phase of the signals being applied to the PA. The phase correction is applied to the data sent to the AD9957, and the gain correction is applied to the signal sent to the pulse-width modulator.

The effects of these corrections on transmitted IMD were very interesting. Applying the gain correction by itself made a barely perceptible improvement, while applying the phase correction by itself reduced third-order IMD by over 12 dB. Applying the gain and phase corrections together made a significant additional improvement of 3 dB. Further refinements in the correction data of the prototype shown in Figure 8 led to the competitive final value of 39 dB down, relative to peak output, shown in Figure 7.

Further Work

We plan to continue our explorations of polar modulation and we encourage others to take up the quest. Our next revision aims to achieve the original goals of producing 100 W at up to 30 MHz, including the ability to band switch the PA output filter. Our ultimate goal is to produce 1500 W output with a single RF output stage and a single set of RF low-pass filters, thus realizing our dream of a cleaner, cheaper, smaller, lighter and quieter legal-limit Amateur Radio transmitter.

Brian Machesney, K1LI, was first licensed at the age of 10. His interest in ham radio was kindled by reading his father's (Ward, K1DXB, SK) back issues of QST throughout the 1950s and 1960s. After graduating from Rensselaer Polytechnic Institute with a BSEE in 1979, he spent more than three decades in both the R&D and business aspects of the semiconductor industry, where he was awarded 14 US patents. Brian has recently turned his radio fascination from DXing and contesting to technical projects that he hopes will address important challenges faced by many hams around the world.

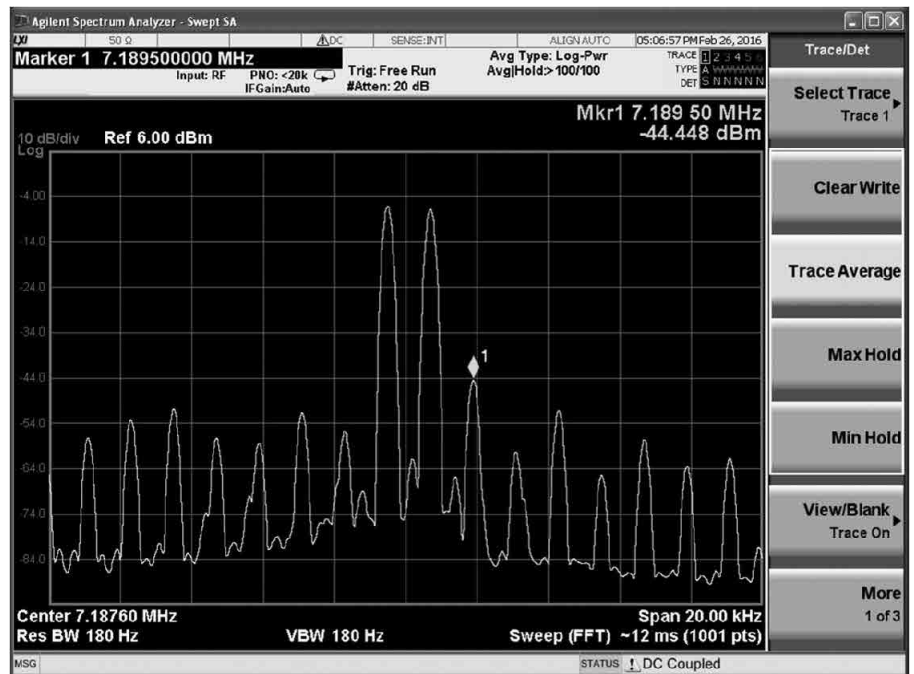


Figure 7 — Polar Explorer transmitted spectrum.

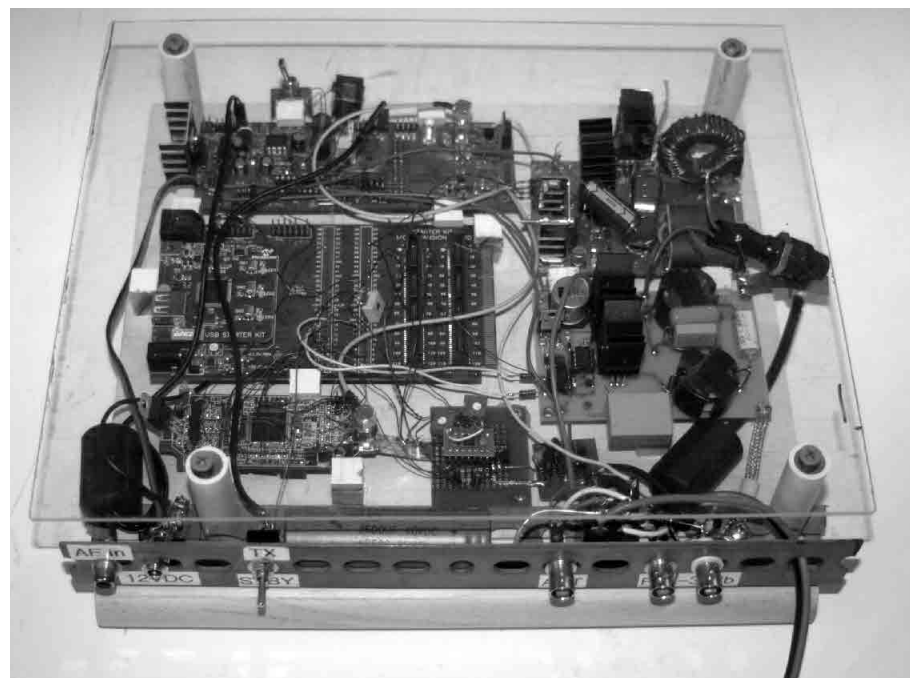


Figure 8 — Polar Explorer prototype hardware.

Tony Brock-Fisher, K1KP, was originally licensed in 1967 as WA1IKP and upgraded to Amateur Extra class license in 1976. He has a BS in Physics and an MS in Ocean Engineering. Tony retired from Philips Electronics in 2013 following a 35 year career in medical ultrasound design. He currently serves as president of Yankee Clipper Contest Club. Tony enjoys contesting, DX, and station construction projects, as well as writing for QST!

Notes

¹Amplifier classes are discussed in the "Types of Power Amplifiers" section of the Transmitters and Transceivers chapter of the ARRL Handbook for Radio Communications, 2017, ARRL item no. 0628, available from your ARRL dealer, or from the ARRL Store, Telephone toll-free in the US 888-277-5289, or 860-594-0355, fax 860-594-0303; www.arrl.org/shop; pubsales@arrl.org.

²L. R. Kahn, "Single-Sideband Transmission

by Envelope Elimination and Restoration”, Proceedings of the IRE, 1952, Vol. 40, Issue 7, pp 803-806.

³D. Cripe, NMØS, “Homebrew Challenge II Co-Winner — The Lowest Cost Entry”, *QST*, Oct 2010, pp 37-41.

⁴For a complete discussion of analytic signals, see the chapter on DSP and Software Design in the *ARRL Handbook for Radio Communications, 2017*.

⁵www.i0cg.com/ad9957_dds.htm.

⁶Sherwood Engineering Inc., www.sherweng.com.

⁷DL4YHF Amateur Radio Software: Audio Spectrum Analyzer (Spectrum Lab), www.qsl.net/dl4yh/spectra1.html.

⁸Bob Allison *et al.*, ARRL “Test Procedures Manual,” Rev. L (2011), www.arrl.org/files/file/Technology/Procedure%20Manual%202011%20with%20page%20breaks.pdf.

⁹F. H. Raab, W1FR, “High efficiency RF power amplifiers”, *Ham Radio*, Oct 1974, pp 829.

¹⁰F. H. Raab, “Power-conserving drive-modulation method for envelope-elimination-and-restoration (EER) transmitters”, U.S. Patent 6,256,482, July 3, 2001.

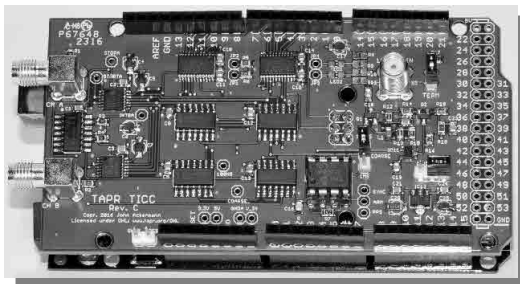
¹¹F. H. Raab, W1FR, M. F. Gladu, N1FBZ, and D. J. Rupp, “Complementary class-D power amplifier for LF and MF”, *QEX*, Mar/Apr 2006, pp 9-13.



20M-WSPR-Pi is a 20M TX Shield for the Raspberry Pi. Set up your own 20M WSPR beacon transmitter and monitor propagation from your station on the wspn.net web site. The TAPR 20M-WSPR-Pi turns virtually any Raspberry Pi computer board into a 20M QRP beacon transmitter. Compatible with versions 1, 2, 3 and even the Raspberry Pi Zero!

TAPR is a non-profit amateur radio organization that develops new communications technology, provides useful/affordable hardware, and promotes the advancement of the amateur art through publications, meetings, and standards. Membership includes an e-subscription to the *TAPR Packet Status Register* quarterly newsletter, which provides up-to-date news and user/technical information. Annual membership costs \$25 worldwide. Visit www.tapr.org for more information.

NEW!



TICC

High-resolution 2-channel Counter

The **TICC** is a two channel counter that can time events with 60 *picosecond* resolution. It works with an Arduino Mega 2560 processor board and open source software. Think of the most precise stopwatch you've ever seen, and you can imagine how the TICC might be used. The TICC will be available from TAPR in early 2017 as an assembled and tested board with Arduino processor board and software included.



TAPR

PO BOX 852754 • Richardson, Texas • 75085-2754

Office: (972) 671-8277 • e-mail: taproffice@tapr.org

Internet: www.tapr.org • Non-Profit Research and Development Corporation

The Antenna Equivalent Radius: A Model for Non-Circular Conductors

K3WQ explains how to model antennas made from angle stock, wires cages, tape measures and other unconventional conductors.

Antennas, sometimes by necessity, are not always constructed from circular conductors. Vertical radiators for medium frequency operation are often constructed from tower sections that may be modeled as either triangular or square radiators. Antennas for VHF or higher frequencies can be conveniently constructed from bar stock, not all of which have circular cross-sections, or segments of a tape measure, as on satellites or portable Yagi antennas, which are nearly flat. This complicates the design and analysis of such antennas through computer modeling because widely available software, much of it based on the Numerical Electromagnetics Code (NEC), models radiating elements as circular conductors. Fortunately, the software can provide realistic results by using an “antenna equivalent radius” for a non-circular antenna element. But with the exception of a few widely published cases, such as square or triangular conductors, there is little guidance on how to do this.¹

This article presents formulas for computing the antenna equivalent radius for several non-circular single- and multi-conductor cross-sections. Some will apply to the construction of antennas from common bar stock (e.g. angle stock), others to the construction of cage antennas with multiple circular wires. Some formulas are in closed form, but detailed calculus-based derivations are not presented in this article — these will be provided by the author upon request. Others were found through numerical integration and curve fitting.

Background

The antenna equivalent radius may

be defined through quasi-magnetostatics, resulting in a problem that only concerns a conductor’s two-dimensional cross section.² Assuming a conductor is infinitely long, that the dimensions of its non-circular cross section are small compared to the wavelength, and electric current is confined to its surface (because of the skin effect) and is uniformly distributed around its circumference (a simplification), the conductor’s equivalent radius is derived by equating the average magnetic potential at its surface with that of a circular conductor. Expressed in logarithmic form, the result is:

$$\ln(r_e) = \frac{\oint_{\ell} \oint_{\ell} \ln|x-y| dx dy}{L^2} \quad [1]$$

where ℓ denotes the conductor circumference that is of length L , \mathbf{x} and \mathbf{y} are vectors locating points along the circumference, and dx and dy are differential segments along the circumference.³ The formula is consistent: (1) if a conductor cross-section is scaled by a positive constant, the equivalent radius is scaled by that same constant; and (2) the equivalent radius of a circular conductor of geometric radius R is simply

$$r_e = R. \quad [2]$$

Non-Circular Antenna Elements

As in the case of a circular conductor, the antenna equivalent radius of a flat conductor is expressible in closed form. Defined as a conductor carrying an infinitely thin “sheet current,” its equivalent radius is

$$r_e = a e^{-3/2} \approx 0.223 a, \quad [3]$$

where a is the width of the conductor. The equivalent radii for all other single-conductor cross-sections presented here were determined through numerical integration; however, the flat conductor provided a test case for selecting an integration method and understanding its convergence with respect to integration step size.

Numerical integration of Equation 1 is straightforward. Mid-point integration is sufficient based on a partitioning of the cross-section’s circumference into integration points (mid-points) and step lengths, which may be used for both the inner and outer integral. The integrand’s singularity (where \mathbf{x} equals \mathbf{y}) may be dealt with by using it as a mid-point and approximating the contribution over the associated integration step by $\Delta(\ln(\Delta/2)-1)$ where Δ is the length of the step. If integration points are uniformly distributed along a line of length $a = 1$ in a manner yielding a constant integration step length, agreement with $e^{-3/2} = 0.22313016\dots$ to 3 and 4 decimal places is achieved with 25 and 320 integration points, respectively. The results in this section are based on numerical integration with points uniformly spaced, either linearly or angularly, along a conductor or a component thereof. Typically 500 equally spaced mid-points were used along the conductor component associated with parameter a , and the number of points on other components chosen in proportion to their lengths.

Figure 1 shows several cross-sections whose size are described by a single parameter a . Most are regular polygons with N sides (a dimensionless number). The antenna equivalent radii for these are listed in Table 1.

Note that for $N \geq 9$, it is sufficient to compute the equivalent radius by dividing the polygon's circumference by 2π , a formula recommended by the Federal Communications Commission (FCC).⁴ This is sensible, because as the

number of sides increases, the better a regular polygon approximates a circle. Numerical studies verified the utility of this formula, as it agrees with the values of equivalent radii computed through numerical integration

Table 1

Antenna equivalent radii for single-conductor cross-sections whose size and shape are described by a single parameter a . Cross-sections are shown in Figure 1.

Cross-section	Number of sides N	r_e
Flat	—	$0.223a$
Half-Circle	—	$0.327a$
Half-Round	—	$0.377a$
Triangle	3	$0.408a$
Square	4	$0.582a$
Pentagon	5	$0.751a$
Hexagon	6	$0.916a$
Heptagon	7	$1.080a$
Octagon	8	$1.234a$
N-gons	9 or more	$Na / (2\pi)$

to within 1.9 percent for $N = 9$. The error decreases as N increases.

Additional single-conductor cross-sections are shown in Figure 2. The size and shape of these are described by two parameters, a and b , which are usually associated with length (width) and height. The antenna equivalent radii for these are provided by the polynomial

$$r_e = a[\beta_0 + \beta_1(b/a) + \dots + \beta_M(b/a)^M] \quad [4]$$

and are listed in Table 2. Coefficients β_0, \dots, β_M were found by numerically evaluating Equation 1 over a range of values for b with $a = 1$, fitting a polynomial to this data using a constrained least squares algorithm, and then rounding the resulting coefficients. The constraints were applied at the upper and lower bounds for b . For $b = 0$, most cross-sections reduce to a flat conductor, constraining the antenna equivalent radius to the exact value of $e^{-3/2}$. At the upper bound of $b = a$ (or $b = a/2$ in the case of the minor circular arc), the radius was constrained to a value based on the specific geometry. For example, the ellipse becomes a circle of radius a and a rectangle reduces to a square with an equivalent radius of $0.582 a$ for $b = a$. The polynomial approximations listed in Table 2 are within 3.3 percent of the values of the equivalent radii (data) used in the least-square fits.

Of practical value is the minor circular arc because, as compared to a flat conductor, it is arguably a more suitable model for a tape measure antenna element. Typically for a tape measure $b = 0.25 a$, which yields $r_e = 0.242 a$, a value 13% higher than that for a flat conductor.

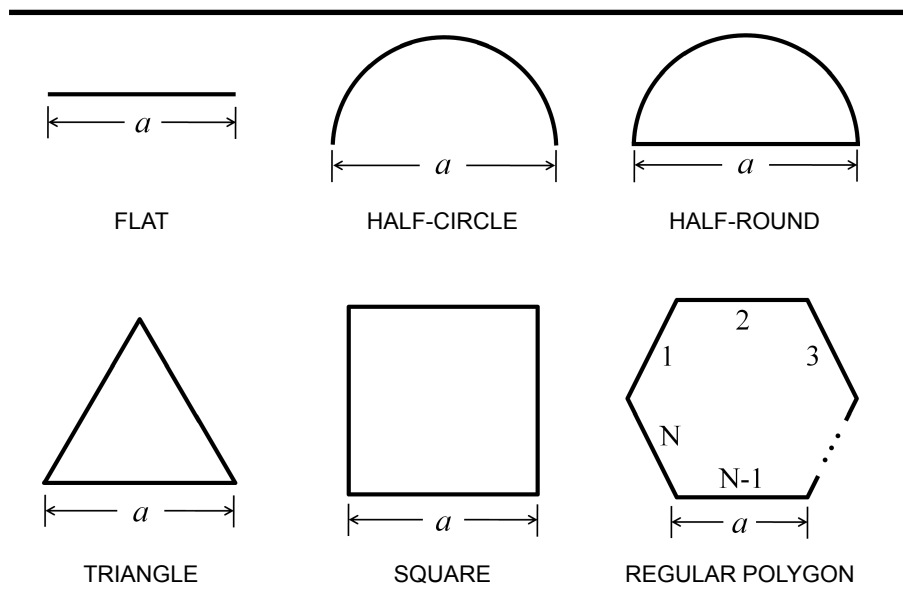


Figure 1 — Single-conductor cross-sections described by a single parameter a . Their antenna equivalent radii are listed in Table 1.

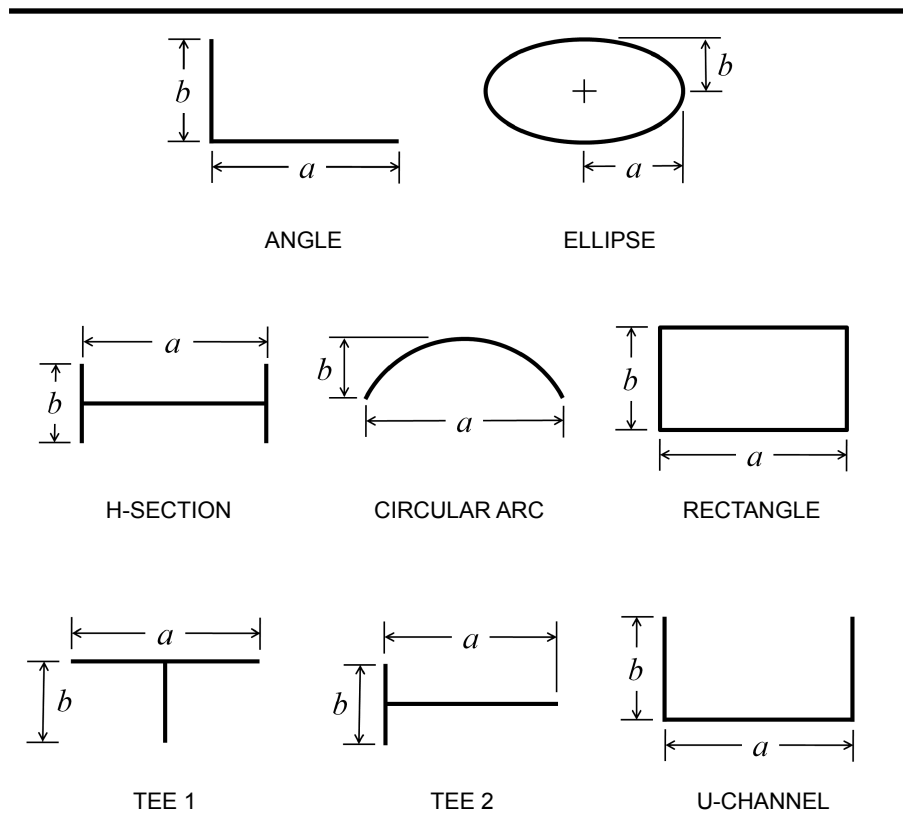


Figure 2 — Single-conductor cross-sections described by two parameters a and b . Their antenna equivalent radii are listed in Table 2.

Table 2

Antenna equivalent radii for single-conductor cross-sections whose size and shape are described by two parameters a and b . Cross-sections are shown in Figure 2.

Cross-section	r_e	Parameter Range
Angle	$0.223a + 0.170b$	$0 < b < a$
Ellipse	$a \left[0.446 + 0.617(b/a) - 0.063(b/a)^2 \right]$	$0 < b < a$
H-Section	$a \left[0.223 + 0.269(b/a) - 0.03(b/a)^2 \right]$	$0 < b < a$
Circular Arc	$a \left[0.223 + 0.029(b/a) + 0.358(b/a)^2 \right]$	$0 < b < a/2$
Rectangle	$a \left[0.223 + 0.464(b/a) - 0.105(b/a)^2 \right]$	$0 < b < a$
Tee 1	$a \left[0.223 - 0.01(b/a) + 0.129(b/a)^2 \right]$	$0 < b < a$
Tee 2	$0.223a + 0.119b$	$0 < b < a$
U-channel	$0.223a + 0.3b$	$0 < b < a$

Multiple-Conductor Antenna Elements

For an antenna element comprised of N conductors, each with a circumference denoted by ℓ_i with length L_i , Equation 1 may be written as

$$\ln(r_e) = \frac{1}{L^2} \sum_{i=1}^N L_i^2 \ln(r_{ei}) + \frac{2}{L^2} \sum_{i=1}^{N-1} \sum_{j=i+1}^N L_i L_j \ln(d_{ij}) \quad [5]$$

where

$$\ln(r_{ei}) = \frac{\oint_{\ell_i} \oint_{\ell_i} \ln|\mathbf{x} - \mathbf{y}| dx dy}{L_i^2} \quad [6]$$

defines the antenna equivalent radius (“self radius”) r_{ei} of the i -th conductor and

$$\ln(d_{ij}) = \frac{\oint_{\ell_i} \oint_{\ell_j} \ln|\mathbf{x} - \mathbf{y}| dx dy}{L_i L_j} \quad [7]$$

defines the “mutual distance” d_{ij} between the i -th and j -th conductors. Application of these formulas is easily demonstrated with the simple case of two circular conductors ($N = 2$) with radii r_1 and r_2 whose center-to-center separation is $a > r_1 + r_2$. Of course, the antenna equivalent radius for each conductor is its geometric radius. The mutual distance between both is a , an exact result for two circular conductors, even if their radii are unequal. The circumference for each conductor is $L_1 = 2\pi r_1$ and $L_2 = 2\pi r_2$, which in turn means the total circumference is $L = 2\pi(r_1 + r_2)$. Using these definitions in Equation 5 yields

$$\ln(r_e) = \frac{4\pi^2 r_1^2 \ln(r_1)}{4\pi^2 (r_1 + r_2)^2} + \frac{4\pi^2 r_2^2 \ln(r_2)}{4\pi^2 (r_1 + r_2)^2} + \frac{8\pi^2 r_1 r_2 \ln(a)}{4\pi^2 (r_1 + r_2)^2} \quad [8]$$

After cancelling common factors and taking the exponential of both sides, this simplifies to

$$r_e = e^{\left(\frac{r_1^2 \ln(r_1) + r_2^2 \ln(r_2) + 2r_1 r_2 \ln(a)}{(r_1 + r_2)^2} \right)} \quad [9]$$

For the case of two conductors with equal radii ($r_1 = r_2 = r$), this further simplifies to

$$r_e = \sqrt{ra} \quad [10]$$

Figure 3 illustrates the more general case of N circular conductors ($N \geq 2$), all with a radius of r , uniformly space around a circle of radius R . Such a configuration is commonly used in the construction of cage dipoles. Here, a closed form formula for the antenna equivalent radius may be found. Using the same approach to derive Equation 9, exploiting the properties of logarithms and rotational periodicity, and recognizing that $L_1, \dots, L_N = 2\pi r$ and $L = 2\pi N r$, leads to

$$\ln(r_e) = \frac{1}{N} \ln(r) + \frac{1}{N} \ln \left(R^{N-1} \prod_{i=1}^{N-1} c_i \right), \quad [11]$$

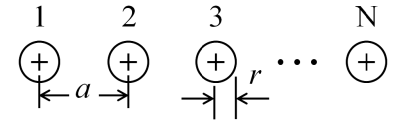
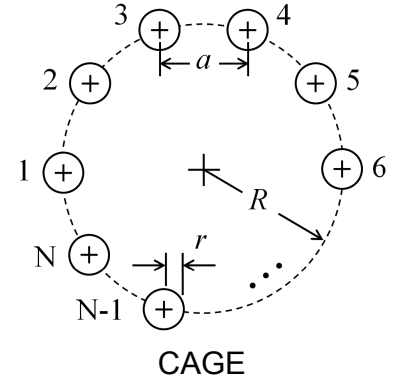


Figure 3 — Cross-sections comprised of circular conductors, each with radius r , uniformly spaced by distance $a > 2r$ either around a circle of radius R , $a/2 = R \sin(\pi/N)$, or along a line. Antenna equivalent radii are listed in Tables 3 and 4.

where c_1, \dots, c_N are the non-zero chord lengths between N points uniformly distributed around a unit circle. The product of these chord lengths is equal to N , a result derived through complex analysis.⁵ This allows further simplification of Equation 11 that, after taking the exponent of both sides, yields

$$r_e = (NrR^{N-1})^{1/N}, \quad [12]$$

which is actually valid for $N \geq 1$. It is convenient to express Equation 12 in terms of the side length a for the regular polygon (N -gon) defined by the conductor centers as shown in Figure 4. This may be done by recognizing that $r < a/2 = R \sin(\pi/N)$, which leads to

$$r_e = \left(\frac{Nra^{N-1}}{(2 \sin(\pi/N))^{N-1}} \right)^{1/N}, \quad [13]$$

and is valid for $N \geq 2$. Specific cases of Equation 13 (as well as Equation 9) likely to be encountered in practice are listed in Table 3.

Figure 3 also illustrates the case of N circular conductors ($N \geq 2$), all with a radius of r , uniformly spaced along a line and separated by distance $a > 2r$. A closed form formula for this configuration’s antenna equivalent radius may also be found and, as in the derivations above, this is a matter of summing the logarithms of mutual distances (see Equation 5):

Table 3

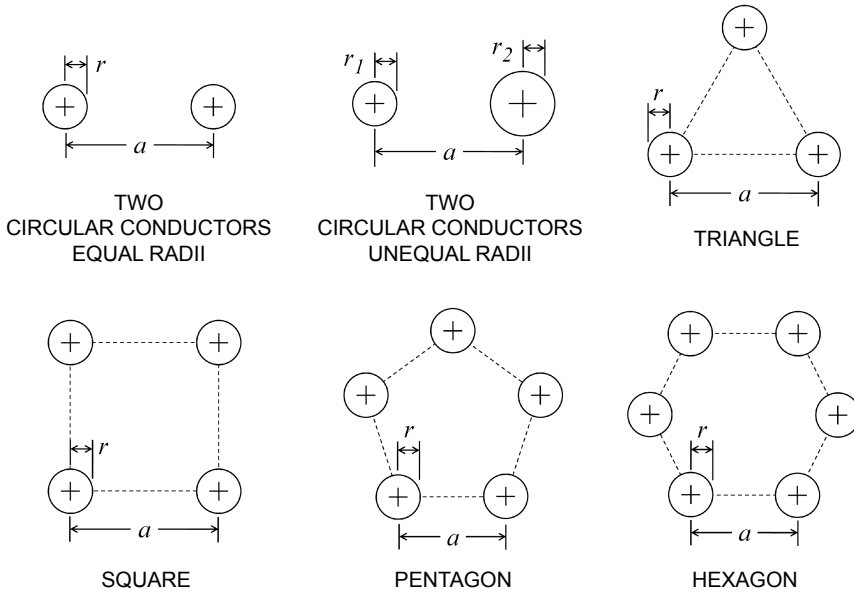
Antenna equivalent radii for elements comprised of circular conductors, each with radius r , uniformly spaced around a circle and separated by distance $a > 2r$ or $a > (r_1 + r_2)$. Cross-sections are shown in Figure 4.

Cross-section	r_e
Two circular conductors, equal radii	\sqrt{ra}
Two circular conductors, unequal radii	$\exp\left(\frac{r_1^2 \ln(r_1) + r_2^2 \ln(r_2) + 2r_1 r_2 \ln(a)}{(r_1 + r_2)^2}\right)$
Triangle	$(ra^2)^{1/3}$
Square	$(\sqrt{2}ra^3)^{1/4}$
Pentagon	$(2.62ra^4)^{1/5}$
Hexagon	$(6ra^5)^{1/6}$

Table 4

Antenna equivalent radii for elements comprised of circular conductors, each with radius r uniformly spaced along a line and separated by distance $a > 2r$. Cross-section is shown in Figure 3.

Number of Conductors, N	r_e
2	\sqrt{ra}
3	$(1.59ra^2)^{1/3}$
4	$(3.46ra^3)^{1/4}$
5	$(9.63ra^4)^{1/5}$
6	$(32.6ra^5)^{1/6}$
7	$(130ra^6)^{1/7}$
8	$(595ra^7)^{1/8}$



and the complex geometries at the feed-point and ends. Furthermore, the effective increase in radius can be significant. Consider the case of four #14 AWG wires arranged in a square (as in Figure 4) with a side length of 3 inches. For this configuration, $r = 0.0321$ inches, $a = 3$ inches, and $N = 4$ in Equation 13, yielding an equivalent radius of $r_e = 1.052$ inches. This is a radius nearly 33 times larger than that of a single #14 AWG wire. If the same four conductors are arranged in a line with a separation of $a = 3$ inches, Equation 15 yields an equivalent radius of $r_e = 1.316$ inches, which is 41 times larger than the radius of a single #14 AWG wire.

Finally, Equation 5 through Equation 7 can provide an accurate approximation for antenna elements comprised of multiple conductors of arbitrary cross-section using the distances between their geometric centers as approximate values for the mutual distances (Equation 7). When the dimensions of all conductor cross-sections are small with respect to all mutual distances, this is certainly true, although what is considered “small” is subjective. However, for pairs of randomly rotated, equal-size triangular cross-sections with side length $a = 1$ and center-to-center displacement of $a = 1.3$ (the approximate mutual distance), numerical studies found antenna equivalent radii computed from Equation 5 to be within 1% of the values computed via numerical integration.

A More General Approach

Using the same approach to derive Equation 1, a more general definition of the antenna equivalent radius is

$$\ln(r_e) = \frac{\oint_{\ell} \oint_{\ell} J(x) \ln|x-y| dx dy}{IL}, \quad [17]$$

Figure 4 — Common cross-sections comprised of multiple circular conductors, each with radius r , uniformly spaced around a circle and separated by distance $a > 2r$ or $a > (r_1 + r_2)$. Antenna equivalent radii are listed in Table 3.

$$\ln(r_e) = \frac{1}{N} \ln(r) + \frac{(N-1)}{N} \ln(a) + \frac{2}{N^2} \sum_{m=1}^{N-1} (N-m) \ln(m) \quad [14]$$

$$K_N = \exp\left(\frac{2 \sum_{m=2}^{N-1} (N-m) \ln(m)}{N}\right) \quad [16]$$

Taking the exponent of both sides yields a formula similar to Equation 12:

$$r_e = (K_N r a^{N-1})^{1/N}, \quad [15]$$

which is valid for $N \geq 1$ with

Specific cases of Equation 15 are listed in Table 4.

It is well known that dipoles constructed with the multiple-conductor elements described above typically exhibit wider bandwidth compared to the same dipoles constructed with single-conductor elements. The antenna equivalent radius allows easy computer-based modeling of such antennas, eliminating the need to model each conductor

where $J(x)$ is the current distribution along the cross-section circumference, I is the total current and

$$I = \oint_{\Gamma} J(x) dx \quad [18]$$

Equation 17 reduces to Equation 1 when $J(x) = I/L$. Although this definition is more accurate, the drawback is that $J(x)$ will most generally depend upon the frequency and the fine details of the conductor cross-section, its electromagnetic properties and proximity to other conductors.

Modeling dipole antennas with software based on NEC and other finite element methods (FEM) revealed, without surprise, that current is not distributed uniformly within any cross-section. However, using non-uniform distributions based on those computations in numerical evaluation of Equation 17 revealed that equivalent radii for some cross-sections, especially those that enclose “convex” areas, are not sensitive to the current distribution. Values were well within 10% of the equivalent radii provided by the formulas presented above (for $b > a/10$ when applicable), which are based on Equation 1. Therefore, for these cases — cage, ellipse, flat-top, half-round, rectangle and all polygons — a uniform current distribution is an acceptable approximation. Of these, the formulas for the cage are the most accurate; for practical purposes, Equation 12 and Equation 13 may be considered exact when $r \ll a$, e.g., $r = a/10$.

Cross-sections comprised of lines with corners — angle, flat, H-section, tee, U-channel — present a more difficult modeling problem. At radio frequencies current will crowd at the corners and ends of these cross-sections, making the uniform current distribution a less accurate approximation. Consequently, the formulas for these cross-sections under-estimate the equivalent radii, but still provide serviceable

values. For example, using current distributions based on FEM computations in the numerical evaluation of Equation 17, the equivalent radius for the flat conductor provided by Equation 3 — which is based on Equation 3 — appears to under-value the equivalent radius by about 10%. For the extreme case of an H-section with $a = b$, the error is also about 10 percent.

Summary and Discussion

The antenna equivalent radius enables quick, simple modeling of antenna conductors with non-circular cross-sections. For NEC-based simulations it eliminates the tedious task of approximating such conductors with a collection of “wires” (circular conductors).

Equation 1 should provide sufficiently accurate values of the equivalent radius for cross-sections that enclose a convex area. For more complicated cross-sections, especially ones that are open curves with corners, evaluation of Equation 17 may be warranted using current distributions determined from electromagnetic modeling codes. If such a modeling capability is unavailable, Equation 1 offers a fall-back option, as it only requires a description of the cross-section. Fortunately, Equation 17 depends primarily on the cross-section geometry, and less so on the current distribution, so Equation 1 should provide a close and practical approximation to Equation 17.

Finally, evaluation of Equation 1 may be carried out on a spreadsheet, often quite accurately, using only a few integration steps. For example, computation of the equivalent radius of a flat conductor using ten integration steps to evaluate Equation 1 yields a value within 1% of that provided by Equation 3.

David M. Drumheller, K3WQ, was first licensed in 1986 as a Novice, originally holding call sign KA3QBQ. A member of the ARRL and the Antique Wireless Association, his interests include restoring antique radio equipment, small analog circuit design and the modeling and construction of HF, VHF and UHF antennas. He earned an A.Sc. in Engineering from Northampton Community College in 1980, a B.Sc.E.E. from Lehigh University in 1982, and an M.Sc.E.E. and Ph.D. in E.E. from the Pennsylvania State University in 1984 and 1989, respectively. He is a program manager for the Department of the Navy.

Notes

¹Several formulas are provided in Table 9.3 in C. Balanis, *Antenna Theory: Analysis and Design*, Chapter 9, John Wiley & Sons, Hoboken, NJ, 2005. However, some appear to be the mean geometric radius of the conductor's circumferential cross-section, and not based on the magnetostatic definition used in this paper.

²E.A. Wolff, *Antenna Analysis*, Chapter 3, John Wiley & Sons, New York, NY, Second Edition, 1966.

³Throughout this article the term “cross-section” will actually refer to the “circumferential cross-section”, which excludes the area bounded by the circumference. This model is consistent with the physical phenomenon of current flowing on the surface of a conductor at radio frequencies.

⁴Federal Communications Commission Rules, Part 73.151, “Directional Antenna Performance Verification,” Section (c)(1)(i): “For arrays using vertical wires to represent each tower, the radii of cylinders shall be no less than 80 percent and no more than 150 percent of the radius of a circle with a circumference equal to the sum of the widths of the tower sides.”

⁵A. P. Mazzoleni, and S. S. Shen, “The Product of Chord Lengths of a Circle,” *Mathematics Magazine*, Vol. 68, No. 1, Feb. 1995, pp 59-60.

Lessons Learned From Four Generations of Satellite Tracking Rotator Designs

KE7FEF reports on his experiences with rotator mechanical designs for tracking satellites.

I started the mechanical design on a portable rotator for working satellites in 2008. In 2016 I finished the firmware for the fourth iteration of these rotators. This article reports some of the things that I have learned in this process. Figure 1 shows all four generations from oldest on the left, to newest on the right.

An Overview

All of these rotators use one or more microcontrollers to translate a stream of position commands from a laptop computer running a satellite position prediction program, to motor control signals. The rotators are designed to position a 144 MHz and 440 MHz *Arrow Antennas* Yagi antenna clamped to an arm, as seen on the rightmost unit in Figure 1. Basic motions for each unit are azimuth and elevation. The last three design iterations support rotating the antenna on its axis (θ rotation axis) to deal with the satellite tumbling in its orbit. The second generation has manual θ operation, and the third and fourth iterations have motorized θ control. Generations one and three use closed loop dc servo motors for actuators, while generations two and four use stepper motors.

First Generation

I designed the mechanical part of the first generation rotator around some motors

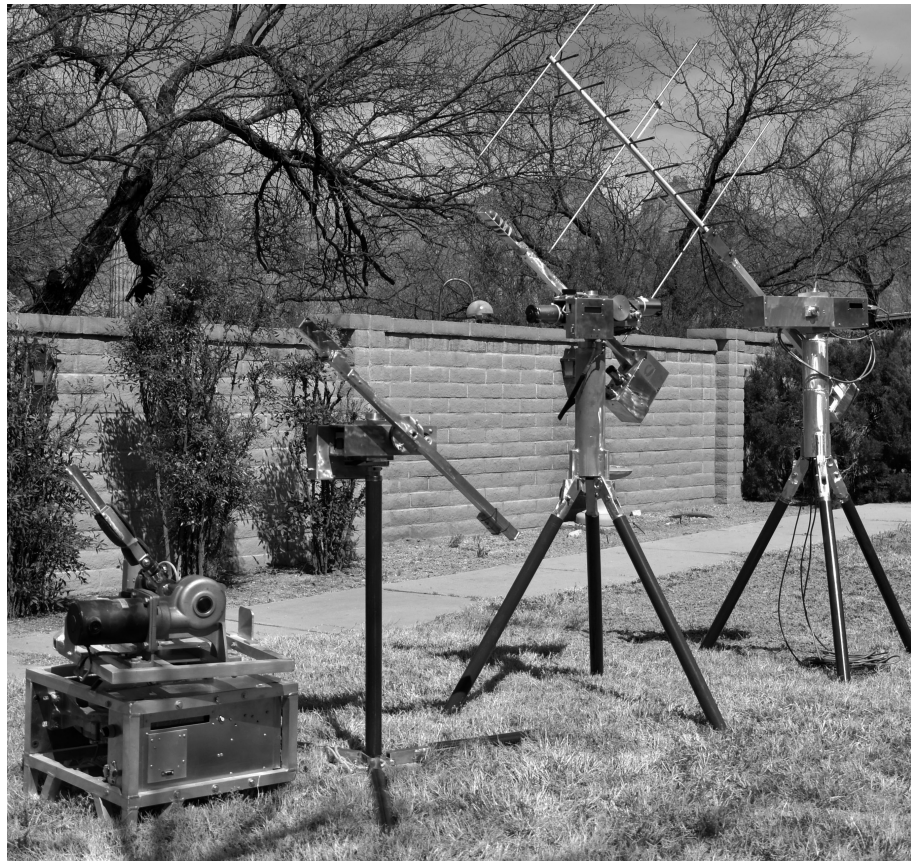


Figure 1 — The oldest of four generations of rotator designs is on the left, newest is on the right. [Bob Harbour, KE7EF photo]

that were left over from another project. This rotator was supposed to be portable, that is, not clamped to a mast or bolted to a roof. Electronics were a combination of a new design using a familiar processor and components from my “junk box” collection.

In the process of building and debugging the first generation unit, I realized that having the antenna counterbalanced was important. Initially, I thought that the elevation motor would just deal with the power required to lift the antenna. This proved to be a bad idea, especially for the motor that I had chosen. In Figure 2, the counterbalance mount is the steel plate with four holes in it, just to the right of the gear case. Counterbalancing the antenna was possible, but because of the very short space available under the antenna arm, it required a lot of weight. A two-pound antenna on the end of a foot long arm, needed 18 pounds of counterbalance 4 inches below the pivot.

The motors chosen for the first generation unit are heavy, around 20 pounds each. I used cast iron pillow block bearings from the

surplus market to support the two axes. The aluminum frame adds very little to the weight of the unit. Including the counterweight, the total weight is approximately 96 pounds. This is just barely “portable”.

Aligning and welding the frame took a lot of time. There were very few machined parts in this project. A lack of capability to rotate the antenna axially is another problem with this first generation design. I wanted to start again on the design. The idea of portability appealed to me. My sense of portability became “put it in a back pack and carry it”.

Second and Third Generations

The second and third generations were designed back-to-back. I had a number of ideas that I thought would make the rotator lighter and easier to build. A friend was talking about building his own rotator, and I volunteered to build a mechanism for him. My friend was adamant about wanting to use stepper motors, while I preferred the servo drive. My solution was to build two

mechanisms, one with stepper motor drive and one with servo drive.

Motors, mechanisms, electronics

NEMA 23 stepper motors are used on the second generation unit shown in Figure 3. Surplus car window gear motors are used on the third generation unit shown in Figure 4. Both units use toothed belts for a 4:1 reduction ratio on all axes. The mechanical reduction increases the torque on each axis and increases the position resolution.

Electronics for both of these units are completely re-designed. A three-axis stepper motor drive board drives the second and fourth generation units. A two-axis servo drive board controls the azimuth and elevation axes, while a single axis servo-drive board controls the θ axis on the third generation unit.

Building all of the azimuth and elevation mechanical components into one piece of 3-inch square aluminum tube seemed like a good approach, as most of the bearing alignment would be free as part of the machining process. The 1/8-inch wall, 3-inch square aluminum tubing is very stiff and holds the motor and bearing loads well, without moving. The second and third generation units have very few welded parts and a number of machined parts. Machining for these two units took about two days each, as opposed to the week of cutting, welding and alignment time for the first generation unit. Bearings are mounted in small aluminum blocks bolted to the outside of the body tube in the new design. Belt drives are on the outside of the body tube. The encoders for the servo unit are also on the outside of the body tube. The motor driven θ axis serves as the antenna counterweight on the servo unit, while a two-pound lead counterweight suffices on the manual θ arm on the stepper motor driven unit.

A single 1-1/4 inch schedule 80 PVC tube mast proved adequate for the stepper motor powered unit, but its flexibility caused problems with the servo stability on the servo powered unit. I tried a 1-1/4 inch aluminum tube mast, but it was not stiff enough either. The 3-inch tube tripod design is very stiff and solved the servo stability issues.

Including the base and antenna mount arm, the stepper motor driven unit weighs about 25 pounds. With the motor driven θ axis and tripod, the servo unit weighs 30 pounds. Either of these units is much lighter than the first generation unit.

Stepper vs. servo motors

Deciding between stepper motor and closed loop servo motor power raises a number of issues. My preference is toward the servo motors because (A) they are quieter, (B) they are capable of a lot more



Figure 2 — Front view of the first generation design. [Bob Harbour, KE7EF photo]

torque, (C) average current consumption is significantly lower, 200 mA vs. 560 mA at idle and (D) operation is smoother.

Advantages of the stepper motors are (A) lower cost to implement, (B) simpler firmware, (C) no hunting or stability problems, (D) simpler mechanical design, because stepper motors have bearings set up for radial loads built in, whereas the gear motors used need external bearings, (E) no encoders to mount, (F) system is lighter because less stiffness is required.

With the antenna correctly counterbalanced, the stepper motors — with 4:1 mechanical reduction — have proven to have enough torque to move and hold an antenna adequately. Torque could be increased by increasing the motor current, but that would require larger batteries. I am still undecided on the use of stepper motors or servo motors. More testing on this is needed.

Battery power

The third generation servo powered system has battery protection hardware in it to support operating from a 2.2 Ah 3S Lithium Ion battery pack. It will run all day without problems. The stepper motor driven systems do not have the battery protection hardware and will run all day on a 12 V 7 Ah cell.

Encoders

Mounting the encoders was a problem on the third generation unit. The only way that I could think of to get the accurate shaft positioning required by the optical encoders was to put the encoders on the opposite end of the gear motor output shafts from the drive pulleys, with their own bearings to locate the shafts. As a result the shafts were constrained in 3 places, which is not a good thing. It took a lot of fitting to get the gear motors to turn freely. Another consequence of this design is that the belt tension is not adjustable. Belts can be bought in many lengths, so I was able to make this work, but it makes assembling the unit harder than it should be. Both of these will be changed if I design another servo unit.

The θ axis

The θ drive on the servo driven design uses a separate, single-channel servo control board for control. This configuration is an advantage, because the satellite prediction software has no understanding of the θ axis. The separate serial channel can be controlled independently from the data stream going to the azimuth and elevation axes. On the stepper motor version of the electronics, all three axes are controlled through a single serial port. This requires another piece of software running on the laptop computer to insert θ axis controls into the azimuth and



Figure 3 — Front view of the second generation design. [Bob Harbour, KE7EF photo]

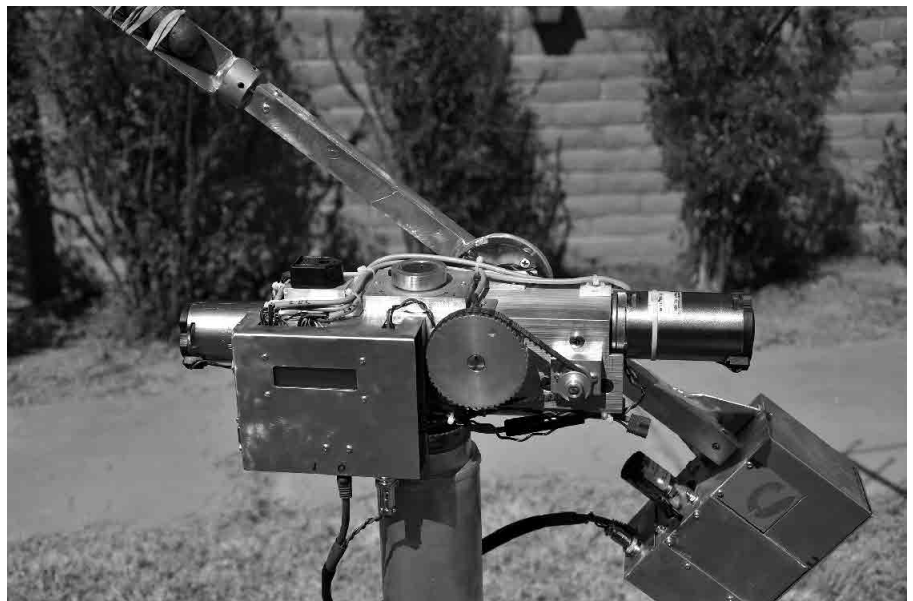


Figure 4 — Front view of the third generation design. [Bob Harbour, KE7EF photo]

elevation control stream.

In a future development control of the θ axis will be based on the signal strength outputs from the receiver.

Fourth Generation

The fourth generation design ruggedizes the second generation stepper motor driven

design and adds the motor driven θ axis. The second and third generation designs seen in Figures 3 and 4 use belts, cables and boards on the outside of the enclosure. While that is okay for a prototype, I wanted something more durable, and look more finished, so I used 4 inch square tubing for the rotator body. All of the motors, belts

**We Design And Manufacture
To Meet Your Requirements**

***Prototype or Production Quantities**

800-522-2253

**This Number May Not
Save Your Life...**

**But it could make it a lot easier!
Especially when it comes to
ordering non-standard connectors.**

**RF/MICROWAVE CONNECTORS,
CABLES AND ASSEMBLIES**

- Specials our specialty. Virtually any SMA, N, TNC, HN, LC, RP, BNC, SMB, or SMC delivered in 2-4 weeks.
- Cross reference library to all major manufacturers.
- Experts in supplying "hard to get" RF connectors.
- Our adapters can satisfy virtually any combination of requirements between series.
- Extensive inventory of passive RF/Microwave components including attenuators, terminations and dividers.
- No minimum order.



NEMAL ELECTRONICS INTERNATIONAL, INC.

12240 N.E. 14TH AVENUE
NORTH MIAMI, FL 33161

TEL: 305-899-0900 • FAX: 305-895-8178
E-MAIL: INFO@NEMAL.COM
BRASIL: (011) 5535-2368

URL: WWW.NEMAL.COM

and the control board fit inside that 4 inch square tubing. Since this design uses stepper motors, the θ axis drive is simpler than for the servo driven design. Comparing Figure 3 and Figure 5 shows the difference in size between the second and fourth generation positioners. The fourth generation unit with tripod and antenna mount arm weighs 26 pounds. Electronics and firmware in the fourth generation unit are identical to those in the second generation unit.

One of the most important things on projects of this complexity, is to make good, accurate mechanical drawings with dimensions to work from.

All told, this has been a fun process. I gave the second generation unit to the

friend mentioned previously. All of the later designs, second through fourth generation, are usable as they are. Now I want to gain some experience using them to see if further refinements are needed before considering a fifth generation design.

Bob Harbour, KE7FEF, enjoyed tinkering with electronic and mechanical gadgets as a youngster. He worked as electronics technician for a number of years, then earned his Bachelors Degree in Computer Engineering. He currently works as an electrical engineer. Bob wanted to learn more about RF, so in 2005 he earned his ham license as a way to get "hands on" experience with radio equipment. Since then, Bob has built several antennas and hardware projects.



Figure 5 — Front view of the fourth generation design. [Bob Harbour, KE7EF photo]

Getting Started with DMR and DSDPlus

This simple tutorial can help get you started on digital modulation.

Digital modulations are becoming quite popular in Amateur Radio. Technologies like DMR, D-STAR, and System Fusion have made the technology accessible and a new platform for experimentation. Recently there was much buzz about the Tytera MD-380, an inexpensive digital mobile radio (DMR) handheld transceiver. Technologies such as the RTL-SDR — software defined radio based on the RTL chip set — have brought software defined radio to the masses. Combining these two technologies can enable additional experimentation.

Recently the Gator Amateur Radio Club, W4DFU, at the University of Florida installed a DMR repeater for Gainesville and the surrounding area. This repeater is a great resource for students and Technician class operators to talk all over the world using UHF locally. It is easy to get started with DMR by just listening to typical DMR contacts. Depending on the talk group, some are quick, others are well organized nets. One option to decode DMR is to purchase a radio. Another is constructing a receiver from an RTL-SDR, an antenna, and some software.

What is DMR?

DMR stands for Digital Mobile Radio. Sometimes it is called MotoTURBO, the DMR product produced by Motorola Solutions. Like D-STAR or System Fusion, DMR digitizes voice using a vocoder and sends the information via digital packet. Unlike D-STAR and System Fusion, DMR uses TDMA (Time Division Multiple Access) with two time slots in 12.5 kHz. This enables one DMR repeater to act as two on a given frequency.

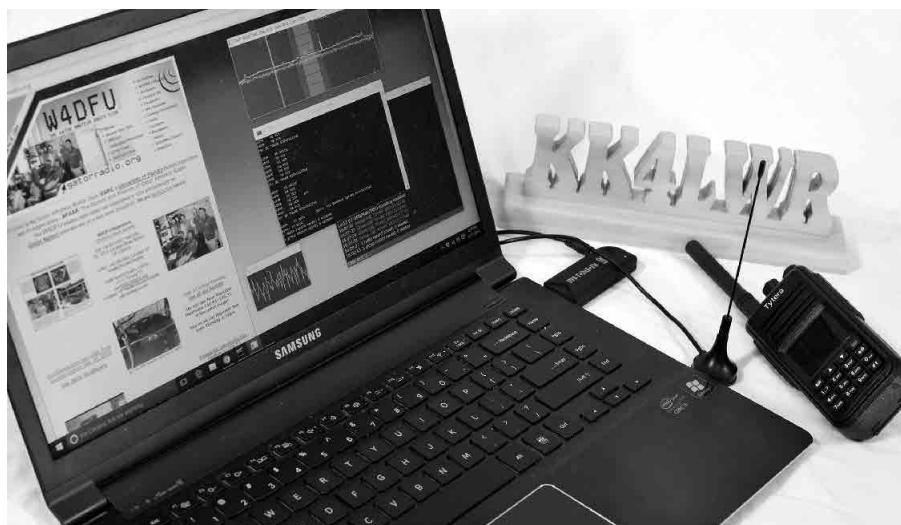


Figure 1 — DMR decoding setup using a Tytera MD-380 handheld transceiver, a laptop computer, and an RTL-SDR dongle. [Andy Milluzzi, KK4LWR, photo]

What is DSDPlus?

DSDPlus is an application that runs on a Windows computer that can decode multiple digital modes.¹ Similar to the open source DSD program, DSDPlus takes an audio stream from a radio and can generate text or audio. The main difference for the scope of this tutorial is that the open source program must be compiled from source code, while DSDPlus offers a Windows binary.

Hardware Setup

My decoding setup requires just a few pieces of physical hardware, seen in Figure 1, and a some virtual hardware. The first thing you need is a DMR source. I already had purchased a Tytera MD-380 handheld

transceiver, since I am quite interested in the ongoing firmware experimentation community. You might already have a DMR source, via other hams and perhaps a local repeater. If you do decided to purchase a DMR radio, Motorola Solutions and Hytera each make some outstanding radios. Both Connect Systems and Tytera make some more inexpensive options.

The second needed piece of hardware is a radio to connect to your computer. You could use a VHF/UHF radio and a sound card to interface with your computer. However, I opted for an RTL-SDR for this project. An RTL-SDR is essentially an inexpensive TV tuner USB dongle for your computer. It can be purchased for less than \$20 and can cover 50 MHz to 1.7 GHz. Your Windows

operating system will most likely need a special driver to use the card as an SDR. You can install the correct driver with assistance from the Zadig web page.² The Zadig website has a simple guide for installing the WinUSB driver. This tutorial will assume you are using an RTL-SDR with the appropriate driver.

The final needed hardware component for this tutorial is virtual. The DSDPlus needs a way to pass the audio. If you are using your computer sound card and an external radio, then you can skip this hardware. I recommend a VB-Audio Virtual Cable as a free solution.³ When you download and install the software, you should notice a new audio input and output device on your computer that acts as a sound card.

Setting up DSDPlus Suite

Download the latest version of DSDPlus and DSDPlus DLL package from the DSDPlus web page.⁴ Extract the contents of the DSDPlus zip file and the DLL zip file to a folder. You should see a few dozen files. For this tutorial, we will focus on FMP-VC.bat and VC.bat. In DSDPlus two programs must be configured: FMP and DSDPlus. FMP is a basic narrowband FM tuner for an SDR. DSDPlus is the decoder.

With all the files extracted, open a command prompt. In the Windows environment, this can be done by pressing the Windows key on your keyboard and typing CMD. Once open, navigate to the folder containing the DSDPlus files. Another option in Windows 8 or Windows 10 is to click on the File menu in your Explorer window. One of the options listed is open a command prompt. If done from the DSDPlus folder, you will not need to navigate.

Setting up FMP

Open the file FMP-VC.bat. You will see several parameters. Modify this script for our use by configuring the four parameters “-I”, “-O”, “-P”, and “-f”. The “-i” parameter followed by number (without a space) indicates which SDR to use as an input. For the SDR we can assume it is the only one on your computer, so set it to “-i1”. The “-o” parameter followed by a number is the output audio device. The “-P” parameter is the parts-per million (ppm) correction for your SDR. The “-f” parameter is the frequency in megahertz.

To determine the values for the other parameters requires some knowledge about your setup. Let’s first tackle the output audio source. Each computer is different. The best way to determine the audio output is to observe what FMP sees. For this next part, you might find it helpful to unplug the SDR from the computer; if it is plugged in

the program will launch. Type “FMP.EXE” in your command prompt window. Without an SDR plugged in, the application should fail to launch, but will still list the audio

devices. For this program, we need to feed the output to our virtual audio port input. On my computer it is “Audio output device #2” seen in Figure 2.

```

C:\Users\... \Desktop\DSDPlus>FMP.EXE
FMP rev 1.4t
FMP -h for help summary

SDR sampling rate = 1.008 MHz
Spectrum window width: 512
FFT size: 32,768
Spectrum update rate: 10 Hz
Step size table: 5.000 6.250 7.500 12.500 15.000 25.000
DSD+ path: '.'
Primary frequency list: '.\FMP-FreqList1.csv'
Secondary frequency list: '.\FMP-FreqList2.csv'
Database search distance: 99.90 miles
Base latitude/longitude: 19.7163 -155.6241

Audio output device #1 = 'Speakers (Realtek High Definiti'
Audio output device #2 = 'CABLE Input (VB-Audio Virtual C'

SDR device count=0
Can't open RTL SDR device #1

C:\Users\... \Desktop\DSDPlus>

```

Figure 2 — Running FMP.EXE produces this text. Note the listed audio output devices.

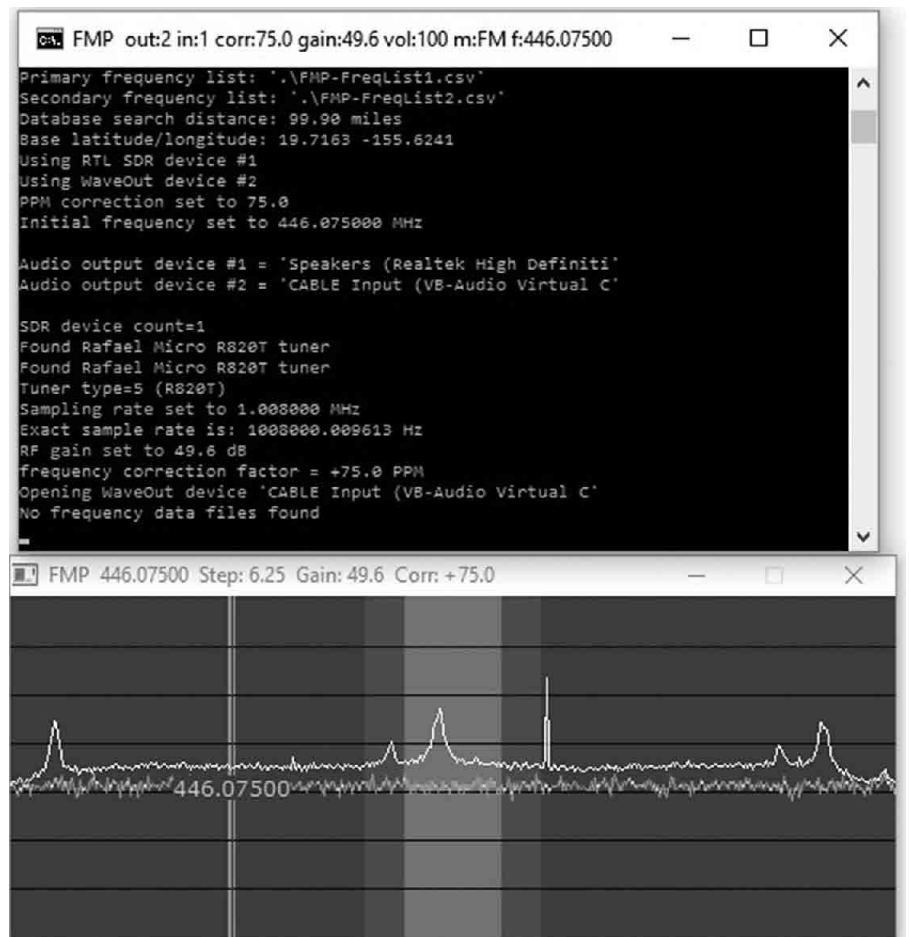


Figure 3 — Screen capture of FMP successfully running, controlling the SDR. Note the command prompt window showing the correct ppm correction and frequency.

Setting the ppm correction for your SDR is specific to your device. You can experiment by leaving it at 0.0. Alternatively you can use another SDR program such as SDR# from the AIRSPY web page to find the ppm correction.⁵ My device required a ppm correction of +75.

The last parameter to set is the frequency to monitor. I do not want to clog the larger DMR network with my testing traffic, so I generated my own signals on 446.075 MHz, one of the UHF simplex frequency. DMR is mostly on UHF in the United States. Once the system is working, you can change the frequency to a local repeater.

If done correctly, your FMP-VC.bat should look like:

```
"FMP -i1 -o2 -P75 -f446.075".
```

Plug in your SDR tuner and run the script. You should see several windows pop up. Your computer screen should look like Figure 3. Save the changes to FMP-VC.bat. You can close FMP by pressing the ESC key.

Setting up DSDPlus

Configure the DSDPlus script with a similar process. Open the VC.bat file and observe the various parameters. The parameters that start with a "w":

```
"-wsl", "-wss", "-wel", and "-wcl"
```

control where the windows are launched. You can set these as you like.

We must configure the audio as we did before by launching DSDPlus from our open command prompt. Unfortunately, there is

no way to stop the program from opening all the windows, so you might need to move the various windows out of the way to see the command prompt and get your results. On my computer I got the results shown in Figure 4.

The input should be set to the virtual audio cable output. The output must be your system speakers. In my case this results in input device #1 and output device #1 respectively. This enables me to hear anyone calling.

A few other parameters must be set to make DMR work. The first parameter, "-rv", tells DSDPlus that we expect voice. DSDPlus must also be set to decode DMR/MotoTURBO, since DSDPlus can do much more than just DMR — DSDPlus documentation indicates that it decodes D-STAR, except audio. It also can also decode P25 Phase 1 and NEXEDGE.

To enable DMR we need to pass the "-fr" parameter. We also need to tell DSDPlus which of the two time slots we want to

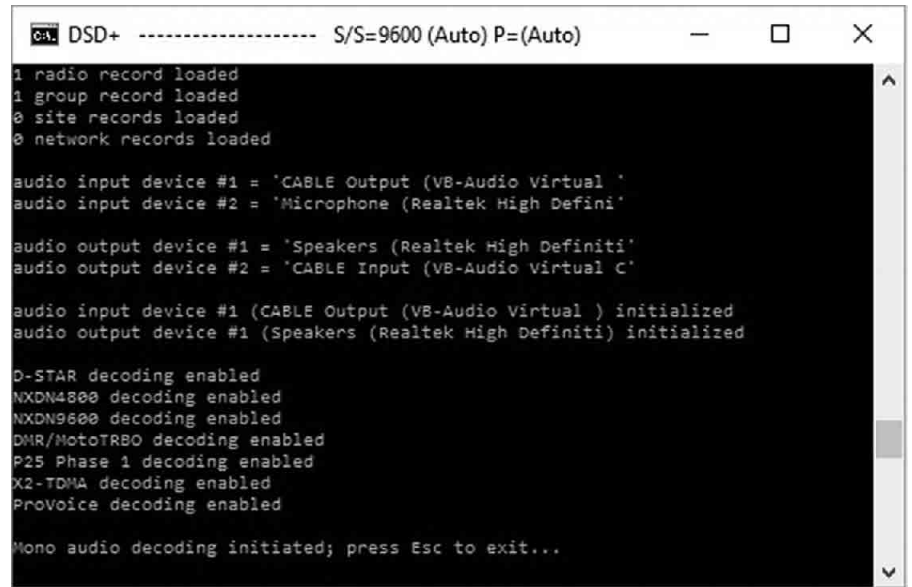


Figure 4 — Running DSDPlus lists both input and output audio devices.

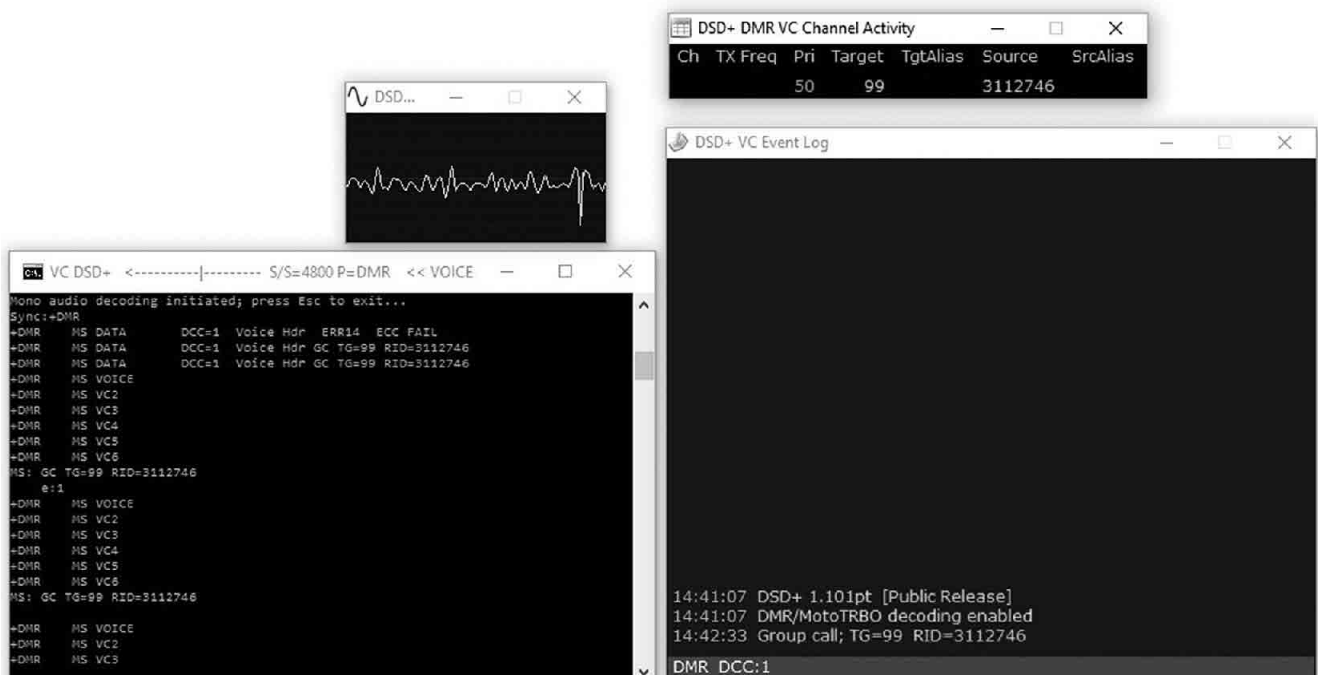


Figure 5 — A screen capture of several windows of DSDPlus while decoding.

monitor. This is done via passing “-1” or “-2” after the “-fr” parameter. Those are the only required parameters to make it work. You can record what DSDPlus decodes using the “-Pwav” parameter to save the audio as a wave file. You might also discover a “-v3” parameter in the sample provided by DSDPlus. This enables verbose logging and I recommend using it, especially for debugging your scripts.

When you are done, you should have a VC.bat script similar to:

```
“DSDPlus -fr -1 -rv -Pwav -i1 -o1 -v3 -wsl400.210 -wss100.200 -wel172.522 -wcl528.0 >>VC.log”.
```

Run VC.bat along with FMP-VC.bat and you should be able to decode DMR audio.

Figure 5 is a screen capture containing several windows of information from my test transmission. If you look at the “DSD+ DMR VC Channel Activity” window you can see my target was Talk Group 99. The signal came from my radio programmed with 3112746, my DMR-MARC registered radio number. “The DSD+ VC event log” also reflects this same information. The “DSD...” window shows a trace of the audio signal. The most useful information comes from the command prompt script, lower left window. You can also see DSDPlus initially locked on my signal before getting regular information. This is because my simplex mode has an “always” admit criteria. If we tweak our script to use slot two, the information for my signal would look the same in the command prompt, but no audio would play. This is because DSDPlus is expecting time slot two to provide the audio. We can also see my radio ID and the talk group in this window.

Test Radio Setup

Testing was done on low power and simplex. I programmed my Tytera MD-380 to use the standard Talk Group 99, Time Slot 1, and Color Code 1, as found on the Amateur Radio guide on the DMR-MARC web page.⁶ I also have the channel admit criteria set to “always” since there is no signal with which to sync up.

Results

The setup easily decodes my DMR test signals from my MD-380. Figure 5, shows that DSDPlus is successfully decoding the incoming DMR voice packets. The software successfully identifies key packet information, such as talk group, device ID, and so on. The audio output is clear and easy to understand. The software saves a “.wav file” of the audio, enabling me to mute the speakers while testing to avoid feedback.

With the setup working correctly, I have configured an old computer with the RTL-SDR to act as a DMR monitor for W4DFU repeater. I used the time slot selection of DSD+ to limit monitoring to time slot 2 (to avoid hearing the near constant traffic on North America or World Wide talk groups). This lets me hear local traffic and just a few larger area talk groups. The W4DFU repeater is part of the K4USD network. Details for time slots and talk groups can be found at the K4USD web page.⁷ I live a few miles from the W4DFU repeater and the small stock antenna that came with the RTL-SDR is easily able to pick up the repeater from my desk.

Next Steps

Like many hams, I am always learning something new. I love the challenge of mastering a new technology. I am far from an expert on DMR, but I am having fun discovering the features of this digital mode. This SDR scanner project is just one way to gain a better understanding of DMR while

also enabling a way to connect with other users.

This tutorial was just the tip of the iceberg in terms of software defined radio. While scanning DMR with DSDPlus is nothing new, the software can be intimidating. We have just scratched the surface in what DSDPlus can do and hopefully this will encourage you to experiment with all the features or get started with DMR. Most of the DSDPlus documentation is in text files with the software. Give it a try and see what you can come up with!

Andy Milluzzi, KK4LWR, is an Amateur Extra licensed ham, first licensed in 2012. He is president of the Gator Amateur Radio Club, W4DFU, at the University of Florida. Andy is 2012 alumnus, receiving a BS in Computer Engineering and a BS in Software Engineering, of the Rose-Hulman Institute of Technology in Terre Haute, Indiana. He is a PhD candidate and 2013 alumnus, receiving a MS in Electrical and Computer Engineering, at the University of Florida in Gainesville, Florida. Andy loves how Amateur Radio affords him the ability to tinker and relax, while still incorporating his passion for engineering.

Notes

¹www.dsdplus.com/

²zadig.akeo.ie/

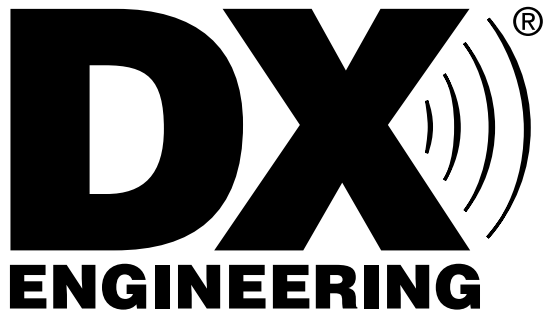
³vb-audio.pagesperso-orange.fr/

⁴www.dsdplus.com/download-2/

⁵airspy.com/download/

⁶www.dmr-marc.net/media/Amateur_Radio_Guide_to_DMR_Rev_I_20150510.pdf

⁷k4usd.org

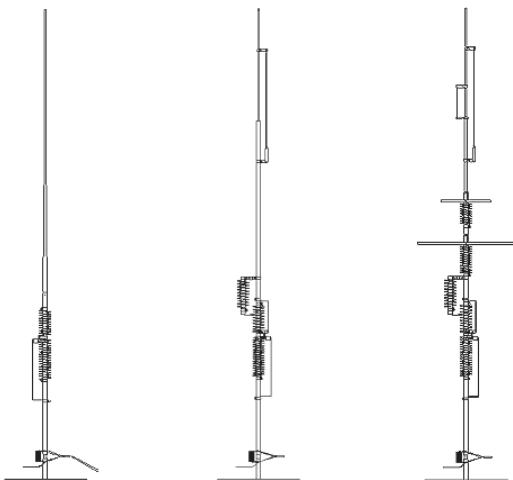


8:30 am to midnight ET, Monday-Friday
 8:30 am to 5 pm ET, Weekends
 International/Tech: 330-572-3200
 8:30 am to 7 pm ET, Monday-Friday
 9:00 am to 5 pm ET, Saturday
 Country Code: +1 Sale Code: 1704QEX

**ORDER BY 10 PM
 SAME-DAY
 SHIPPING**
 Mon-Fri, 10 pm ET
 In-Stock Items

800-777-0703 | DXEngineering.com

DX Engineering is Your #1 Antenna Source!



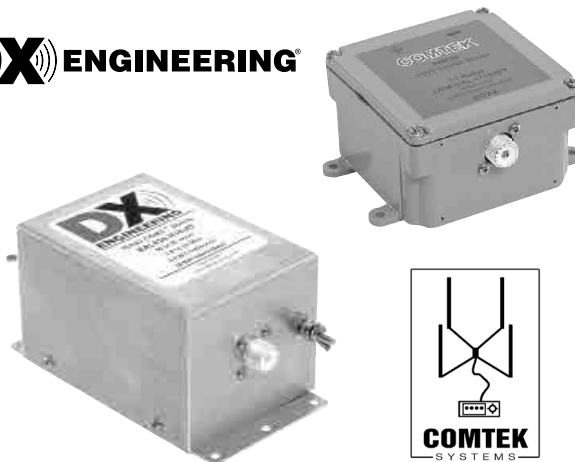
HF Vertical Antennas

DX Engineering's Butternut Antennas line boasts three renowned designs, including 2-band, 6-band, and 9-band vertical antennas. The antennas' compact size makes them easy to install, yet they will deliver outstanding performance on each band. DX Engineering also carries repair, add-on, and replacement parts for Butternut Antennas.



BTV Packages

DX Engineering has kits based around Hustler's popular multi-band verticals that let you work HF with performance and flexibility. They're perfect if you want a versatile HF setup with a small footprint. Each kit includes an antenna, a radial plate with exclusive patented Tilt-Base, a set of radial staples, radial wire, and important brackets, connectors and hardware.



Baluns

Based on time-tested designs from noted Balun expert W2FMI, DX Engineering and COMTEK baluns offer the perfect balanced/unbalanced transition for superior SWR across all HF bands. The baluns are available in 1:1 and 4:1 matching ratios, with single or dual cores.



Coaxial Cable Assemblies

These pre-made low-loss cable assemblies are available with DX Engineering's revolutionary new PL-259 connector, featuring the best qualities of both crimp-on and solder-on connectors.

Use the free online Custom Cable Builder at DXEngineering.com to build assemblies made to your exact specs. DX Engineering's coaxial cable is also available by the foot or in bulk spools.



Antenna Tuners An antenna tuner can mean the difference between making or missing a critical contact. In addition to improved transmit performance, a properly tuned antenna is more efficient, saving valuable power in portable stations. Find over fifty manual and automatic antenna tuner models for virtually any antenna setup at DXEngineering.com.

Email Support 24/7/365 at DXEngineering@DXEngineering.com



Using FDMA in HF Multimedia Modes

WA6NUT discusses how FDMA technology can be used for new sound card modes.

In the past, Amateur Radio multimedia modes have been restricted to UHF and above. ATV is a UHF multimedia mode, combining voice and video. The High Speed Multi Media (HSMM) mode, usually associated with 2.4 GHz 802.11 access points, can be used to transmit and receive the media found on the Internet.

This article describes how an older technology, FDMA, can be used to implement multimedia modes on HF, using sound card techniques. For several years the author has been developing FreeDV plus Video, an HF multimedia mode using FDMA, combining voice and video.

FDMA Described

FDMA, or Frequency Division Multiple Access, is a multiple access technique that permit various users — voice, video, data, etc. — to share a common transmitter or satellite transponder. FDMA assigns a separate frequency subchannel to each user, and if multicarrier modes are used, each frequency subchannel might include many subcarriers. FDMA accommodates multiple users using frequency multiplexing.^{1,2} Other multiplexing modes such as Time Division Multiple Access, or TDMA, assign a time slot to each user or like Code Division Multiple Access, or CDMA, assign a distinct coding to each user. FDMA is much easier to implement than either TDMA or CDMA.

A Sound Card Implementation of FDMA

FDMA is readily implemented using a sound card as found in your PC, or as an external USB adapter, together with the associated driver software. I show an

implementation that uses a sound card feature known as “input monitoring.”

Most sound cards can be set up to pass the input signal through so it appears at the output together with software-derived audio. This is useful in PC gaming applications. When input monitoring is a built-in hardware feature, gamers can monitor their own voice commentary without the annoying delay caused by software buffering. It is also useful for monitoring voice commentary when producing on-screen tutorials. This feed through is variously referred to in the literature as, (1) Input monitoring, (2) Mic monitoring, (3) Sidetone/Voice feedback, (4) Pass-through mixing.

Some USB sound cards are designed with input monitoring as a built-in hardware feature, which cannot be disabled. Conversely, some software drivers cannot be

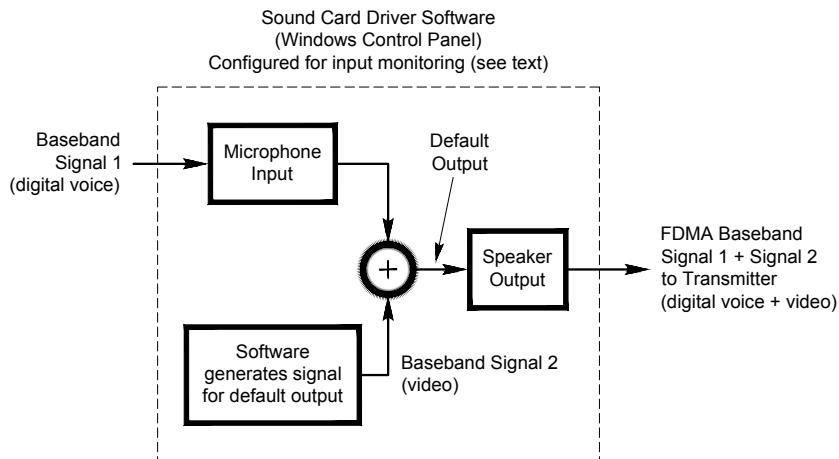
configured for input monitoring. In general, input monitoring can be configured by:

(1) Using USB sound cards having input monitoring as a built-in hardware feature.³

(2) Unchecking the “Mute” checkbox for the Microphone on the Speaker GUI in the Windows Control Panel “Sounds and Audio Devices” option. However, some sound card drivers do not include a “Mute” checkbox for the Microphone⁴ or,

(3) Checking the “Listen to this device” checkbox in the “Listen” tab of the “Microphone” GUI under “Manage Audio Devices” under “Hardware and Sound” in the Windows Control Panel.⁵

Let’s examine one scheme to obtain an FDMA signal by summing multicarrier baseband signals using a Windows sound card driver. See the software signal flow diagram in Figure 1.



QX1701-Peterson01

Figure 1 — Software signal flow diagram for FDMA transmitter.

Setup — Configure the sound card for input monitoring and designate the sound card output as the default output.

Signal 1 — Baseband signal applied to sound card input

Signal 2 — Baseband signal generated by software; software directs the output to the sound card default output. Of course, to avoid interference, subcarriers within Signal 2 must be located so they will not overlap Signal 1 subcarriers.

Result — Signal 1 summed with Signal 2 as a composite baseband FDMA signal.

For example, if Signal 1 is a baseband digital voice signal, and Signal 2 is a baseband video signal, then the output of the sound card is a baseband FDMA signal combining voice and video.

Figure 2 is a software signal flow diagram showing how the received baseband FDMA signal is processed by the sound card, with a separate processor for each component. Other FDMA implementations using sound cards are possible. The implementations in Figures 1 and 2 were compatible with the hardware and software in the author's setup.

FDMA Issues

When multicarrier signals are combined as in FDMA, several issues arise, including intermodulation distortion (IMD), peak-to-average power ratio (PAPR), and power sharing. When multiple signals are applied to a nonlinear device, mixing occurs, adding outputs at sum and difference frequencies, including sums and differences between the signals and their harmonics. Transmitters are designed with mixers — analog mixers are nonlinear by design — and amplifier stages — designed to minimize nonlinearity. So the mixing products — intermodulation distortion, or IMD — are inevitable. In an

FDMA system, when multicarrier signals are combined with other multicarrier signals, spurious multicarrier signals — the IM products — are formed. Formulas for calculating the locations of the third-order IM products (IM_3) are found in the literature. Higher order products exist but are usually negligible.⁶

The locations of these spurious IM_3 multicarrier signals are calculated as follows. For multicarrier Signals 1 and 2, comprising an FDMA signal, where Signal 1 extends from frequencies f_{1lo} to f_{1hi} , and Signal 2 extends from frequencies f_{2lo} to f_{2hi} , the intermodulation products form spurious multicarrier signals covering the frequency bands,

$(2f_{1lo} - f_{2hi})$ to $(2f_{1hi} - f_{2lo})$ and $(2f_{2lo} - f_{1hi})$ to $(2f_{2hi} - f_{1lo})$, spread over bandwidths

$(2B_1+B_2)$ and $(2B_2+B_1)$, where $B_1 = f_{1hi} - f_{1lo}$ and $B_2 = f_{2hi} - f_{2lo}$

Care must be taken so that those signals do not interfere with the desired multicarrier signals, and/or interfere with other users located outside the bandwidth occupied by the composite FDMA signal. It may be possible to provide spacing — guard bands — between the multicarrier signals comprising the FDMA signal so that IM products do not interfere with the desired signals. Other means of dealing with IMD include,

(1) — Keeping transmitter output signal levels low enough (back off) to avoid saturation in the amplifier chain, considering the signal's peak-to-average power ratio (PAPR).

Output power back off for PAPR: The average output power of an FDMA signal must be set so that signal peaks are not close to saturation in the output amplifier.

Assuming that, for the FDMA signal, the signal peak power level exceeds the average level by a factor of six (PAPR = 6), the average output power should be maintained at about 15 to 20 W or less when used with an amplifier rated at 100 W output.⁷

(2) — Balancing power levels between the multicarrier signals comprising the FDMA signal.

IM products are introduced when the power levels of the multicarrier signals comprising the FDMA signal are not balanced.^{8,9} The required power level for each multicarrier signal is a function of its bandwidth, so that for balance, power levels should be set as follows:

$$P_1 = (B_1 / B_i) P_i$$

$$P_2 = (B_2 / B_i) P_i$$

$$P_3 = (B_3 / B_i) P_i$$

where

P_1, P_2, P_3 are the required power levels for multicarrier Signals 1, 2 and 3

B_1, B_2, B_3 are the bandwidths of multicarrier Signals 1, 2 and 3,

$B_i = B_1+B_2+B_3$ is the total bandwidth of the FDMA signal, and

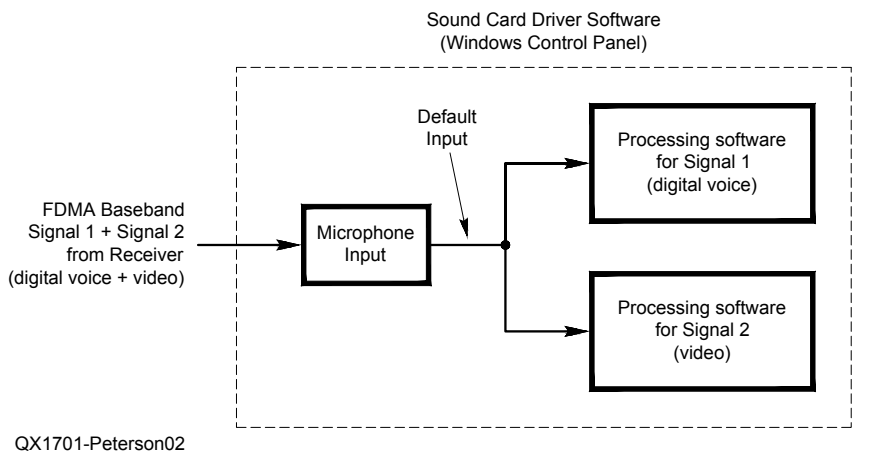
$P_i = P_1+P_2+P_3$ is the total power of the FDMA signal including back off allowed for PAPR.

(3) — Using hardware and/or software to linearize the processing of the FDMA signal.

Several techniques are available to linearize the processing of the output signal.¹⁰ One technique, adaptive pre-distortion, has recently become available in Amateur Radio HF SDR transceivers. Adaptive pre-distortion (APD) samples the transmitted signal at the output of the transceiver (or at the output of an external amplifier) using a second receiver dedicated to APD monitoring. The receiver output is compared with the transmitter audio modulation signal using a special software algorithm — called PureSignal in Apache Labs SDR products. The algorithm generates a correction signal, which when summed with the transmitter audio modulation signal, linearizes the processing of the transmitted signal.

An Example: A Multimedia Sound Card Mode

In recent years Skype™, Facetime™ and other forms of video conferencing have become a part of everyday life, adding a new multimedia dimension to voice-only communications. In Amateur Radio, our amateur TV colleagues have been combining voice and video since long before the Internet. But they have been restricted to the 70 cm band and higher frequencies, because of the bandwidth required for NTSC and DVB-T TV signals.



QX1701-Peterson02

Figure 2 — Software signal flow diagram for FDMA receiver.

On HF, SSTV proponents have been sending and receiving high-resolution images for years, but at very slow frame rates and without simultaneous voice. Analog SSTV with simultaneous voice has been implemented with the Adonis Electronics ST-12, or equivalent.¹¹ But the use of low-pass filtering makes the voice quality less than ideal.

The need for simultaneous video and voice over HF is unmet because the analog voice bandwidth alone occupies the entire bandwidth of HF transceivers. But, with the recent advent of digital voice — FreeDV and its predecessor FDMDV — the digital voice bandwidth occupies less than half the bandwidth of some HF transceivers, leaving room for a low resolution, low frame rate video signal.

The remainder of this article describes FreeDV plus Video, a new experimental sound card mode providing simultaneous voice and video on HF.

In General

Today's FreeDV plus Video owes its existence to recent advances in Digital Voice, Narrow Band TV (NBTv), and to Frequency Division Multiple Access (FDMA).

Digital voice

Prior to 2013, Frequency Division Multiplex Digital Voice (FDMDV) was the most widely used sound-card digital voice mode. Developed by Cesco Lanza,

HB9TLK, it worked well but there were issues with a proprietary CODEC (COder-DECoder). In 2013, another sound card implementation of digital voice, FreeDV, was introduced. Developed by David Rowe, VK5DGR, and Dave Witten, KDØEAG, FreeDV is still a work in progress, but has already gained wide acceptance in the HF community. Several modes have been offered in the various implementations of FreeDV “1400”, a narrower bandwidth mode, with no forward error correction (FEC). “1600” is a wider bandwidth mode with FEC. “1600 Wide” is an even wider bandwidth mode more useful for weak signal work. “700” is a recent, even more robust, mode.

FreeDV plus Video uses the “1600” mode, with the digital voice signal composed of 17 subcarriers spaced at 75 Hz intervals, centered at 1500 Hz baseband.

Narrow Band TV (NBTv)

Con Wassilieff, ZL2AFP, is the leading proponent and developer of sound card NBTv software. In 2004 he developed a version, called “FFT-TV”, providing a 36-line resolution image, with color, at 0.9 frames/sec. The signal is composed of 49 subcarriers, originally spaced at 43.0664 Hz (WA6NUT modified the ZL2AFP software for 37.5 Hz spacing with the 13 chroma subcarriers relocated below the FreeDV subcarriers and the 36 luminance subcarriers relocated above the FreeDV subcarriers). ZL2AFP continues to develop new software for NBTv.¹²

Frequency Division Multiple Access (FDMA).

FDMA provided transmission of simultaneous multiple signals from satellite transponders. FreeDV plus Video is a sound

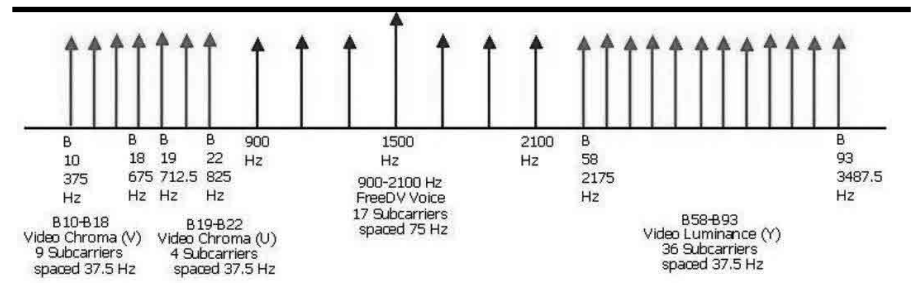
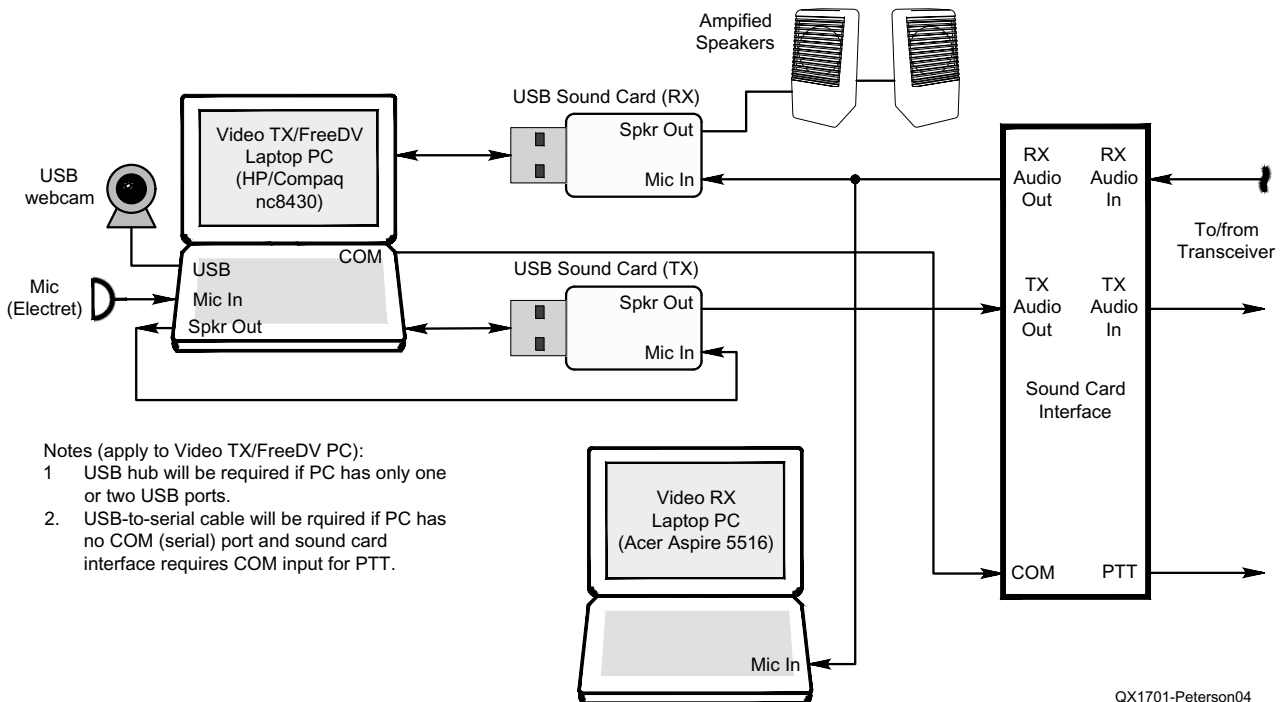


Figure 3 — FreeDV+ video base-band spectrum.



- Notes (apply to Video TX/FreeDV PC):
1. USB hub will be required if PC has only one or two USB ports.
 2. USB-to-serial cable will be required if PC has no COM (serial) port and sound card interface requires COM input for PTT.

QX1701-Peterson04

Figure 4 — FreeDV+ video hardware block diagram.

card mode combining FreeDV and ZL2AFP “FFT-TV” NBTv, as modified by WA6NUT, using FDMA techniques. Video resolution is 36 lines at a 0.9 FPS frame rate, with a total bandwidth of 3.5 kHz. The signal consists of 13 video chrominance subcarriers with 37.5 Hz spacing, 17 digital voice subcarriers with 75 Hz spacing, centered at 1500 Hz baseband, and 36 video luminance subcarriers with 37.5 Hz spacing.¹³

For brevity “FreeDV plus Video” will be referred to as “FreeDV+”.

Description of FreeDV plus Video (FreeDV+)

Figure 3 shows the spectrum of the 66-subcarrier FreeDV+ signal. The 17-subcarrier digital voice (FreeDV) signal is located above the 13 video chroma subcarriers and below the 36 video luminance subcarriers.

FreeDV+ is a hybrid mode. The digital voice component is a digital signal, and the video component is an analog signal. The digital voice signal is QPSK with data occurring in 2-bit binary groups (00, 01, 10, or 11) transmitted at any instant on each subcarrier. The video signal is analog, with each subcarrier frequency modulated. The FM deviation on each video subcarrier at any instant represents the luminance (Y) for subcarriers B58-B93, or chrominance (U or V) for subcarriers B10 to B22, for the pixels being transmitted. Each luminance subcarrier corresponds to a line in the FreeDV+ image.

Hardware for FreeDV plus Video (FreeDV+)

Figure 4 shows a block diagram of the various hardware components required for FreeDV+, and how they are connected. The components of FreeDV+ shown in the diagram are readily available with no special requirements. But there are special requirements for the HF transceiver. The most important requirement is the transmitting and receiving bandwidth must be at least 3.5 kHz. Almost any HF transceiver suitable for eSSB will also be suitable for FreeDV+.¹⁴

Tuning of the received video signal requires adjustment of the receiver frequency in 1 Hz steps. The hues in the received video image are sensitive to frequency drift, so good frequency stability in the transmitter and receiver is required. Frequency stability is usually not a problem with modern synthesized transceivers with TCXO master oscillators, if adequate warm-up time is allowed before a FreeDV+ contact.

The FreeDV+ digital voice SNR and video quality should be greatly improved if the HF transceiver RF output is processed using adaptive pre-distortion. This technology

has been recently introduced in amateur HF SDR transceivers. Two laptop PCs running the Windows™ operating system (OS) are used for FreeDV+. One PC runs software for transmitting video and for transmitting and receiving digital voice. The other PC runs software for receiving video and for tuning the received video with WinWarbler software.

Almost any sound card interface may be used with FreeDV+. However, VOX operation must be disabled because the multicarrier video signal is issued from the video transmit software regardless of the state of the push-to-talk (PTT) button. PTT is implemented with the PTT button on the FreeDV digital voice Graphical User Interface (GUI). More details of the FreeDV+ hardware are found on the FreeDV+ website.

Software for FreeDV plus Video (FreeDV+)

FreeDV+ consists of add-on software for FreeDV, adding video capability to FreeDV digital voice, “1600” mode. Figure 5 is a software signal flow diagram for the Video TX/FreeDV PC. One USB sound card — shown as “Turtle Beach USB Audio (2)” — together with the FreeDV software, is used to process and decode the received digital voice signal from the sound card interface and to provide an audio signal to the amplified speakers.

The PC motherboard sound card, together with the FreeDV software, is used to encode and process the audio from the microphone and provide the multicarrier digital voice transmit signal. The digital voice transmit signal is applied to the input of a second USB sound card — shown as “Turtle Beach USB Audio (1)”. The digital voice transmit signal is summed with the video transmit signal, and the composite multicarrier FreeDV+ transmit signal is applied to the input of the sound card interface, to be applied to the HF transceiver audio input.

A description of the summing process follows.

The baseband FreeDV signal path

This signal appears at the “Speakers” output of the transmit USB sound card, summed with the video signal, as a result of “input monitoring” in that sound card. Input monitoring allows the output to monitor the signal applied at the input.

Input monitoring is a built-in feature for some USB sound cards, such as the Turtle Beach Amigo II, but more commonly depends on user-defined settings in the Windows Sound driver software.

The baseband video (TXfftCO5L) signal path

This signal appears at the “Speakers” output of the transmit USB sound card,

summed with the FreeDV signal, since the output is set by the user as the “default output” in the Windows sound driver software. The TXfftCO5L software is designed so that its output appears at the output designated by the user as the default output.

Figure 5 shows an implementation of the scheme in Figure 1. FDMA systems require a means for adjusting the level of one signal with respect to the levels of other signals to prevent interference from IM products. This process is termed “power sharing” or “power balancing” in the FDMA literature. The adjustments labeled TX LEVEL 1 and TX LEVEL 2 establish correct power sharing in the FreeDV+ output signal.

In the FreeDV+ setup, the sound card playback (speakers) and record (microphone) slider controls are accessed from the “Sounds” option of the Windows™ Control Panel.

TX LEVEL 1, TX LEVEL 2 and TX LEVEL 3 adjustments

The TX LEVEL 1 Playback Level slider control for the motherboard sound card, and TX LEVEL 2 Record Level slider control for the transmit USB sound card, shown as “Turtle Beach USB Audio (1)” — are used to adjust the digital voice signal level. The video signal level is not adjustable. TX LEVEL 1 and TX LEVEL 2 are set for the best compromise between low-noise video and best digital voice signal-to-noise ratio (SNR), while monitoring the received FreeDV+ spectrum and SNR on the FreeDV GUI. The author sets the TX LEVEL 1 and 2 slider controls for a peak FreeDV SNR reading of 10 to 12.

The TX LEVEL 3 Playback Level slider control for the transmit USB sound card, shown as “Turtle Beach USB Audio (1)” is used to set the transceiver power output. Figure 6 shows a screen shot of the receiving station Video TX/FreeDV PC running with the Windows XP™ OS. The TX LEVEL 3 slider control is set to about 60% in the “Master Volume” GUI.

The digital voice GUI is displaying the spectrum of the signal being received from WA6NUT (see the GUI textbox). The video transmit software shows the first frame of a video clip ready to be transmitted to WA6NUT. The digital voice SNR reading is 16.

Figure 7 is a software signal flow diagram for the Video Receive PC. The motherboard sound card, together with the video receive software, is used to process the received video signal from the sound card interface and to display the FreeDV+ video image. Note how Figure 7 is an implementation of the scheme in Figure 2 — except that the digital voice receive processor is located on the other PC, as shown in Figure 5.

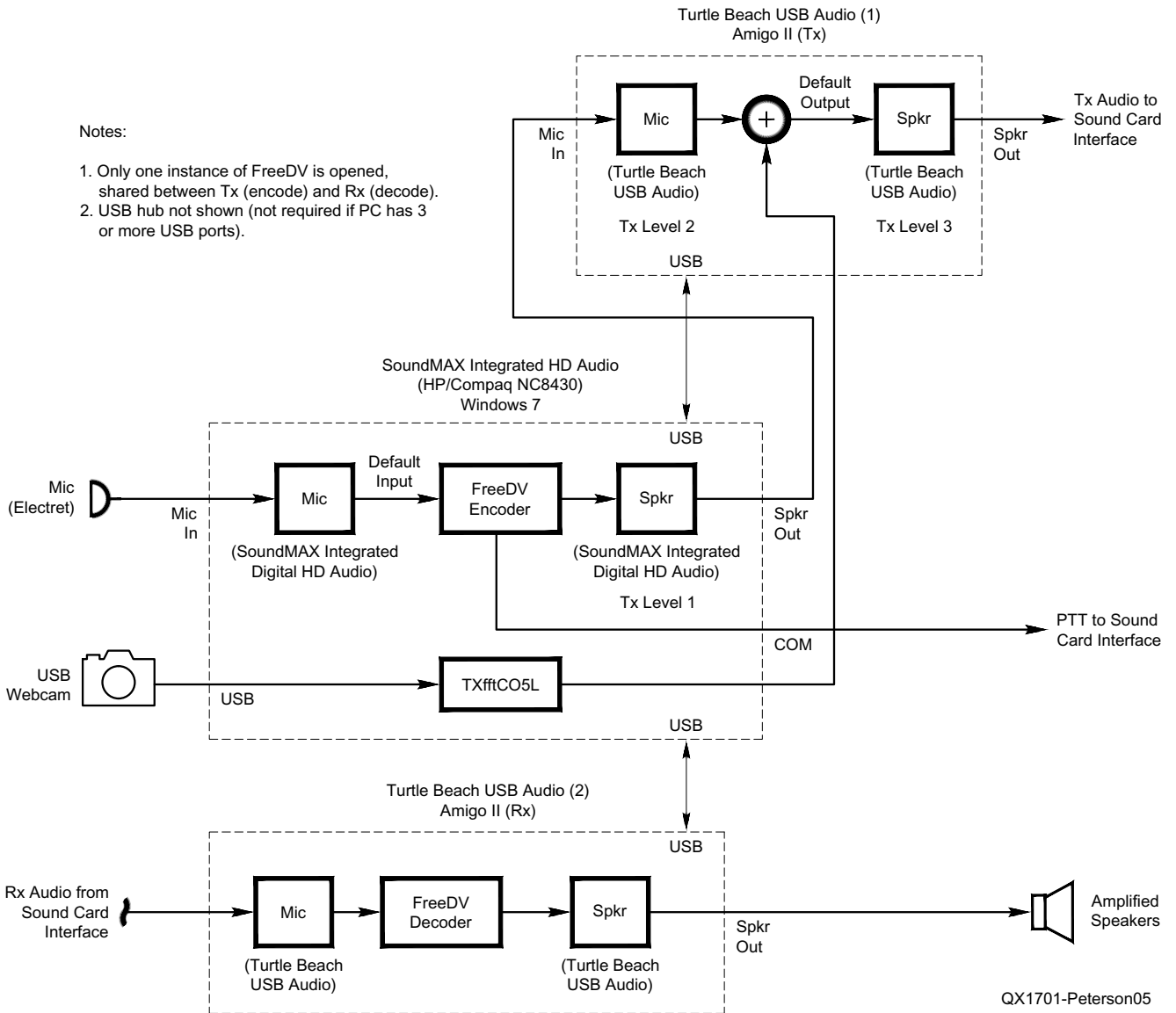
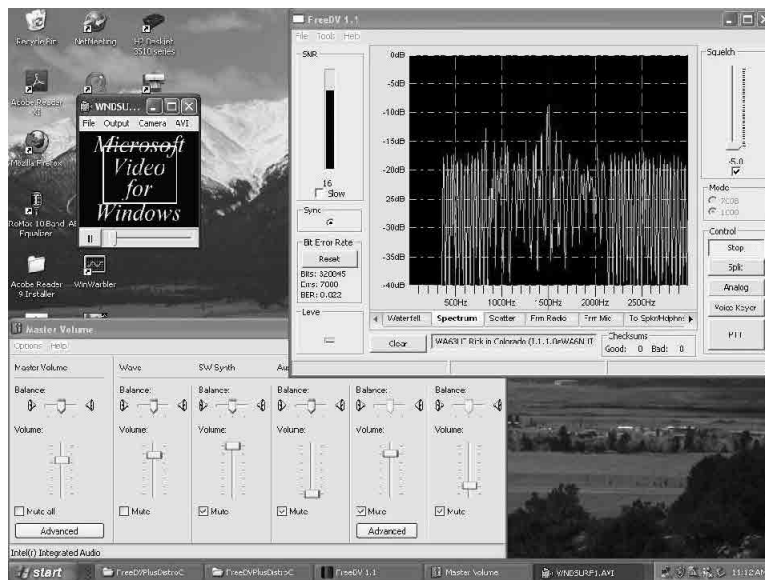


Figure 5 — Software signal flow diagram of FreeDV+ transmit setup.

Figure 6 — Video TX/ FreeDV+ computer screenshot.



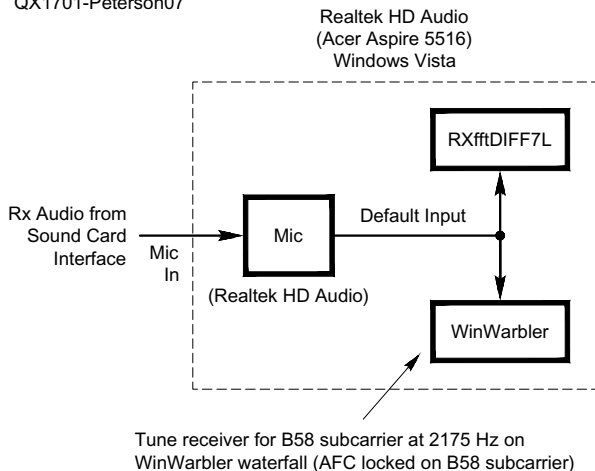


Figure 7 — Video RX/Free DV+ video receive computer setup.

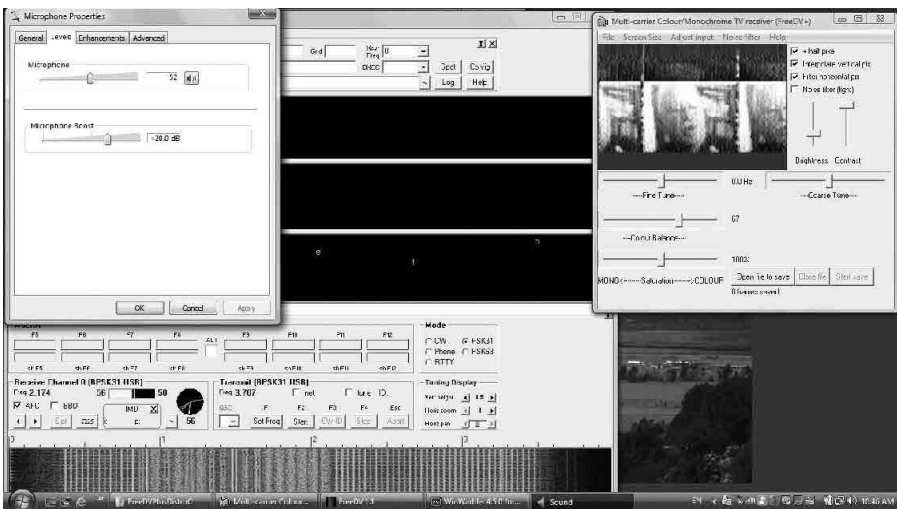


Figure 8 — Video RX/FreeDV+ computer screenshot.

The received FreeDV+ signal is also processed by the WinWarbler application. WinWarbler's AFC is used to read out the frequency of one of the video subcarriers (B58, with a nominal frequency of 2.175 kHz). Figure 8 shows the receive tuning of the transceiver set so the AFC readout indicates 2.174 kHz, 1 Hz low, since the receiver is tuned to compensate for frequency drift in the transmitter and/or receiver.

Figure 8 shows a screen shot for the receiving station Video Receive PC running with the Windows Vista™ OS. Note that the Record (Microphone) slider control for the motherboard sound card is set to 52 (GUI titled "Microphone Properties"). Live video from WA6NUT is displayed on the video receive software GUI. The display consists of one complete frame and whole or parts of one or two other frames. This "feature"

greatly simplifies the software required for horizontal sync. The video lags the digital voice by 2 to 3 frames. Note that the effects of IMD are visible in the video image as vertical noise. The WinWarbler waterfall is shown at the bottom, with the AFC locked to the B58 video subcarrier — shown as a yellow trace. See the FreeDV+ website (Note 13) for a full-color version of Figure 8.

Each frame of the displayed FreeDV+ video is like a snapshot of a sideways waterfall display, with 36 horizontal lines (one for each luminance subcarrier). The upper lines in the FreeDV+ image correspond to the higher luminance subcarrier frequencies. Noise, due to QRN or IMD, appears as vertical lines in the displayed image.

The video receive software (RXfftDIFF7L), along with the video transmit software (TXfftCO5L), is part of the FreeDV+ software suite, which can be



Figure 9 — FreeDV+ video from WA6NUT received by W4BCX 1,600 miles away.

downloaded from the FreeDV+ website. The AA6YQ WinWarbler software can be downloaded from the WinWarbler website.¹⁵

More details for setting up and adjusting the FreeDV+ software is found on the FreeDV+ website, and in the PDF document included with the FreeDV+ download.

The author's station uses an Apache Labs ANAN-10E SDR transceiver, and transmitted video and audio are monitored with a Ten Tec Omni VII transceiver. Adaptive pre-distortion (PureSignal in the ANAN-10E) is necessary to avoid splatter on adjacent frequencies. An HF Packer, with an Ameritron AL-811 amplifier are used to obtain an average output power of 60 W. Best DX to date is about 1,600 miles, from WA6NUT in Colorado to James Knighton, W4BCX, in Florida. WA6NUT transmitted FreeDV+ while W4BCX transmitted FreeDV (without video). Figure 9 shows one frame of the WND SURF1.AVI video clip as received by W4BCX. The windsurfer is silhouetted against the yellow sail of the sailboard.

Rules and Regulations

In the US, FCC regulations, Part 97 paragraph 97.307(f)(2) specifically places bandwidth requirements on "a multiplexed image and phone emission." The regulation states that the bandwidth "shall not exceed that of a communications quality A3E emission." The 3.5 kHz bandwidth required for FreeDV+ is much less than the 5 to 6 kHz bandwidth allowed for "a communications quality A3E emission" (double sideband AM).

However, the "rule of the considerate operator" also applies here. The "considerate operator" will refrain from causing QRM on adjacent frequencies, especially with a wide-bandwidth mode like FreeDV+. Such an operator will carefully check adjacent frequencies for activity before putting a FreeDV+ signal on the air. The operator will also keep sound card output levels low to avoid IM products on adjacent frequencies.

Problems with FreeDV plus Video (FreeDV+)

FreeDV+ requires HF transceivers with good frequency stability and tuning resolution in order to obtain acceptable quality in the received video image. Manual tuning of the receiver in one Hertz steps is required to compensate for frequency drift in the transmitter and/or receiver. However, only minimal receiver tuning is required after the transceiver warms up and stabilizes. This problem could be eliminated by adding automatic frequency control (AFC) to the video receive software.

The author encountered a “problem” when testing FreeDV+ with an AL-811 linear amplifier while monitoring the signal on the station Kachina 505DSP receiver. After adding the AL-811 to the setup, the S meter reading on the monitor receiver read S-9+ compared with S-6 previously. Also the video image become noisy, with lower FreeDV SNR of 6-7 dB. The author immediately, and incorrectly, assumed nonlinearity in the amplifier was the culprit. But further testing showed that the receiver was at the onset of overload, with receiver IM products causing the noisy video and poor SNR. By switching the receiver preamp off, and the receiver attenuator on, the author was able to obtain good video quality with a FreeDV SNR of 10-12 dB, with a received signal level of S-6 with 60 W output power using the AL-811.

Conclusions

The author has shown how FDMA can be used to combine software applications resulting in a new multimedia mode. When multicarrier modes are combined, the only software modification required is the adjustment of subcarrier frequencies for compatibility between the combined modes. FreeDV+ is a work in progress, and like any experimental mode, there is room for improvement. For ease of use, the mode

would benefit from the following added features in the video receiving software (RXfftDIFF7L).

Horizontal sync

In the present design, horizontal sync requires the display of two received images. The software could be redesigned with a horizontal sync scheme allowing the display of a single received image. More recent versions of the ZL2AFP NBTv software incorporate horizontal sync with a single displayed image.

Automatic frequency control (AFC)

The present design requires manual retuning of the receiver to keep correct hues in the received image. Retuning compensates for frequency drift in the transmitter and/or receiver. Retuning would be unnecessary if (a) the transceiver frequency synthesizers with OCXO or GPSDO frequency sources are used — this is not really a practical solution — or (b) AFC is added to the video receiving software — similar to the AFC in the FreeDV digital voice software. It might be possible to adapt the AFC scheme used by Moe Wheatley, AE4JY, in his PSKCoreDLL software. The AA6YQ WinWarbler PSK31 software is based on the PSKCoreDLL engine.¹⁶

Richard R. Peterson, WA6NUT, is an Amateur Extra class licensee. He has been licensed since 1960 and is active on digital voice, narrowband TV and other HF sound card modes. He has had articles published in QEX previously. Rick retired in 1995 from Delco Systems, General Motors Corporation, where he was a Senior Engineer responsible for analog circuit design for inertial navigation systems. He holds one patent related to electric vehicles. He received a BS degree in Engineering from UCLA in 1963. Rick is a member of the Radio Club America, the British Amateur Television Club, the Chaffee-Lake Amateur Repeater Association and is an ARRL Volunteer Examiner.

Notes

¹See, [electronicdesign.com/communications/fundamentals-communications-access-technologies-fdma-tdma-cdma-ofdma-and-sdma](http://www.electronicdesign.com/communications/fundamentals-communications-access-technologies-fdma-tdma-cdma-ofdma-and-sdma).

²T. Pratt, C. W. Bostian, and J. E. Allnutt, *Satellite Communications*, 2nd edition, John Wiley & Sons, New York, 2003, pp. 223-233, describe FDMA. Errors have been found in some of the worked-out examples, but that the formulas are believed to be correct.

³PC-Microphone ‘Echo’ caused by Mic Monitor feature, Turtle Beach Knowledgebase <https://support.turtlebeach.com/hc/en-us/articles/221179108-DP11-PC-Microphone-Echo-caused-by-Mic-Monitor-Feature>.

⁴Search in your browser, “How to set up USB Audio in Windows”.

⁵Search in your browser, “How to Listen to Your Own Voice in Windows”.

⁶See **Note 2**: example p. 228 describes calculating locations of third-order IMD products. Note errors in worked-out example; but formulas are correct.

⁷A. Gangwar, M. Bhardwaj, “An Overview: Peak to Average Power Ratio in OFDM system and its Effect,” www.ijccts.org/books_pdf_dwd/An%20Overview%20Peak%20to%20Average%20Power%20Ratio%20in%20OFDM%20system%20&%20its%20Effect.pdf.

⁸D. R. Cheruku, *Satellite Communication*, IK International Publishing House, New Delhi, 2010, p. 205 describes power sharing.

⁹See **Note 2**: example pp. 231- 232 describes power sharing.

¹⁰A. Katz, “Linearizing High Power Amplifiers,” describes linearization techniques in high power amplifiers, including adaptive pre-distortion, www.lintech.com/PDF/hpa.pdf.

¹¹www.adonis.ne.jp/e-other.html.

¹²Introduction to NBTv software, www.qsl.net/zl1bpu/NBTv.

¹³FreeDV plus Video web page www.qsl.net/wa6nut/FreeDVplusVideo.

¹⁴Transceivers suitable for eSSB, most are also suitable for FreeDV+, www.nu9n.com/essb_ready_rigs.html.

¹⁵WinWarbler, www.dxlabsuite.com/win-warbler.

¹⁶See Section 3.2.8 in www.moetronix.com/ae4jy/files/pskcoredll141.pdf.

An Improved Audio-Frequency Bandpass Filter for Morse Code Reception

A look into the filter design rationale that explains why receivers with “rounded top” selectivity curves sound better to the CW operator, no matter how that selectivity is achieved.

In April of 2013 I proposed to Ed Wetherhold, W3NQN, that an unusual design should be used for an audio-frequency band-pass filter for Morse Code (“CW”) reception. The filter was to be added on to the output of receivers used for CW work. Over the years, Ed had accumulated a number of toroidal inductors with a nominal 77 mH value and was using these inductors for building audio-frequency band-pass filters. Hence his well-known *nom de plume* “Filter Builder” in the Amateur Radio fraternity. I suggested to him a passive filter design, which used only one value of inductor. It was tailor-made to use some of Ed’s stash of 77 mH inductors. Ed thought the design had merit and built several, and put them out into the field for testing. Feedback revealed the concept was quite satisfactory.

This article examines the CW filter design rationale, and explains why receivers with “rounded top” selectivity curves sound better to the CW operator, no matter how that selectivity is achieved.

The Problem

The IF response of the receiver used by a typical CW operator has a flat top with a width of typically 400 Hz. Figure 1 illustrates such an IF response. We have set the filter center frequency to 500 Hz for our tests. The filter bandwidth extends from 300 Hz to 700 Hz and drops off rather sharply beyond those limits. We are looking here at the response down at audio, not at the IF itself. Now we will apply a single CW “dit”, a burst, into that IF and see what exits. We can expect it to be distorted — and to sound distorted as well. In fact, it appears as shown in Figure 2.

Such a signal corresponds to a 24 WPM Morse signal, typical of CW operators. The signal can be seen to be somewhat distorted at the leading and trailing edges. Time-domain analysis is being done here by *Elsie*, the filter design and analysis program.¹ *Elsie* also has

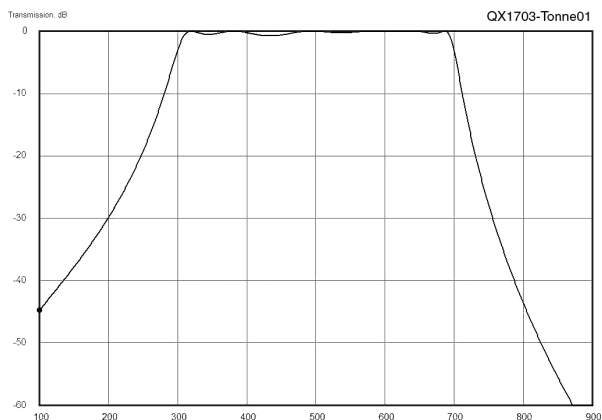


Figure 1 — Response of typical IF strip.

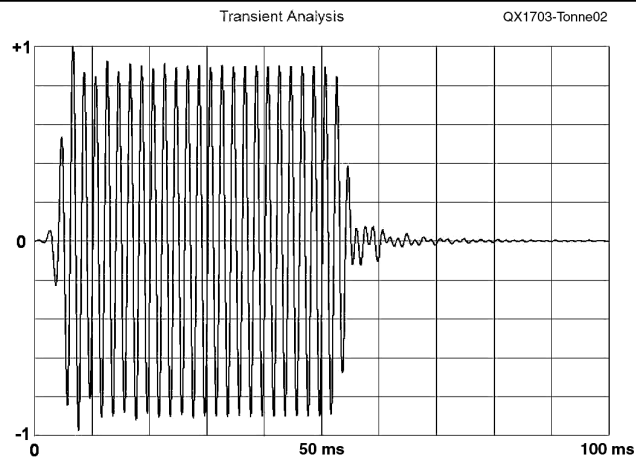


Figure 2 — A test pulse as it exits from that IF viewed at audio.

a very useful option of revealing the *envelope* of that time-domain waveform. Using this option reveals the distortion more clearly.

Figure 3 shows the envelope of this burst. The clearly visible ringing seen in this graphic forecasts an audibly obnoxious sound, the kind of sound CW operators find objectionable. This distortion is caused in large part by the group (envelope) delay distortion resulting from the sharp cutoff at the IF filter band edges. Group delay distortion is a common byproduct seen in a filter with a sharp band edge. Group delay equalization can reduce these effects to a limited extent. Figure 4 shows the amplitude response (top trace, left scale), and the group delay (lower trace, right scale) of the same IF filter.

Consider the keyed CW signal as a modulated wave. As we go out from “carrier” (500 Hz in this discussion), the “sidebands” go down uniformly in amplitude. But if they are not handled correctly in both time and amplitude, the signal will not sound pleasing. If some of those sidebands happen to be delayed more than they should we will have ringing. This is what we see in Figures 2 and 3.

The ringing gets worse as the CW speed increases to 30 or 35 WPM. If we can’t change the shape of that filter response then we’ll have to do something else to improve the sound quality.

A Solution

One way to improve the situation is to modify the *system* response

by adding a second filter to the system at the receiver output. This “add-on” filter would have a somewhat rounded top and it would be noticeably narrower than the usual IF bandwidth. The responses of this add-on filter are shown in Figure 5, where the upper trace is amplitude and the lower trace is group delay.

This add-on filter is narrower than the IF strip and has a more gentle response in both magnitude and time. The system magnitude responses with (solid line) and without (dashed line) the add-on filter are shown in Figure 6.

The added audio band-pass filter adds some selectivity to the receiver. When we have added the new filter to the receiver we have narrowed the system bandwidth, but we’ve also rounded the top of the response. The impact of the rounded top on signal response at band-edges as can be seen in Figure 7. That pair of plots shows the system magnitude response (the upper plot) and group delay (the lower plot). The group delay of the sidebands at the band edges is significant, but notice that the add-on filter has reduced the magnitude of the sideband components at band edge to a very low amplitude. As a result, group delay problems at those frequencies are of much less consequence. We can expect the behavior of the system to be improved over the behavior of the receiver IF filter alone.

Passing the “dit” burst through the system now results in an output as shown in Figure 8. Compare this with Figure 3. The burst waveform shape is obviously improved. Reports from the units

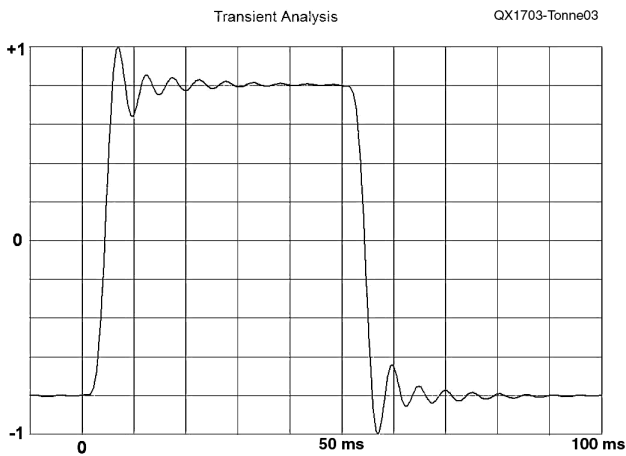


Figure 3 — The envelope of the burst shown in Figure 2.

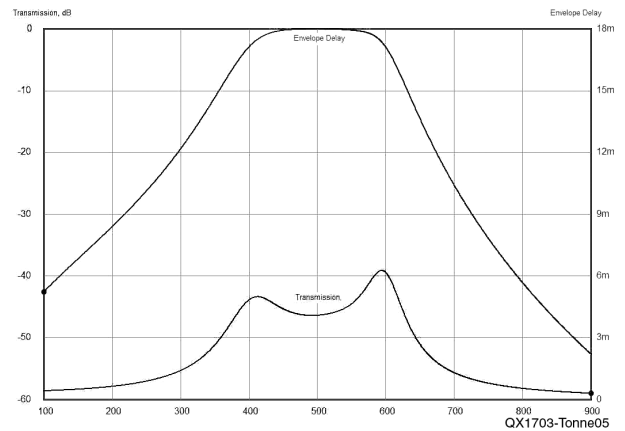


Figure 5 — Magnitude response of the add-on filter (upper plot) and group delay (lower plot).

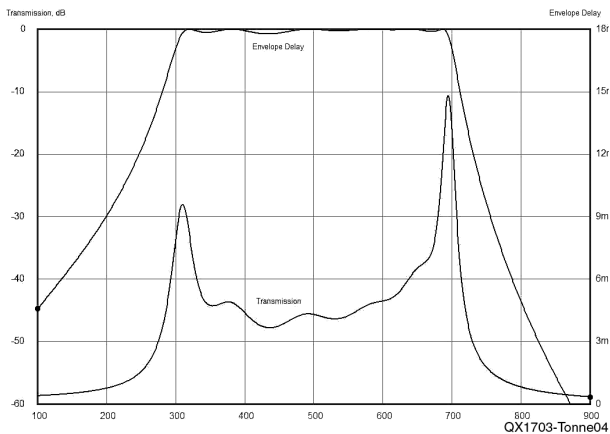


Figure 4 — Magnitude response of the receiver IF strip (upper plot) and the associated group delay (lower plot).

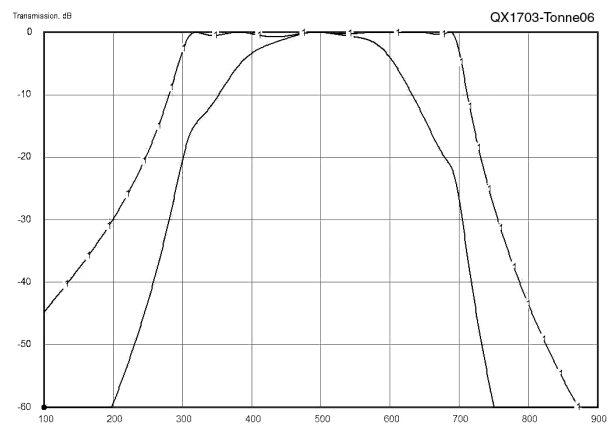


Figure 6 — The original receiver magnitude response (upper plot) and overall magnitude response with the add-on filter (lower plot).

delivered to the field consistently report that a CW signal passing through this filter sounds better than does a signal from the receiver IF alone — our expected result.

The add-on filter effectively masked the overshoot problem caused by the flat-topped IF filter in the receiver. This is because the add-on filter has removed the band edge components that would have caused the overshoots in a controlled manner. Another feedback item we see from the field is the reduction of noise when this filter is switched into the system. Let's see why this might be.

When the filter is analyzed using *Elsie* we see that the noise bandwidth of the filter is somewhat under 200 Hz (close to the 3 dB bandwidth displayed in Figure 5) using the analysis of Figure 9. Because the add-on filter is narrower in bandwidth than the receiver IF bandwidth, it determines the system noise bandwidth. Recall that the receiver IF noise bandwidth (Figure 1) is about 400 Hz.

Waveforms and Spectra

The pulse waveform used for this article has envelope rise and fall times of zero. The behavior of the system does not change until those times are increased to greater than about 1 ms. An interesting observation was made during the data-gathering portion of this research. The recommended rise and fall time of 5 ms in the transmitted signal essentially negates the need for the filter such as

the one under discussion. The next set of graphics illustrates this point using the *LTspice* analysis tool.²

Figure 10 shows the raw keyed CW signal applied to the filter with envelope rise and fall times set to zero. The spectrum of this signal is shown in Figure 11. The sidebands extend outward symmetrically and slowly drop off in amplitude. This situation results in “key clicks”. Applying a 5 ms rise time and fall time to the envelope of the

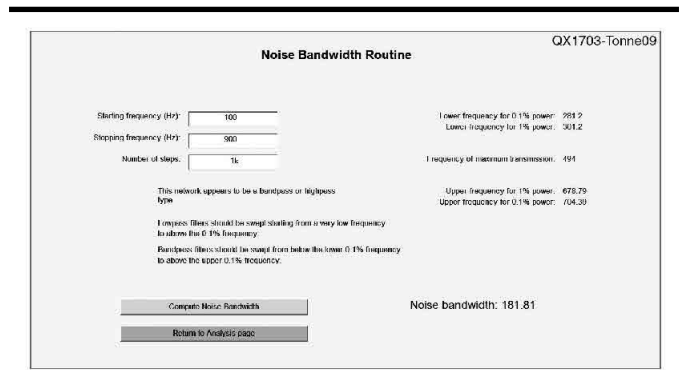


Figure 9 — Noise bandwidth analysis capability in *Elsie* software.

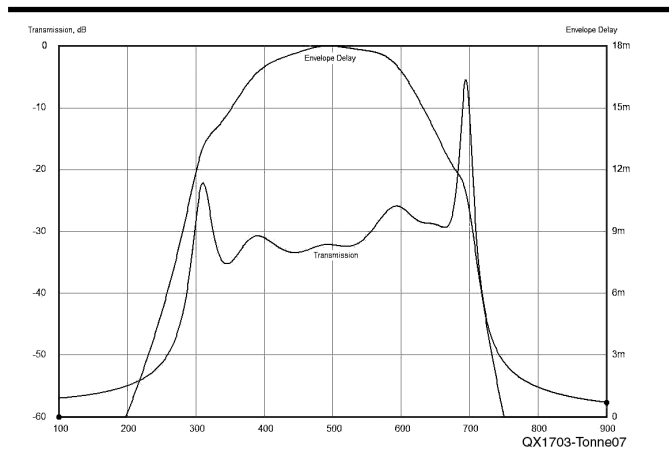


Figure 7 — Magnitude response of the overall system with the add-on filter (upper plot) and system group delay (lower plot).

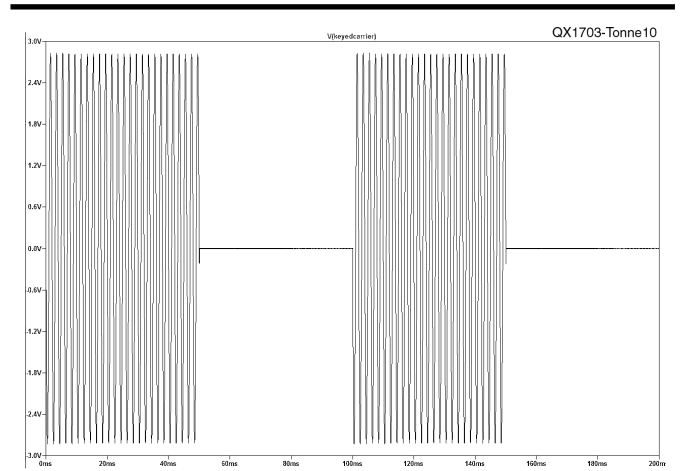


Figure 10 — Excitation waveform applied to the add-on filter.

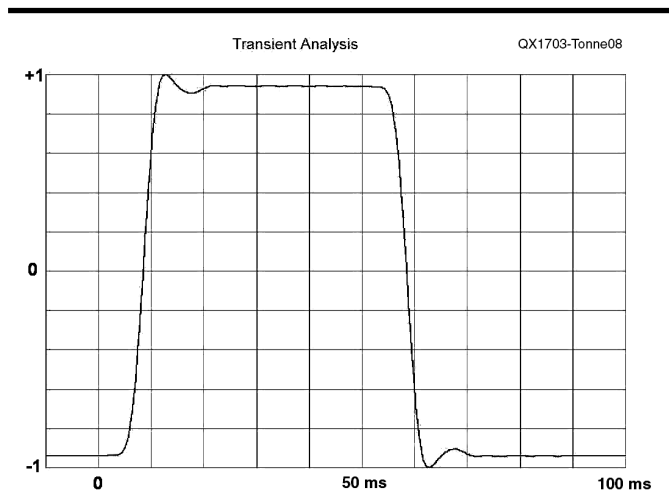


Figure 8 — The envelope of the burst when the add-on filter is used.

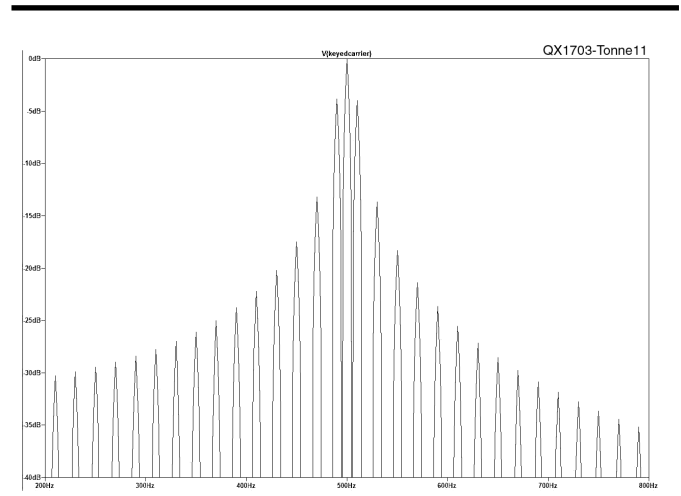


Figure 11 — The spectrum of a raw (unshaped) keyed CW signal.

pulse results in the response shown in Figure 12. The signal has a narrower bandwidth as can be seen in Figure 13. The signal occupies a noticeably narrower bandwidth, as compared with the spectrum in Figure 11. Passing this transmitted signal through our narrowband add-on filter should not result in significant alteration because the signal has already been made narrowband.

The rise and fall times were controlled by using a single-pole low pass (an RC network) filter with a rise time to 90% of 5 ms. Now we'll apply that narrowband signal (shown in Figure 12) to our add-on band-pass filter, to get the response seen in Figure 14. The difference between the waveforms of Figure 12 and Figure 14 is small and we see little ringing. Ringing causes the harsh sound that is objectionable to the CW operator.

The transmitted signal, narrow banded by controlling the rise and fall times of the envelope, is hardly altered in wave shape when additionally passed through the add-on filter. Bandwidth limiting of a transmitted CW signal is further discussed in the *ARRL Handbook*.³

I did not include the effects of the receiver IF filter for the *LTspice* analyses because the add-on filter band width is smaller than the IF bandwidth. The IF filter effect would be slight.

An Equivalent Active Filter

During the data-gathering portion of this paper, some correspondents asked about an active filter equivalent. Active band-pass filters are generally symmetrical on a geometric basis. Rephrased, they attenuate a given amount when the test frequency is changed by a given *factor* rather than by a specified frequency *shift*. As a simplistic example, the attenuation of the filter is typically the same when the test frequency is an octave below or an octave above the center frequency. When their responses are plotted on a linear frequency scale it can be seen that they commonly have poor attenuation on the high side of center.

A correctly behaving active filter design, that is to say one that attenuates about the same on both sides of the center frequency, has its response shown by the dotted points in Figure 15. The solid line in Figure 15 shows the response of our passive filter. The bandwidth of the active filter has been adjusted to be about the same as the field-proven passive filter. The top is somewhat narrower, and is more rounded. This active version has not yet been field tested. The output of this active filter subjected to our test burst is shown in Figure 16. This active filter is shown schematically in Figure 17.

Note that we have two multiple-feedback band-pass filter sections and three low-pass

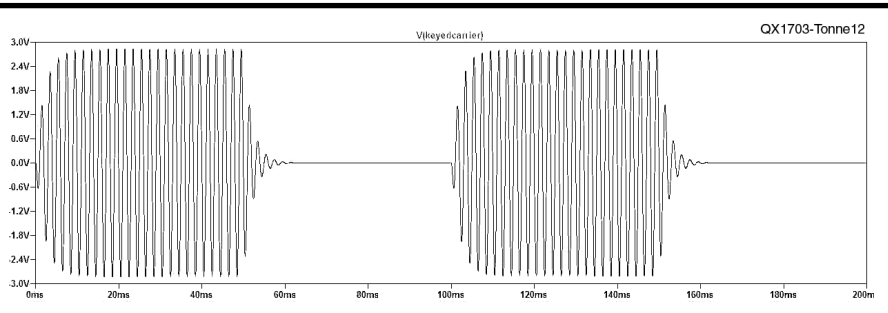


Figure 12 — The narrow banded pulse. The pulse was subjected to a 5 ms rise and fall time.

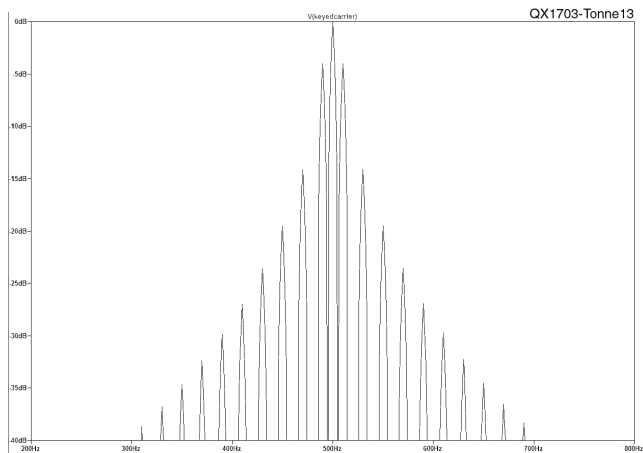


Figure 13 — Spectrum of the pulse when shaped by the 5 ms rise and fall time constraint.

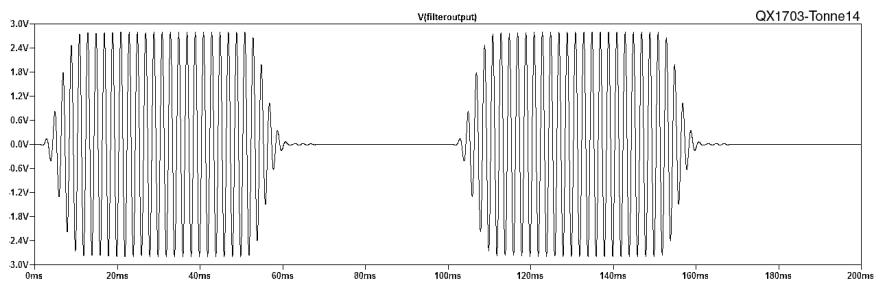


Figure 14 — The narrow band pulse of Figure 12 after it has passed through the add-on band-pass filter.

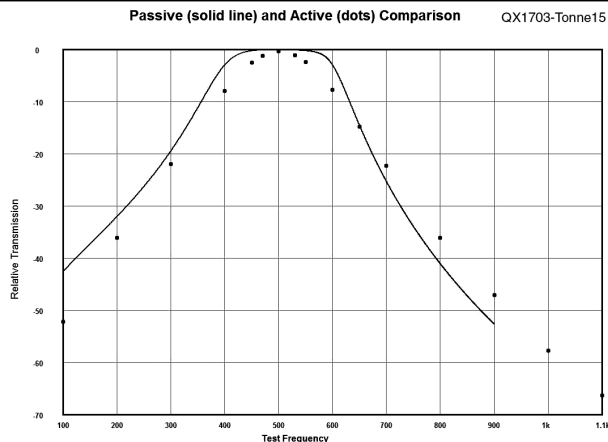


Figure 15 — Responses of the passive version of the filter (solid line) and an active filter approximation (dots) using a linear frequency scale.

filter sections. This complexity is required to achieve the transmission shown by the dots in Figure 15. This active filter has a modest gain at its center frequency of 500 Hz. It is noticeably more complex than the passive filter seen schematically in Figure 18. Furthermore it requires power, although physically it is more compact.

The Passive Filter Schematic

Figure 18 shows the schematic for the passive filter with a center frequency of about 500 Hz, and shows optional input and output matching transformers. Exact component values were computed to use 77.5 mH inductors. All of the inductors are of the same specified value — an attractive feature of the design. A practical filter could use 5% tolerance component values, although tighter tolerances would be preferred. This design closely exhibits arithmetic symmetry about the center frequency.

The passive filter is to be driven from, and terminated in, impedances of about 125 Ω. Transformers are shown on the input and output for matching from an 8 Ω source and to an 8 Ω load. Be aware that the transformers can cause distortions and can cause false responses to appear. If driven into saturation, some degree of nonlinearity can result, and the transformer can have a non-linear frequency response.

Final Comments

The passive design topology is mesh-capacitor coupled. All inductors are of the same value. The response has arithmetic symmetry. That is, the responses on either side of the center frequency are treated equally. This filter is from the Butterworth family, hence has a smooth top in the passband and a smooth descent into the stop bands.

The inductor Q values are somewhat low,

about 40. This, too, contributes to a smooth, rounded pass band and a smooth descent into the stop band. Those filter attributes work together in a filter that has garnered numerous favorable reviews on eham.net.⁴ Ed Wetherhold has offered to supply components for this filter.⁵

James L. Tonne holds the Amateur Extra class call sign W4ENE, and was first licensed in 1951. His current Amateur Radio interests are largely focused on speech processing and filter design. He has written several articles for QST and QEX and was a major contributor to the RF and Filters chapter in the ARRL Handbook. He is the author of the Tonne Software package on the CD accompanying the ARRL Handbook and included as part of the downloadable package available on the ARRL website.

Notes

- ¹Free student edition, www.arrl.org/arrl-handbook-reference, professional edition, tonnesoftware.com/elsie.html.
- ²LTspice, Linear Technology Corp., www.linear.com/designtools/software/#LTspice.
- ³See the Digital Modulation section, Fig. 8.11 and associated text; *The ARRL Handbook Book*, 2017 Edition. ARRL item no. 0628, available from your ARRL dealer, or from the ARRL Store, Telephone toll-free in the US 888-277-5289, or 860-594-0355, fax 860-594-0303; www.arrl.org/shop/; pubsales@arrl.org.
- ⁴www.eham.net/reviews/detail/58.
- ⁵Ed Wetherhold, w3nqn@comcast.net.

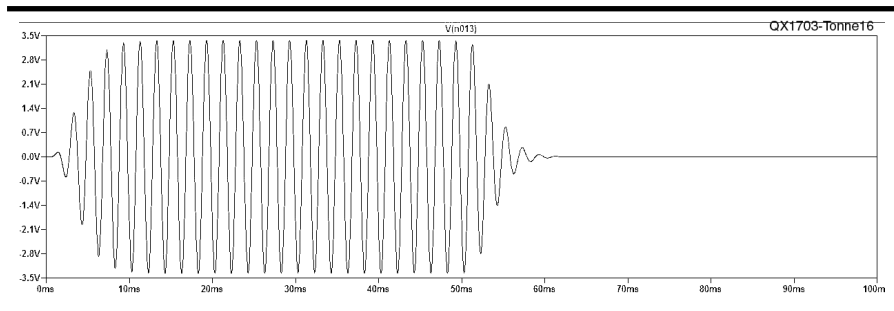


Figure 16 — Output of the active filter with the applied burst.

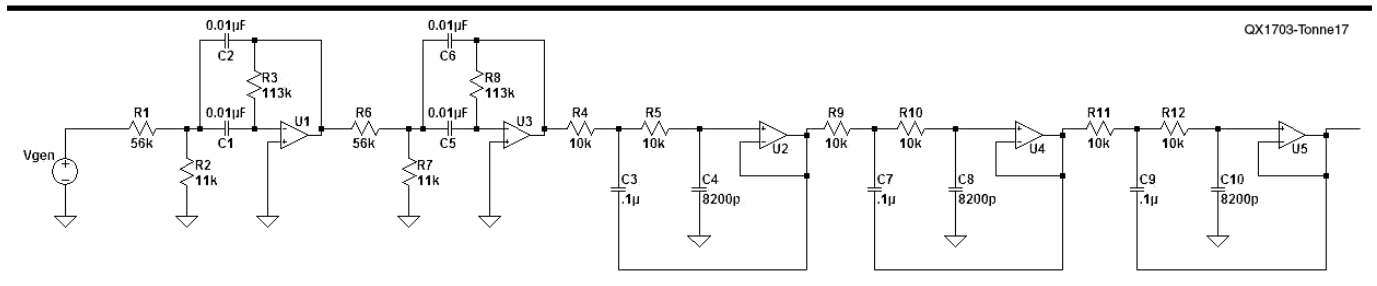


Figure 17 — Schematic of an equivalent active filter.

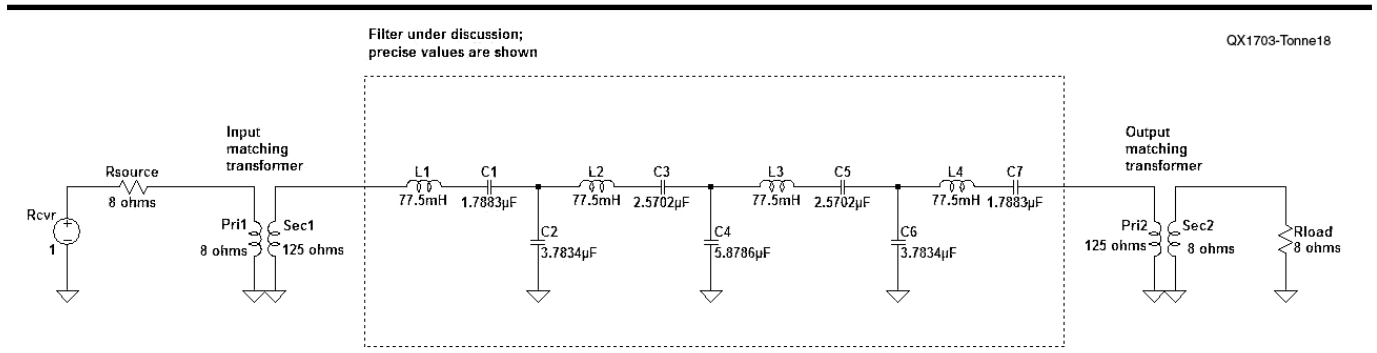


Figure 18 — Schematic of the passive add-on band-pass filter.

Apparatus for RF Measurements

This inexpensive test set needs just an ac digital voltmeter along with the inherent precision of modern components to generate precise, very low level digitally modulated RF signals in the amateur HF bands.

We describe an RF test set that provides very accurate, very low power levels down to -150 dBm or less for testing the sensitivity of digital radios or for testing analog radios. While working to determine the sensitivity of receivers for digital modes, we needed an easy and convenient means to make low level RF measurements. An objective was to generate stable, low-noise signals and use them to accurately test digital modulation modes at very low signal levels, below -150 dBm. We wished to achieve this with relative simplicity, using methods that a home experimenter could apply to investigate receiver and transmitter performance, and the performance of digital modulation modes. Other key objectives were to produce a test set that was simple to calibrate, would be much lower in cost, and be smaller than a typical array of test equipment previously needed for this type of application.

The usual equipment list for these types of measurements includes several expensive pieces of RF test and measurement hardware. We launched into a project to design a digital radio test set. This is a brief discussion of the results.

Test Set Features

The test set is simple, low cost and can be used on a table top. It requires just an ac digital voltmeter for set-up and calibration, and features continuous level adjustment of the input audio signal. It provides for high performance, accurate, low level RF measurements.

The test set uses low cost microprocessor-type crystal controlled oscillators along

with frequency division for stable, low noise signals. It enables comparisons of analog and digital modulation modes, and can be used with computer sound-card generated signals or with specialized digital modems commonly used with Amateur Radio communications, or with audio signal generators.

The test set can generate signals on the 20, 30, 40, 80 and 160 m bands in its standard basic configuration. It can be extended for use on other bands if desired, for a modest additional cost and parts count.

No electrical adjustments or measurements are necessary to change frequencies on the basic unit, which provides for standard receiver and transmitter measurements. The test set linearly translates modulated analog and digital RF signals to different frequencies in various amateur bands.

Features and uses are realized without the need for expensive test and measurement equipment. There is no need for RF step attenuators, stable well shielded laboratory grade RF generator, sensitive, accurate RF power meter, die cast aluminum or other shielded enclosures, costly RF connectors.

The Standard Test Set

Our original intent for this design was to make a test set that was low in cost, could be used on a table top, and not require large physical separation between transmitters and receivers. Especially important was the design goal of providing accurately known levels of RF power without requiring expensive test equipment, other than a good digital voltmeter.

The basic test set also generates accurately

known RF power level unmodulated CW signals in the 10 and 15 m bands and signals within a few kilohertz of other bands. Provisions are made for adding modulated RF signals in other bands, with additional components and materials. However, an analysis of typical amateur band receiver architecture and operation will show that digital signal radio performance can be adequately measured using only one or two frequency bands, so additional frequencies are not really required. Receiver front ends are used at low levels of RF power, and handle signals in a very linear manner, so there is negligible distortion. Receiver noise figures may vary somewhat from band to band, but this is not a significant factor.

As usual, due to the external sources of noise at HF frequencies, the HF noise figure of the receiver is not a significant contributor to the signal to noise ratio of the desired signal to be processed. So, the performance of the digital signal modes, along with other modes, is determined by the RF receiver IF through to the audio systems, not the linear frequency-translating front ends, and primarily by the computer software performing the actual base-band signal processing and demodulation. Therefore, the modulation modes can be tested and compared using only the 160, 80, 40, or 20 m band where leakage signals can be more easily controlled using inexpensive cables and connections.

Local oscillator (LO) leakage into the receiver is mostly from the LO amplifier and its power supply circuits, causing RF energy on the coax shields and into the RF/IF printed circuit board, and from leakage across the

mixer package — a surface mount package would be better but we had many of the metal can versions on hand. RG-400U double shielded coax with SMA connectors is used to connect the test board to the receiver. These leakage paths are manageable using 20 m signals due to the receiver's ability to filter out the LO that does get into it. The LO leakage is much reduced at 40 m and almost non-existent at 80 m when using inexpensive cable and RF connectors. However, fastening the 40 dB external attenuator directly to the receiver — through one SMA adaptor to the usual SO-239 connector — and using short lengths of RG-405 0.085 in/0.086 in semi-rigid cable — LO leakage is low enough to be of no concern at all frequencies.

Receiver Testing

For receiver, modem, and software testing, a modem — or a computer — provides the modulating audio signal to the test set. The ac voltmeter can be used to calibrate audio level, and hence ultimately the RF signal level. The test set is built on small PC boards using surface mount parts in order to reduce undesired RF radiation from the circuits and to provide predictable RF performance.

The RF output power from the test set is -73 dBm (nominal S9 level) for the fundamental frequency component on all bands, using only an audio range digital voltmeter at a level of 1 V. The 1 V signal passes through an accurate attenuation, and jumper-selected attenuation on the PC board, along with a means for variable attenuation, and into the mixer IF. This provides a continuously variable RF signal of known amplitude from -73 dBm down to -152 dBm. All attenuators are constructed using SMD 1% resistors — costing around 10 cents each — mounted on PC boards.

PSK31, RTTY, CW, and other modes have been successfully tested with these test sets, and basic minimum discernible signal (MDS) was measured on various receivers.¹ PSK31 signals have been decoded at known RF levels well below the receiver MDS (specified in the SSB bandwidth), or noise floor, at levels below -140 dBm. *Digipan* and *MMTTY* software were used to drive a Signalink USB digital modem to modulate and demodulate signals.

Measuring Transmitters

The process could be reversed and a transmitter can be modulated with a modem, attenuated and used to insert a +10 dBm or less signal into the mixer at the RF port through the first 20 dB attenuator on the board. This makes a low gain, low sensitivity receiver to control unwanted RF signal radiation from the transmitter. This receiver is linear and has predictable performance. The IF output routes into the buffer amplifier to provide a modem

with a signal to decode. This process tests the transmitter without a complex receiver in the path. Alternatively, once a receiver, modem, and software have been tested, transmitters can be operated into that combination and checked for signal quality.

Test Set Hardware and Techniques

A picture of the test set in use on the development bench is shown in Figure 1. The test set comprises two PC boards that are separated by the straight piece of coax cable seen in the photo. For lowest cost, we soldered cable connections, eliminating intermediate connectors.

One PC board, the LO generator portion of the test set, is seen in the upper center of Figure 1. The second board, the IF/RF portion of the test set, is seen in the lower center of Figure 1. The physical separation of the boards helps to avoid the need for shielded enclosures and expensive connectors. A different arrangement, better

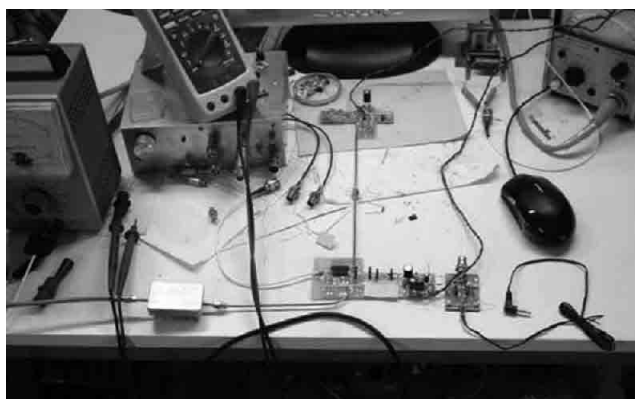
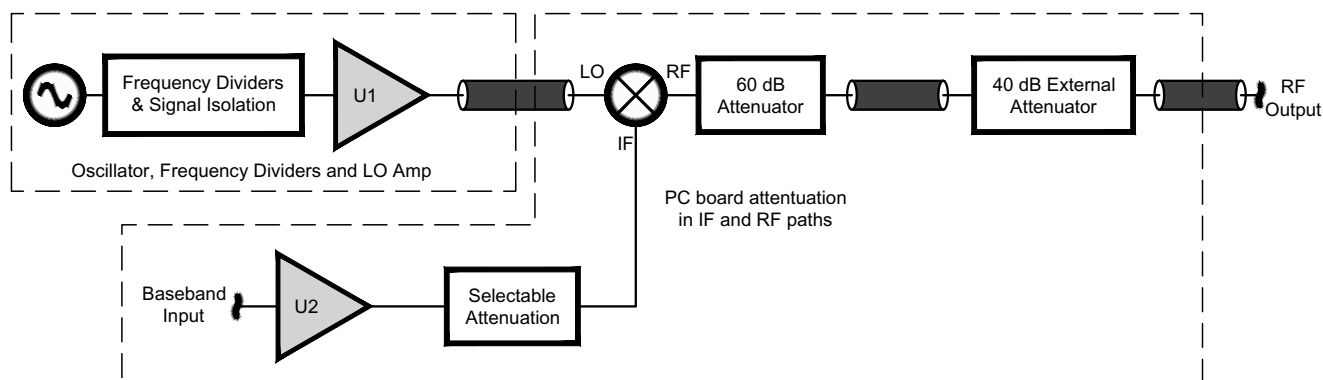


Figure 1 — The complete RF test set consists of the two PC boards separated by the straight piece of coax cable. For lowest cost, soldered-only cable connections can be used, eliminating any intermediate connectors. One board is at the top center, and connects by the vertical coax to the other board seen near the bottom center.



QX1701-Pontius02

Figure 2 — Block diagram of the RF test set shows the oscillator, frequency divider, LO amplifier portion, and the mixer and attenuator portion.

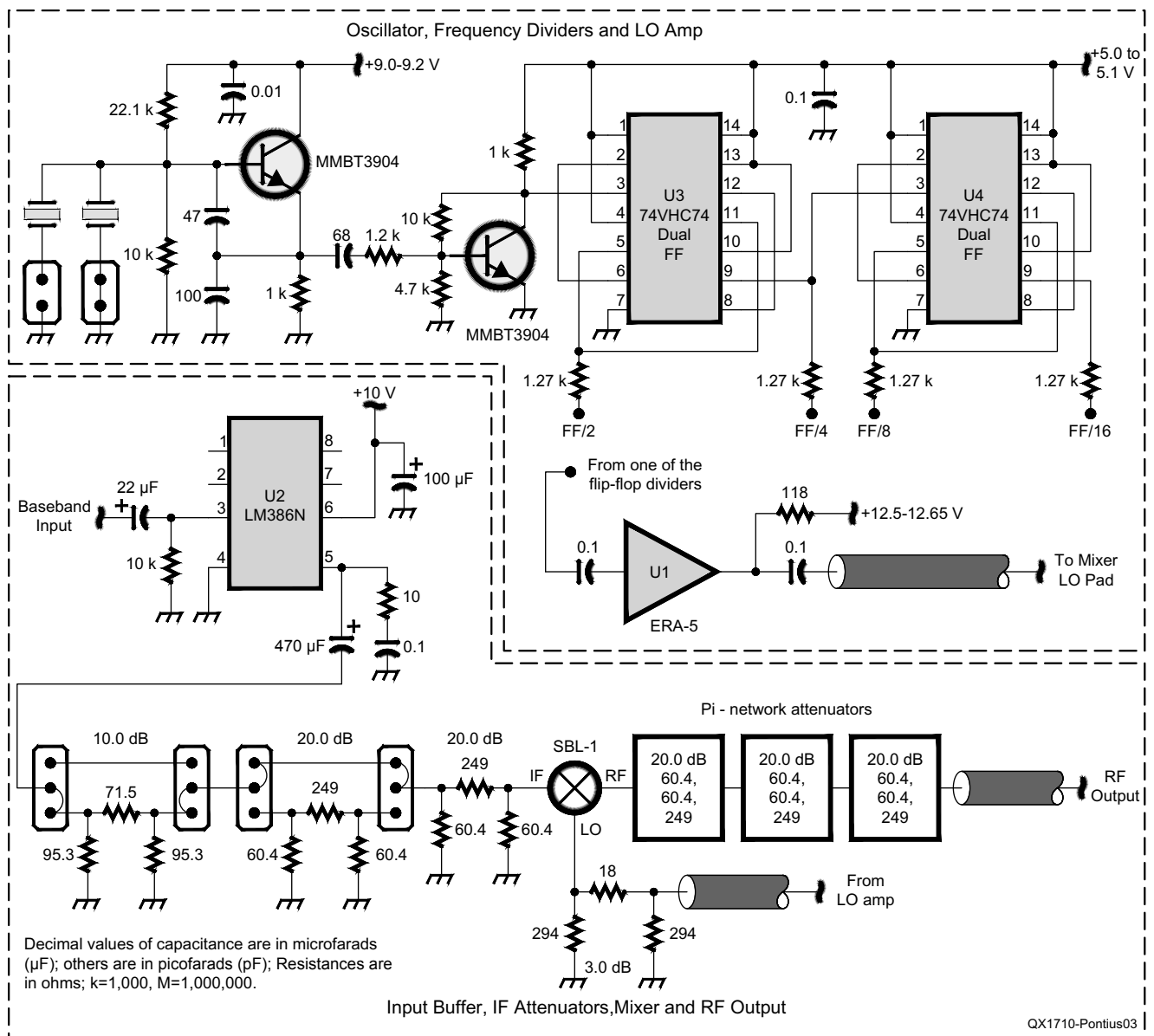


Figure 3 — Schematic diagram of the RF test set shows the components of the oscillator, frequency divider, LO amplifier PC board, and the components of the mixer and attenuator PC board.

than that shown in the picture, is a straight, in-line connection of the test set boards, as implied by the linear arrangement of the test set blocks shown in Figure 2.

When the external attenuator is used, it is screwed directly onto the receiver antenna connector through one adaptor. An RG405 coaxial cable attaches to the attenuator and is soldered to the RF output pad on the PC board. This in-line arrangement saves a cable and connectors, provides for low LO leakage into the receiver. Use a short piece of wire from the cable center conductor to a PC board pad. This makes it easy to connect and disconnect a cable, since the short wire is removed first, making it easy to then unsolder

the cable jacket. The cable jacket can be soldered only on one side, rather than all around, making disconnections easier.

The external 40 dB attenuator is on the lower left side in the small shiny box — an Altoids box will also work — in the RF output line at the lower left in Figure 1. The circuit board on the lower far-right of the lower PC board, with the black audio cable attached, was used to connect to a computer for digital signal sources. This circuit is not required for normal use of the test set, but was utilized here for flexibility of sources that were used during development. A Signal Link USB modem with a low noise internal sound card was used along with a computer.

The short white cable on the left side of the lower section was used during design and evaluation. Three of the units have been built and all accomplish the desired functions. To keep costs and complexity low, the test set was designed for use primarily with amateur transceivers having adjustable frequency, and available narrow crystal filters. However, there are techniques for working with crystal controlled, narrow tuning range, or fixed frequency low power PSK transceivers.

Block Diagram

A block diagram of the test set is shown in Figure 2, with schematic diagram shown in Figure 3. A crystal oscillator operating in

the 28 MHz band is divided down by two dual flip-flops (FF), U3 and U4, to produce signals in the 20, 40, 80 or 160 m bands. Amplifier U1, a Minicircuits Labs (MCL) ERA-5 feedback amplifier, serves as the LO amplifier, and connects to one of the four frequency divider outputs corresponding FF/2, FF/4, FF/8 or FF/16 to the frequency desired. The mixer in Figure 2 is the MCL SBL-1.

In Figure 2 the signal at the LO mixer port is an RF tone. The signal in the IF mixer port is an audio tone or a baseband digital waveform. Its level is well known by measurement with a digital volt meter at the baseband input, measured at the U2 output. The signal out of the RF mixer port is a double sideband suppressed carrier RF signal — remember we are using a double-balanced mixer here. The output level is very nearly 6 dB below the level of the IF port signal.

Figure 3 shows the schematic diagram of the test set. The attenuators at the output of the mixer are surface mounted on the PC board, their implied topology is a Pi-network with 60.4 Ω shunt and 249 Ω series resistors. A 40 dB external attenuator, like the ones on the PC board, is also used. It is housed in a shielded Altoids box enclosure.

Figure 4 shows the IF/RF portion of the test set, also seen in the lower center of Figure 1. The LO signal comes in the top coax, and RF leaves by the lower coax. The IF path is in between. At the right is U2, a standard LM386N audio power amplifier driving the IF attenuators at 1000 mV. The IF attenuators are adjustable using the pins (headers) and shunts. The RF fundamental frequency output power is accurately set at -73 dBm (nominal S9 level) using only an audio range digital voltmeter.

Calibration Not Explicitly Needed

Levels are set by the inherent repeatable and reproducible characteristics of the components, as in the 1% resistor networks. The double-balanced diode mixers from Minicircuits have well known signal level characteristics. The transfer function of these devices, IF to RF and RF to IF, and LO to either RF or IF ports are well defined, controlled and specified, with much data available from MCL.

A signal at the IF port is mixed with an appropriate LO signal at the LO port to generate a known RF signal, by the well known transfer functions, both calculated and measured values. These transfer functions are consistent, and almost frequency independent, over the range of 3.5 to 29 MHz for a 1 to 500 MHz mixer device, like the MCL SBL-1. The SBL-1 uses a 7 dBm LO.

You can measure these responses with

a wide-band thermal power meter like the HP-478A/432A power meters, a spectrum analyzer, a DSO, or a calibrated receiver. We used them all to verify performance. The output at the RF port from a 0.1 V (100 mV) ac source, at say 1 kHz, at the IF port, will result in predictable stable signals at the RF port of -13 dBm (within a few tenths of a decibel) for each sideband of the fundamental signal.

For a “calibrated result” all we need to do is measure the voltage available to the IF port using a low frequency ac voltmeter in order to know the RF output within a few tenths of a decibel. The fundamental value of each sideband of the ac IF signal at the RF output will be very close to -13 dBm. Then the accurate 60 dB attenuator on the PC board will yield the -73 dBm signal.

Three 20 dB precision attenuators on the PC board provide 60 dB of RF attenuation. A 40 dB external RF attenuator, like the one seen in Figure 1, plus a jumper selectable 0, 10, 20, or 30 dB of IF fixed attenuation is used, along with variable IF attenuation by adjusting the audio range signal level at the LM386N buffer amplifier output (10 to 12 dB range) using the ac digital voltmeter. This provides a continuously variable RF signal of known amplitude from -73 dBm to -152 dBm. The SMD attenuators on the PCB and the external 40 dB attenuators correlated well when compared to two HP 355D and two Kay Elemetrics 439A attenuators, and Pasternack attenuators.

The 1 V ac IF input signal results in a 0.1 V signal available to the mixer IF port. This creates an upper and a lower sideband at the mixer RF port. The receiver selects either sideband and rejects the other. When a 1 V dc signal is inserted at the IF attenuator chain, by opening the connection from the IF buffer amplifier, the sidebands merge into a single signal at the frequency of the LO. The power measured at the RF port of the mixer will be exactly 3 dB higher than the individual sidebands were when an ac IF signal was used.

Figure 5 shows the LO generator portion PC of the test set, also seen in the upper center of Figure 1. The circuit includes, left to right, a crystal oscillator, TTL type conditioner/FF driver, dual flip-flops U3 and U4, and (bottom) LO amplifier. The LO signal exits the bottom center at a level of about +10 dBm. This level is set by the consistent, frequency independent, and known level at the FF outputs, and by the consistent, frequency independent, and known gain of the feedback RF amplifier (the SMD ERA-5). The LO frequency is changed, if desired, by attaching the appropriate FF output wire to the LO amp input. No adjustments are required.

The crystal oscillator typically runs

From **MILLIWATTS**
To **KILOWATTS**SM
*More Watts per Dollar*SM

In Stock Now! Semiconductors for Manufacturing and Servicing Communications Equipment

- **RF Modules**
- **Semiconductors**
- **Transmitter Tubes**

Se Habla Español • We Export

Phone: **760-744-0700**
Toll-Free: **800-737-2787**
(Orders only) **800-RF PARTS**
Website: **www.rfparts.com**
Fax: **760-744-1943**
888-744-1943
Email: **rfp@rfparts.com**



RF PARTS
COMPANY

From Milliwatts to KilowattsSM

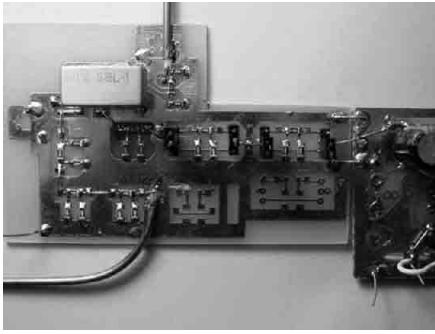


Figure 4 — The IF/RF PC board portion includes the mixer and attenuators.

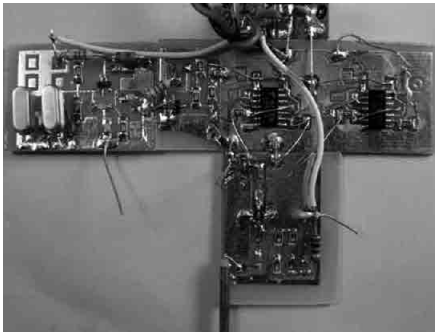


Figure 5 — The local oscillator, LO amplifier, frequency divider / flip-flop PC board.

at 28.220 MHz, or with other 70 cent microprocessor crystals in the 7 to 28.5 MHz range. The four (two per package) FFs in the center divide the 28.220 MHz by 2, 4, 8 or 16 to obtain 20, 40, 80 or 160 meter signals from the 28.220 MHz (or some other frequency in that range). The LO amplifier at lower center is simply jumper-tapped onto the desired FF output. There are no tuned circuits and no adjustments required for changing bands of operation. The conditioner circuit limits the oscillator signal to a 5 V square wave for the FFs. RF levels are determined by known levels at the FFs and the constant known gain of the LO amplifier to yield an LO drive

within about -0.5 to +1 dB of the desired +7 dBm without needing to make any RF measurements. There is a 3 dB attenuator at the mixer LO input on the IF/RF PC board.

The voltage from the adjustable IF buffer amplifier, and the precision attenuators determine the RF output. Signal leakage is adequately low and LO leakage and feed-through are controlled, to afford accurate measurements. The FFs divide the frequency for stability and lower noise, but they also provide a degree of signal isolation by separating the oscillator signal from the LO value being used. The small size of the SOIC packages keeps unwanted radiation down. These features help to avoid the need for expensive shielded enclosures and expensive RF connectors.

Conclusions

By exercising care, all receiver measurements can be accomplished with adequate accuracy, and modem performance can be evaluated. The process can be reversed and a transmitter can be modulated with a modem, attenuated and used to insert a +10 dBm or less signal into the mixer at the RF port through the first 20 dB attenuator on the board. This makes a low gain, low sensitivity receiver to control unwanted RF signal radiation from the transmitter. This receiver is very linear and has predictable performance. The IF output is routed into the buffer amplifier to provide a signal for the modem to decode. This process tests the transmitter without a complex receiver in the path. Alternatively, once a receiver, modem, and software have been tested, transmitters can be operated within that combination and checked for signal quality.

Our circuit boards were cut apart from one 5 in long by 3.3 in wide PC board that was manufactured by Far Circuits.

Modulators could be tested using RF links by linking two of these test sets together. The set on the transmitter side can use fewer on-board attenuators. Modems can

also be tested by directly connecting them to each other without any RF. Additionally, controlled noise levels can be inserted into the test procedures using op amps and a noise generator.

Bruce Pontius, NØADL, holds a BSEE degree and has been involved in the development of RF semiconductors, radio equipment and systems for many years. He participated in the development of early cellular radio equipment, digital trunking radios and narrowband data radio equipment. Bruce served as Engineering Vice President at E.F. Johnson Company for 15 years and worked with other companies in similar roles. He served as President of TRM Associates, working in wireless communications and RFID, until he retired. Bruce first got involved with Amateur Radio at age 11, building radios and test equipment with his father. He holds an Extra Class license and enjoys operating with simple equipment, portable operation, and doing RF tests and measurements.

Kazimierz (Kai) Siwiak, KE4PT, earned his PhD specializing in antennas, propagation and digital communications. He is a registered Professional Engineer and Life Senior Member of IEEE. Dr. Siwiak holds 41 US patents, has authored many professional papers and several textbooks. His writings appear in QST, QEX, and other ARRL publications. Kai holds an Amateur Extra class license, is a life member of AMSAT, and member of ARRL where he serves on the RF Safety Committee, is a Technical Advisor, QEX Editor, and QST Contributing Editor. He is an avid DXer and QRP operator, and was a team member with SAREX (Space Amateur Radio Experiment). His interests include flying (instrument and multiengine commercial pilot), hiking, and camping.

Notes

¹K. Siwiak, KE4PT, and B. Pontius, NØADL, "How Much 'Punch' Can You Get from Different Modes?", *QST*, Dec 2013, pp 30 – 32.

Letters to the Editor

How to Tune an L-network (Nov/Dec 2016)

Dear Editor,

I very much enjoyed the Chuck MacCluer, W8MQW, article. Although I knew how to determine if the resistive component of a complex impedance is 50 Ω by comparing voltage *magnitude* measurements, I had not seen it done by comparing voltage *phases*, and I was impressed both with this method and with its mathematical derivation.

But note that first transforming a load impedance so that its resistive component is 50 Ω applies only to half of the impedances represented by a Smith Chart: those that can be first tuned to lie on the Smith Chart's 50 Ω resistance circle. W8MQW's series *L*, parallel-*C* (*LsCp*) *L*-network does this tuning. But to tune the other half of the chart's impedances, the parallel-*C* must be moved to the front of the *L*-network, thus changing it from an *LsCp* to a *CpLs* topology. Then the series-*L* instead is first tuned so that the *conductance* of the transformed load *admittance* becomes 20 millimhos, after which the parallel-*C* would be tuned to reduce the remaining susceptance to 0.

W8MQW's phase comparison of V_r to $(V_f - V_r)$ lets us identify when the impedance lies on the 50 Ω circle, but not when the admittance lies on the 20-millimho conductance circle. So this measurement technique works only when tuning *LsCp* and not *CpLs* *L*-networks.

However, we can use his mathematical approach to develop a way to identify when a load conductance has been transformed to 20 millimhos (thus allowing us to cover the *CpLs* half of the Smith Chart). If we note that admittance $Y = I/V = G + jB$ and then we follow a path similar to his derivation, we discover that $Y - 0.02 = -0.04V_r/(V_f + V_r)$.

In other words, to determine if the conductance of the transformed admittance lies on the Smith Chart's 20-millimho conductance circles, we still use a V_r sample for one of our measurements, but we now compare its phase against a *voltage* sample $(V_f + V_r)$, rather than against the *current* sample $(V_f - V_r)$ previously used to determine if the transformed impedance is on the 50 Ω circle. So, for those impedances best matched with a *CpLs* *L*-network, W8MQW's two-step tuning technique would be: first tune *Ls* until V_r is 90 degrees out of phase from the voltage sample $(V_f + V_r)$. Then tune *Cp* until V_r is 0 (i.e. SWR = 1:1).

My thanks for a great, thought-provoking article. — *My best regards, Jeff Anderson, K6JCA.*

[The author replies]

Jeff Anderson, K6JCA, is entirely correct. My two-step tuning of an *L*-network will not work for low-*Z* loads, when the tuning capacitor is on the exciter side of the inductor. I leaned upon duality and symmetry rather than brut calculation. When actually calculated, assuming the load *R* is resistive and less than 50 Ω, the exciter in fact sees

$$Z = \frac{RX_C^2}{R^2 + (X_L - X_C)^2} + j \frac{R^2 X_C + X_L X_C (X_L - X_C)}{R^2 + (X_L - X_C)^2}$$

where at tune, the values of *L* and *C* are determined by the following two equations, which are obtained by looking backwards toward the source and applying equations,

$$\frac{50X_C^2}{50^2 + X_C^2} = R \quad \text{and} \quad \frac{50^2 X_C}{50^2 + X_C^2} = X_L$$

The equation for *Z* shows that the real part *Z* is affected by both *C* and *L* and thus my two step algorithm fails. However, Jeff's Smith Chart approach, when displayed analytically is

$$\frac{1}{Z} = \frac{1}{R + jX_L} + \frac{1}{-jX_C}$$

and the real part of the admittance is indeed determined solely by the single variable X_L and can be brought to the correct conductance of 20 millimhos, followed by a tuning of the capacitor to null the reactive part.

Moreover, Jeff is also correct in that we must now watch instead the phase of $(V_f + V_r)$ versus V_r since

$$\frac{1}{Z} - \frac{1}{50} = \frac{V_f/50 - V_r/50}{50} - \frac{1}{50} = -\frac{1}{25} \frac{V_r}{V_f + V_r}$$

We have reached the correct conductance circle only when $V_f + V_r$ and V_r are in quadrature. — *Chuck MacCluer W8MQW.*

Send your *QEX* Letters to the Editor to, ARRL, 225 Main St., Newington, CT 06111, or by fax at 860-594-0259, or via e-mail to qex@arrl.org. We reserve the right to edit your letter for clarity, and to fit in the available page space. "Letters to the Editor" may also appear in other ARRL media. The publishers of *QEX* assume no responsibilities for statements made by correspondents.

From **MILLIWATTS**
To **KILOWATTS**

More Watts per Dollar



Transmitting & Audio Tubes



COMMUNICATIONS
BROADCAST
INDUSTRY
AMATEUR

Immediate Shipment from Stock

3CPX800A7	4CX1000A	810
3CPX1500A7	4CX1500B	811A
3CX400A7	4CX3500A	812A
3CX800A7	4CX5000A	833A
3CX1200A7	4CX7500A	833C
3CX1200D7	4CX10000A	845
3CX1200Z7	4CX15000A	6146B
3CX1500A7	4CX20000B	3-500ZG
3CX3000A7	4CX20000C	3-1000Z
3CX6000A7	4CX20000D	4-400A
3CX10000A7	4X150A	4-1000A
3CX15000A7	572B	4PR400A
3CX20000A7	805	4PR1000A
4CX250B	807	...and more!

Se Habla Español • We Export

Phone: **760-744-0700**

Toll-Free: **800-737-2787**

(Orders only) **RF PARTS**

Website: **www.rfparts.com**

Fax: **760-744-1943**

888-744-1943

Email: **rfp@rfparts.com**



RF PARTS
COMPANY

Upcoming Conferences

MicroHAMS Digital Conference 2017 Operating Specialty Convention

March 18, 2017, Redmond, WA
www.microhams.com/mhdc

Check website for details.

1st Annual Amateur Radio Utah Digital Communications Conference

March 25th, 2017, Sandy, Utah
utah-dcc.org

The conference will be a fusion of amateur radio communications and maker topics. Amateur radio is the pioneer of digital modes. This conference will focus on the amateur radio hobby that surrounds utilizing digital modes. Current emerging topics such as digital modes for emergency communications and building your own components.

Call for Presenters: Interested in presenting at the conference or volunteering to help? Contact: utahdcc@gmail.com

Registration: Registration is now open using the EventBrite system (see website). Cost is \$12 per person pre-registration.

Session Topics

- Introduction To Mesh
- Advanced Mesh Topics
- Introduction to DMR
- Universal Modem For Ham Radio
- Getting started with WinLink
- Introduction to APRS
- Exploring capabilities with 3D Printing
- Introduction to D-Star
- D-STAR System Administration
- Eagle Cad – Printing Circuit Boards
- Building your first Arduino Project
- Orientation to System Fusion
- Getting started with FLDIGI
- AMSAT – Amateur Radio Satellite
- Getting started with Raspberry Pi

Southeastern VHF

April 28 – 29, 2017, Charlotte, NC
svhfs.org

The SVHF Society will hold our convention in Charlotte, NC this year on April 28 and 29 at the Doubletree by Hilton Hotel Charlotte Airport, 2600 Yorkmont Rd., Charlotte, NC 28201. We have arranged rooms at \$95; you can call 800-222-TREE and ask for this rate under the name "South East VHF Society." We will have the registration information on the web site soon, so watch for the sign up details. The conference fee for pre-registration is \$30, Friday's Luncheon is \$15, and the Saturday's banquet is \$40.

Call for Paper

Papers and presentations are solicited on both the technical and operational aspects of VHF, UHF and Microwave weak signal amateur radio. Some suggested areas of interest are:

- Transmitters
- Receivers
- Transverters
- RF Power Amplifiers
- RF Low Noise Pre Amplifiers
- Antennas
- Construction Projects
- Test Equipment And Station Accessories
- Station Design And Construction
- Contesting
- Roving
- DXpeditions
- EME
- Propagation (Sporadic E, Meteor Scatter, Troposphere Ducting, etc.)
- Digital Modes (WSJT, etc.)
- Digital Signal Processing (DSP)
- Software Defined Radio (SDR)
- Amateur Satellites
- Amateur Television

In general papers and presentations on non-weak signal related topics such as FM repeaters and packet will not be accepted but exceptions may be made if the topic is related to weak signal. For example, a paper or presentation on the use of FM simplex in contests or on the use of APRS to track rovers during contests would be considered.

The deadline for the submission of papers and presentations is March 13, 2017. Please indicate when you submit your paper or presentation if you plan to attend the conference and present your paper in person or if you are submitting solely for publication. Papers and presentations are being handled by Jim Worsham, W4KXY. Jim can be contacted at w4kxy@bellsouth.net. Papers and presentations are also to be sent to w4kxy@bellsouth.net.

2017 SARA Western Regional Conference

Socorro, New Mexico
March 17 – 19, 2017
www.radio-astronomy.org

The 2017 SARA Western Regional Conference will be held at the Pete V. Domenici Science Operations Center in Socorro, New Mexico on March 17 to 19, 2017.

Please contact conference coordinator Dave Westman if you have any questions about the conference or if you would like to help: westernconf@radio-astronomy.org.

Registration for the 2017 Western Regional Conference is just US\$60.00. This includes breakfast and lunch on Saturday and Sunday. Payment can be made on-line, or you can mail a check to SARA, 2946 Montclair Ave., Cincinnati, OH 45211 USA. Please include an e-mail address so a confirmation can be sent to you upon receipt of payment.

Lodging during the conference can be reserved at the Best Western Hotel & Suites in Socorro for a special rate of \$101.48 per night (89.24 + tax per night single or double by calling (575) 838-0556 or bestwesternsocorro@yahoo.com.

SARA Annual Conference

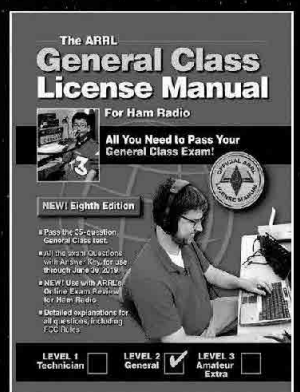
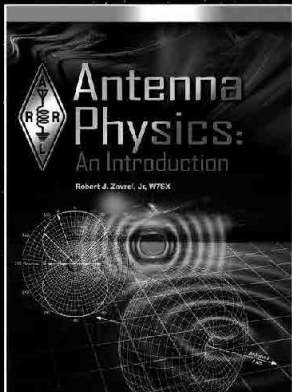
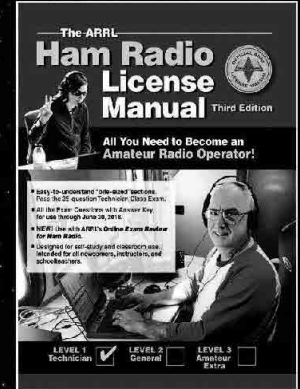
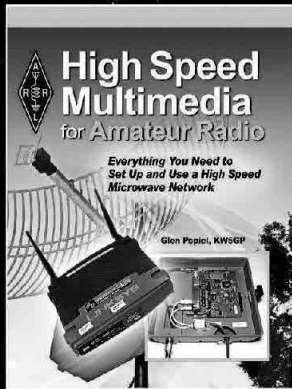
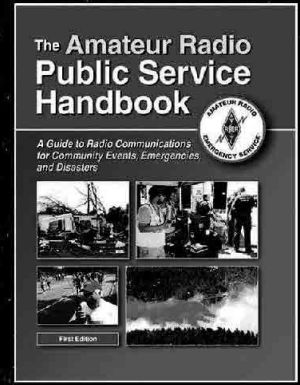
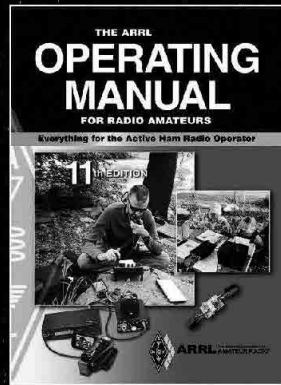
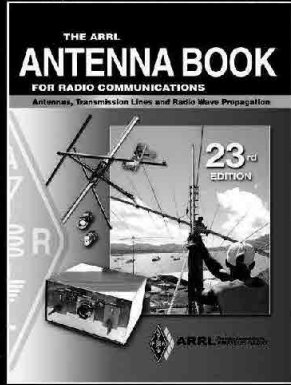
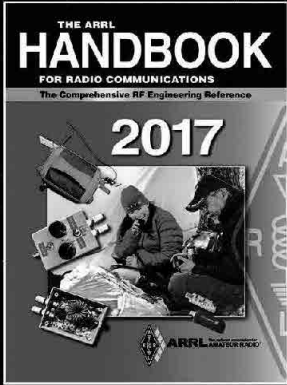
NRAO Green Bank, WV
July 23 – 26, 2017
radio-astronomy.org

See website for details.

Central States VHF Society 2017 Conference

Albuquerque, New Mexico
July 27 – 30, 2017
Sheraton Albuquerque Airport
Hotel
2017.csvhfs.org

See website for details.



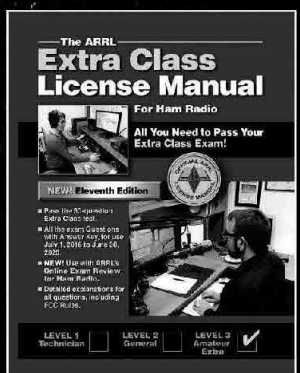
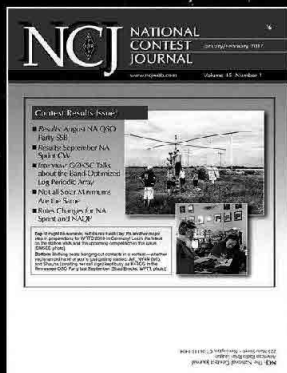
Stay in the Know!

ARRL Publications
and Journals
www.arrl.org/shop



The national association for
ARRL AMATEUR RADIO

Advancing the Art, Science, and Enjoyment of Radio
Since 1914



Members, Enjoy Your Online Benefits!



- QST Digital Edition**
 View monthly, online digital editions of *QST* at no additional cost (web and app versions).
- FREE E-Newsletters**
 ARRL weekly Letter, ARRL ARES e-Letter, Division and Section news, special offers, and more.
- QST Archive and Periodicals Index**
 Browse ARRL's extensive online *QST* archive, and a searchable index for *QEX* and *NCJ*.
- Product Review Archive**
 Download and view *QST* Product Reviews from past to the present.
- E-Mail Forwarding Service**
 YourCallSign@arrl.net
 E-mail sent to your arrl.net address will be forwarded to any email account you specify.



The national association for
ARRL AMATEUR RADIO

www.arrl.org/myARRL

Membership Application

Membership options (circle your choice/s)

	1 Year	2 Years	3 Years	
US	\$49	\$95	\$140	Monthly <i>QST</i> via standard mail for US members
Youth	\$25			Must be 21 years old or younger AND the oldest licensed Radio Amateur in the household
Canada	\$62	\$120	\$177	Monthly <i>QST</i> via standard mail for Canadian members
International	\$76	\$147	\$217	Monthly <i>QST</i> via standard mail for international members
International/Canada – no print <i>QST</i>	\$49	\$95	\$140	Digital <i>QST</i> only
Family	\$10	\$20	\$30	Must reside with primary member and have corresponding membership dates; no extra copies of <i>QST</i>
Blind	\$10	\$20	\$30	No <i>QST</i> delivery; all other member benefits apply. Requires a one time signed and dated statement of Legal Blindness.

Additional membership options are available at www.arrl.org/join Membership includes \$21 per year for subscription to *QST*. Dues subject to change without notice and are nonrefundable.

Name _____ Call Sign _____

Street _____ City _____ State _____ ZIP _____

E-mail _____ Phone _____ Date of Birth _____

Family Member Name _____ Call Sign (if any) _____

Payment Options

- Total enclosed payable to ARRL \$ _____
- Visa MasterCard Amex Discover Check Enclosed

I do not want my name and address made available for non-ARRL related mailings.

Card Number _____ Expiration Date _____

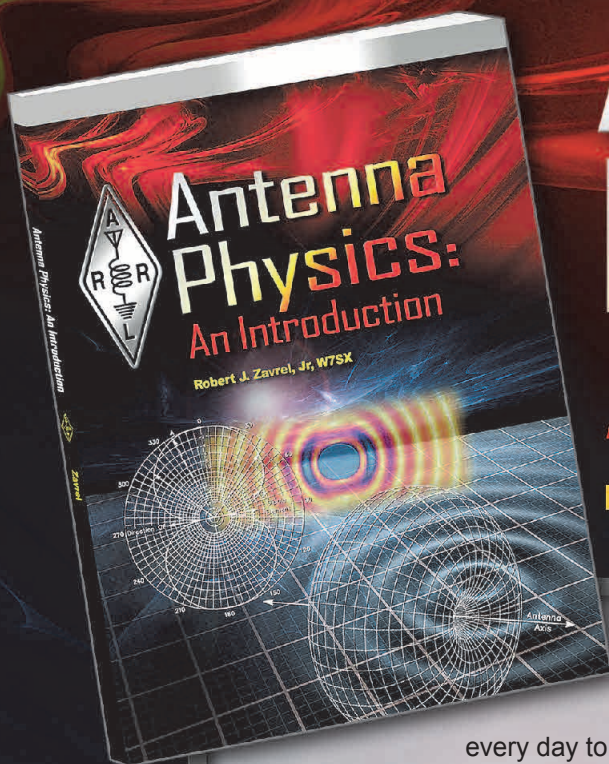
Cardholder's Signature _____



ARRL, 225 Main St.
 Newington, CT 06111

1-888-277-5289

www.arrl.org/join



Antenna Physics: An Introduction

by Robert J. Zavrel, Jr, W7SX

Delve Deeper into Antenna Theory

Radio amateurs are familiar with antennas and use them every day to communicate on the air. We learned some basic antenna theory while studying for license exams, and most of us have built an antenna or two. We know the basics and turn to the *ARRL Handbook*, *ARRL Antenna Book*, and other general texts when thinking about our next antenna project.

We know how long to make a dipole or vertical antenna for a particular frequency, but do we know how the antenna really works? ***Antenna Physics: An Introduction*** was written to bridge the gap between basic theory and graduate-level engineering texts. **Robert J. Zavrel, Jr, W7SX**, a well-known author and professional antenna engineer, explains many of the underlying principles of antennas and antenna physics and introduces the reader to the mathematics behind these principles. Note that this is not a book of “how-to” projects, but rather a theoretical and mathematical approach to the topic.

Although some competence in mathematics is required to get the most from this book, readers may follow along and understand the concepts without needing to solve the complex equations presented. In later chapters, examples tie the concepts learned in earlier chapters to a number of antenna types familiar to radio amateurs.

Includes:

Antenna Physics

- Development of Antenna Physics
- Fundamentals
- Radiation of Radio Waves
- Transmission Line
- Antennas Using Multiple Sources

Applied Antenna Physics

- Dielectric Effects Upon Radio Waves
- Vertical Antennas
- Yagi-Uda and Cubical Quad Antennas
- Specialized Antenna Configurations
- Noise, Temperature, and Signals

Antenna Physics: An Introduction

ARRL Item No.0499

Only **\$29.95** plus shipping and handling

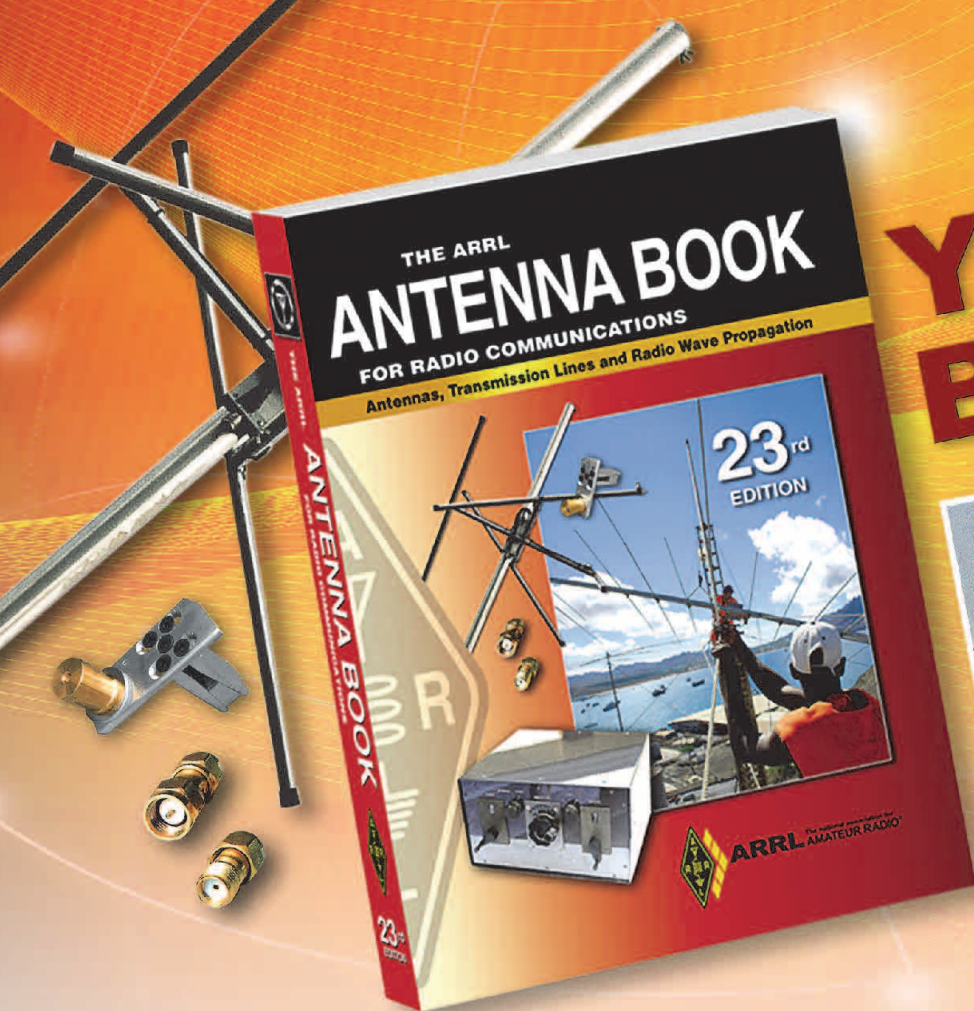


ARRL The national association for
AMATEUR RADIO®

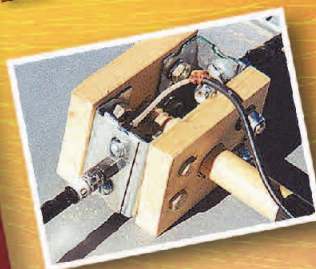
www.arrl.org/shop

Toll-Free US 888-277-5289 or
elsewhere +1-860-594-0355

QEX 3/2017



You Can Build It!



The ARRL Antenna Book
Softcover Book with CD-ROM
ARRL Item No. 0444
Only \$49.95

The ARRL Antenna Book has everything you need to design your own complete antenna system. Since 1939, it has maintained its place at the forefront of Amateur Radio technology—a single resource covering antenna theory, design and construction, and practical treatments and projects. It describes hundreds of antenna designs: wire, vertical, portable and mobile, and new high-performance VHF/UHF Yagi designs. Updated to reflect the latest advances and technologies, this 23rd edition is full of antenna designs pioneered by dozens of radio amateurs:

New Projects

- Multiband HF antennas from 160 through 10 meters
- A simple omnidirectional satellite antenna system
- More popular Moxon antenna projects on CD-ROM
- Stealthy and portable antenna designs for home and away

New Information

- How short vertical antennas affect the performance of antenna systems
- New section on grounding and bonding, both key to effective station design and protection
- Updated Propagation chapter now includes a discussion of MF and LF propagation
- Expanded content on CD-ROM, including references and classic articles on antennas

System Requirements: A fully searchable PDF version of this book is included for Windows® 7, Windows Vista®, or Windows® XP, as well as Macintosh® systems, using Adobe® Acrobat® Reader® software. The Acrobat Reader is a free download at www.adobe.com. PDF files are Linux readable. Utility programs are Windows® compatible, only.



ARRL The national association for
AMATEUR RADIO®

www.arrl.org/shop
Toll-Free US 888-277-5289,
or elsewhere +1-860-594-0355

QEX 3/2017

